

5.3 NaCl-05: NaCl (MR=0.7) Test with Diamond Packing

5.3.1 Background

Since the NaOH-03 test confirmed that the crevice chemistry instrumentation worked properly, the bulk water chemistry was returned to NaCl. Test NaCl-05 involved only one diamond-packed crevice having a radial gap of 10 mils. The crevice was packed with 127-165- μm -dia diamond grit. The estimated crevice porosity was 40 %. This arrangement allowed us to focus more carefully on only one crevice producing hideout for the NaCl chemistry. The initial Na-to-Cl MR in the bulk water was set at 0.7. The previous test with MR=0.7, NaCl-04, followed the NaCl-03 test without opening of the secondary chamber. As discussed in Section 4.4, the NaCl-04 test appeared to be affected by the NaCl-03 test. The NaCl-05 tests will permit verification of the NaCl-04 tests. As a result of the cracking of the alloy 600 tubing in the NaCl-04 test, the SG tubes were replaced with 7/8-in. dia. alloy 690 TT for the NaCl-05 test. An unpacked crevice having 20-mil radial gap was not tested during the NaCl-05 and following tests.

5.3.2 Temperature Data

As shown in Figure 115, the crevice temperature started to increase right after the solution injection in NaCl-05. One thermocouple was installed near the crevice electrode assembly labeled "Near Electrodes" in Figure 115. This reading showed similar behavior to other thermocouples but was about 1°F higher than others at $\Delta T=40^\circ\text{F}$. At $\Delta T=60^\circ\text{F}$, the "Near Electrodes" thermocouple was about 6°F higher than T2. After the increase in ΔT , two of the thermocouples exhibited noisy behavior, followed by stabilization at the secondary saturation temperature. T2 also started to decrease followed by gradual recovery, and T1 recovered its original temperature value when T2 returned to its original value. The "Near Electrodes" thermocouple exhibited a noisy signal and did not come back to the original value. The temperature variation observed at $\Delta T=60^\circ\text{F}$ was not evident in the earlier MR=0.7 test (NaCl-04). After increasing the ΔT from 60 to 80°F, T1 and T2 did not show a noisy signal. The post-test examination indicated that all the diamond powder was secure inside the crevice, but that the thermocouples may have slipped since they were not tightly secured. Therefore, a reasonable explanation for the unexpected temperature oscillation is that the thermocouples slipped during the test and were pushed backward from the tube wall, which led to the decrease of temperature. Then, as concentration proceeded at the thermocouple tip area, the temperature returned to the original value or even higher. The temperature data obtained after the occurrence of instability was not used for further analysis. The "Near Electrodes" thermocouple started to malfunction at 215 hours, probably because the protective alloy 600 sheath failed by corrosion. At $\Delta T=80^\circ\text{F}$, a second solution was injected to confirm that the crevice had become saturated but it is difficult to determine the saturation from the temperature data because of the thermocouple problem. In the next test, a new method of positioning and tightening the thermocouples was used.

In Figure 116, the normalized crevice temperatures are plotted as a function of time. The temperature elevation after the solution injection is clearly evident. The normalized crevice temperature, however, did not change significantly after the increase of ΔT from 40 to 60°F.

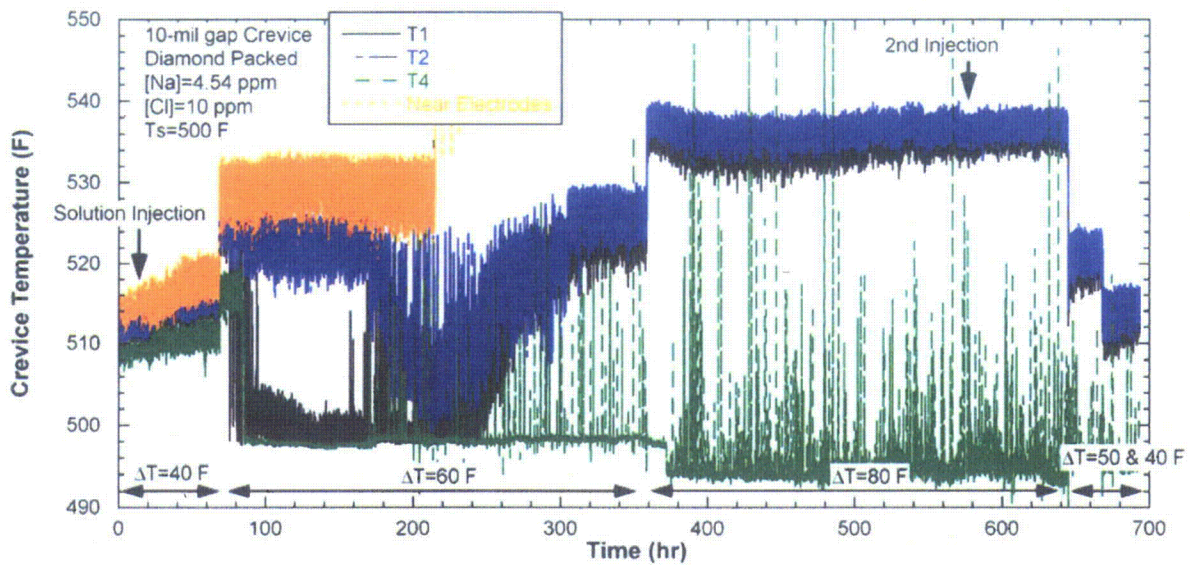


Figure 115. Crevice temperature variation with time in the 10-mil gap crevice packed with diamond powder (initial MR=0.7; NaCl-05).

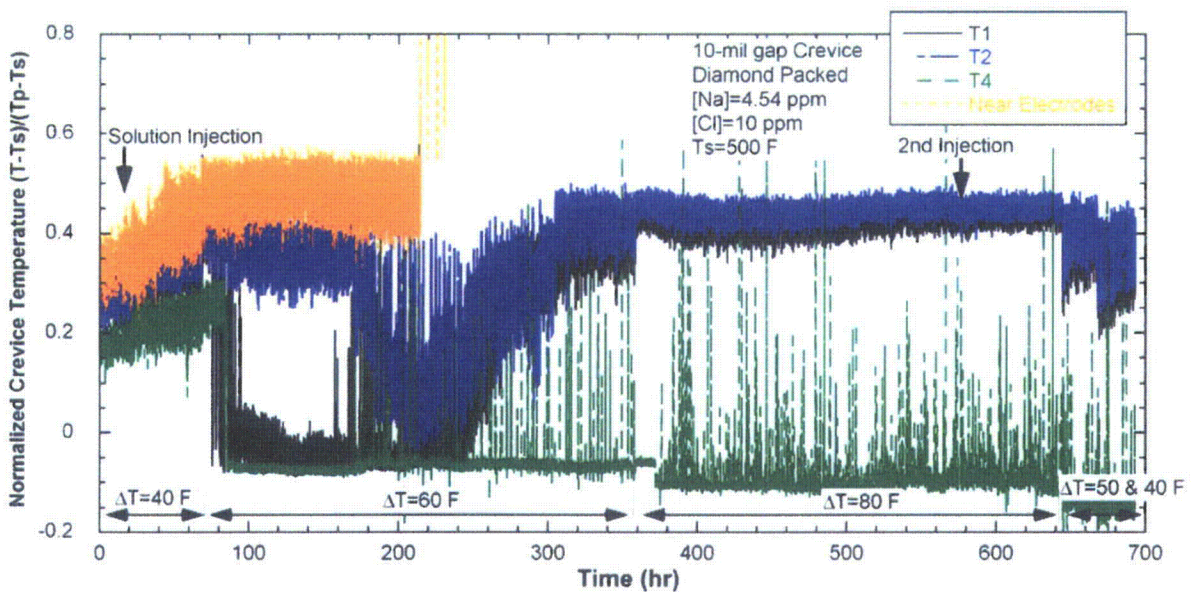


Figure 116. Normalized crevice temperature variation with time (initial MR=0.7; NaCl-05).

5.3.3 Bulk and Crevice Chemistry

Figure 117 shows the conductivity variation with time for the bulk solution in NaCl-05. Most of the bulk conductivity reduction occurred at $\Delta T=60^\circ\text{F}$. Based on the MULTEQ code prediction, NaCl precipitation can occur if the boiling point elevation exceeds 46°F . Therefore, it is likely that the NaCl precipitation occurred inside the crevice and became saturated after about 100-hours operation at $\Delta T=60^\circ\text{F}$. The occurrence of the NaCl precipitation will be verified by a mass balance analysis, discussed

in Section 5.3.6. When increasing ΔT from 60 to 80°F, the bulk conductivity initially decreased and became stabilized in a short time, indicating that most of the NaCl precipitation had already occurred at $\Delta T=60^\circ\text{F}$. The bulk conductivity increased immediately after injecting more MR=0.7 NaCl solution and did not decrease with time, indicating that the crevice is in a fully saturated state. During the test period of 240-320 hours, the Cl concentration decreased while the Na concentration increased slightly. The concentration change is slightly higher than analysis error ($\pm 10\%$) and, considering that the tube surfaces were corroded (based on post-test inspection), electromigration might have occurred during this time period; the dissolved metal cations from the corrosion drove Na^+ out of the crevice and Cl^- into the crevice.

The variation in crevice conductivity with time is plotted in Figure 118. The crevice conductivity increased suddenly a few hours after the first solution injection. It then quickly stabilized at $\Delta T=40^\circ\text{F}$. After the increase of ΔT from 40 to 60°F, crevice conductivity did not change significantly, but about 30 hours later it started to decrease and stabilized at another value. However, the crevice conductivity started to increase again and stabilized at the same value as before. The crevice conductivity variation at $\Delta T=60^\circ\text{F}$ is unexpected and difficult to be explained by simple impurity hideout mechanism. After ΔT was increased from 60 to 80°F, the crevice conductivity slowly increased, followed by a slow decrease. If the NaCl precipitation occurred around the conductivity probes, the crevice conductivity should decrease. Therefore, the conductivity change at $\Delta T=80^\circ\text{F}$ may be attributed to the NaCl precipitation around the conductivity probe.

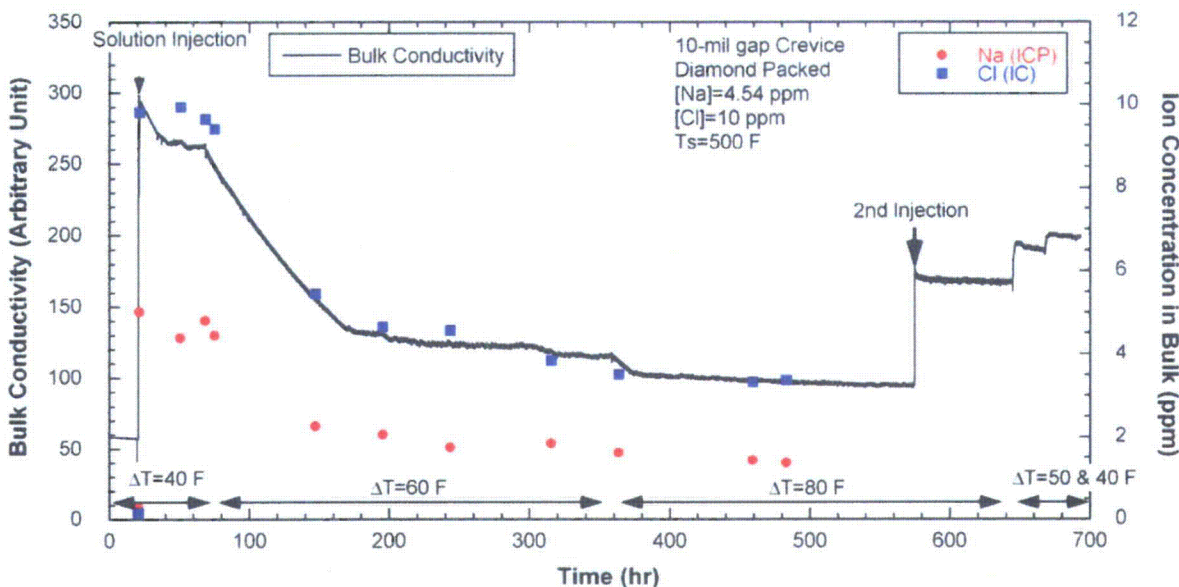


Figure 117. Bulk conductivity variation with time and the chemical analysis results for bulk samples (initial MR=0.7; NaCl-05).

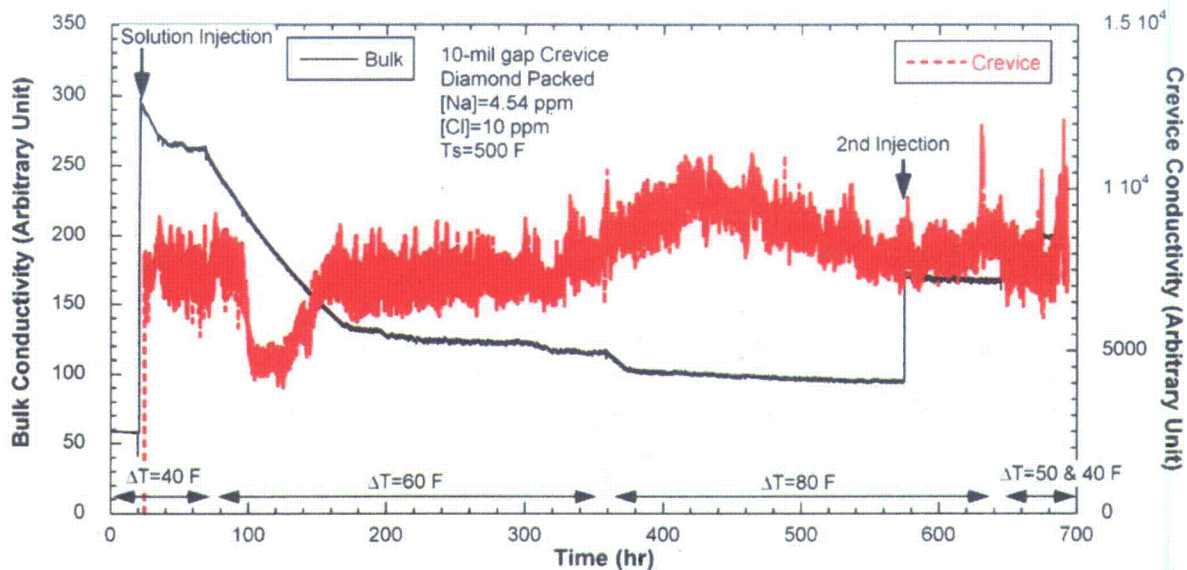


Figure 118. Bulk and crevice conductivity variation with time (initial MR=0.7; NaCl-05).

Figure 119 shows the variation in ion concentration based on the analyses of crevice samples. As discussed earlier, the sampling time correction was applied to minimize the effect of the sampling-line dead volume. The initial ion concentration in the crevice increased rapidly but suddenly dropped to about the bulk concentration before the change in ΔT from 40 to 60°F. About 60 hours later, it recovered to the initial high value. The timing is not exactly consistent with the crevice conductivity drop but, as shown in Figure 118, the crevice conductivity showed similar behavior. These results suggest the possible instability of the crevice hideout. Additional investigations could lead insights on whether or not this crevice instability is generic and repeatable and can occur in a magnetite-packed crevice and in the actual field SG crevice. The Na and Cl concentrations in this test are much higher than those in the NaCl-04 test (Figure 73) at $\Delta T=40$ and 60°F. These results support the earlier observation that the crevice concentrations in the NaCl-04 test were affected by the previous NaCl-03 test.

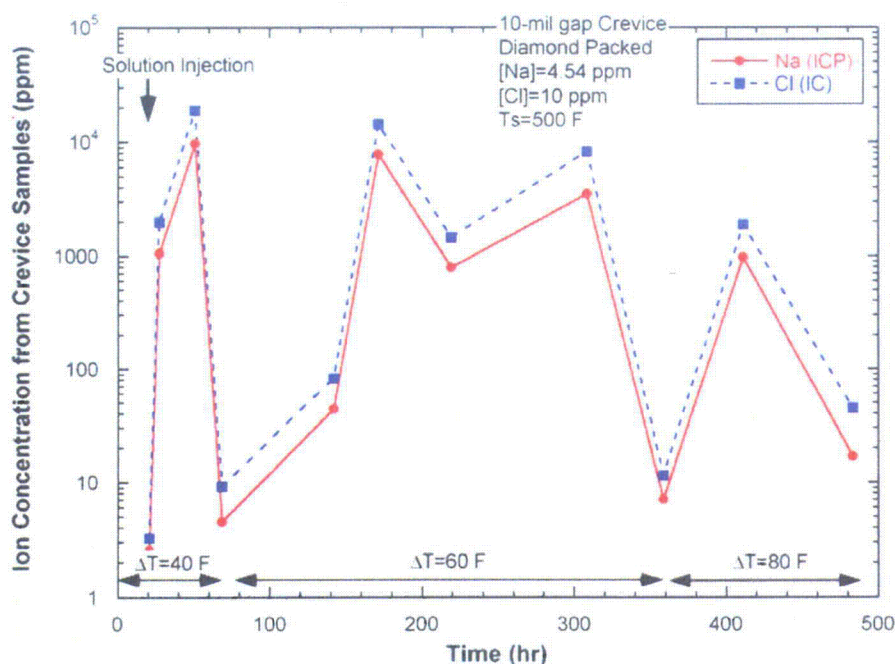


Figure 119.
Chemical analyses of
the crevice samples
(initial MR=0.7; NaCl-
05).

5.3.4 ECP Measurements

Figure 120 shows the tungsten potential changes in the bulk and the crevice during NaCl-05. The bulk potential drop after the solution injection is 164 mV. The pH change calculated by MULTEQ using the chemical analyses of the bulk samples is 1.95, which corresponds to a potential change of 185 mV. The calculated potential change is close to the measured bulk potential change. Two tungsten/tungsten oxide electrodes were installed in the 10-mil gap crevice separated by 30 degrees at the same crevice elevation. The two tungsten potentials showed very similar behavior. The bulk tungsten potential gradually decreased during the test period at $\Delta T=60^{\circ}\text{F}$ and stabilized at $\Delta T=80^{\circ}\text{F}$. If the Na-to-Cl MR in the bulk water remains at 0.7, the bulk water pH will increase because the absolute amount of H^+ ions needed to maintain charge neutrality will decrease as the absolute Na and Cl amounts decrease in the bulk water. This explanation is supported by the pH calculations for bulk samples, as described in Section 5.3.6. The crevice tungsten potential was almost insensitive to the change in ΔT , except for the initial 20 hours after the first solution injection. The initial increase after the first solution injection was caused by the transition from pure water to the acidic NaCl solution. The following abrupt potential decrease was caused by the volatility effect of Cl, which is supported by the finding that, in the same short time period, bulk tungsten potential slightly increased, indicating preferential Na concentration and resultant acidification of the bulk water. However, the crevice tungsten potentials increased again, and this change suggests that the volatility effect of Cl became less significant. Based on the post-test examination showing the gouging on the tube surfaces, the insensitiveness of the crevice tungsten potential might be due to the crevice tungsten wire tip being too far from the tube surface to represent the active chemical change near the tube surface.

The Ta/TaO_x electrode was introduced for the first time during this test and was expected to serve as a pH electrode, just as the W/WO_x electrode did. As shown in Figure 121, the bulk potential decreased 160 mV after the chemical injection at 20 hours, which is very close to the tungsten potential change of 164 mV. The bulk Ta potential stayed almost the same for the test period; this behavior differs from that

of the bulk tungsten potentials shown in Figure 120. Detailed comparisons between tungsten and Ta electrodes are discussed in Section 5.3.6. There was no advantage observed in using a Ta electrode over a tungsten electrode.

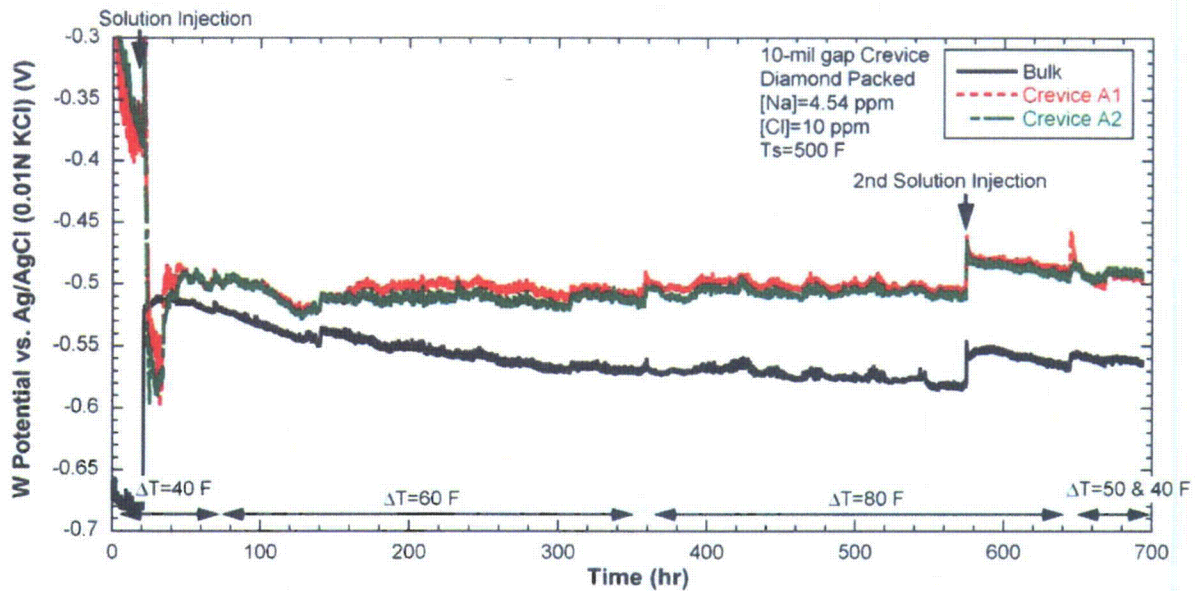


Figure 120. Tungsten potential variation with time in the bulk and 10-mil gap crevice packed with diamond powder (initial MR=0.7; NaCl-05).

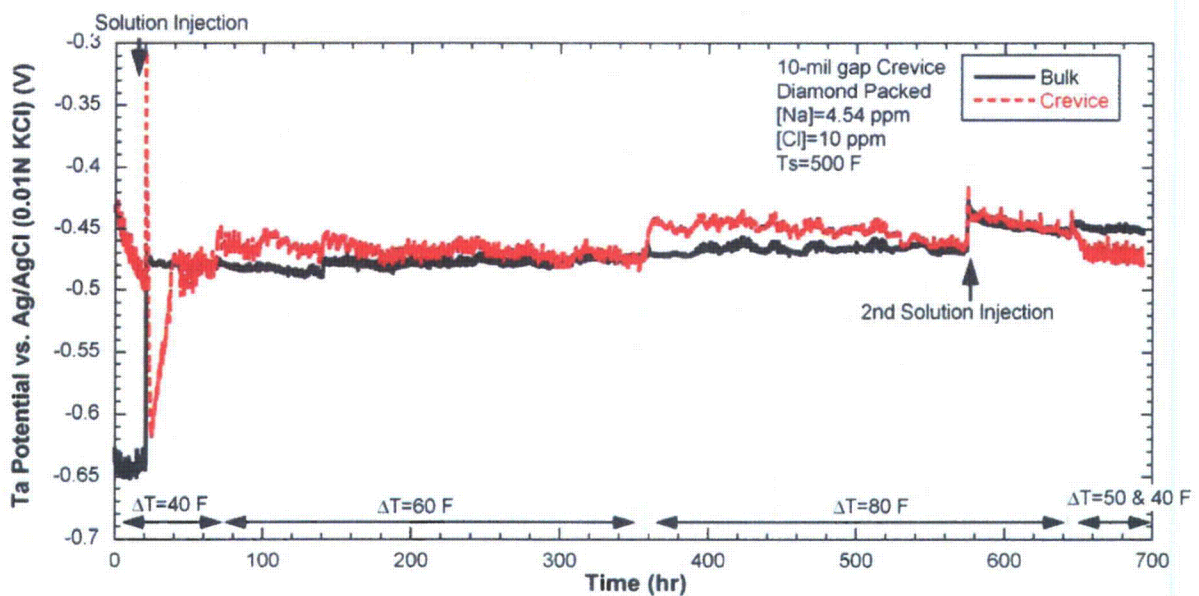


Figure 121. Ta potential variation with time in the bulk and the 10-mil gap crevice packed with diamond powder (initial MR=0.7; NaCl-05).

5.3.5 Post-Test Examination

Figure 122 shows the top of the crevice ring after removal of the Ni-Cr-Mo alloy foam and retaining ring, and shows that the diamond dust was secure inside the crevice. Gouging was apparent over the alloy 690 TT tube surfaces, as shown in Figure 123. The degree of gouging is comparable with that observed on the alloy 600 surfaces after the NaCl-03 and -04 tests, as shown in Figure 84. The corrosion data of alloy 690 TT under strong acid environments are very limited. Based on this gouging observation, the corrosion resistance of alloy 690 TT in a strong acid is comparable with that of alloy 600 MA. The severe gouging on the tube surfaces suggests that a strong acid chemistry developed in the crevice in this test. As discussed in Section 3.2.1, the abrasion of hard diamond particles might enhance this gouging. For this reason and others, a magnetite-packed crevice test similar to NaCl-05 should be conducted and compared with the results of the diamond-packed crevice test. The calculated pH from the crevice samples supports the development of acidic crevice chemistry, but the crevice tungsten potentials, shown in Figure 120, do not support this observation. No evidence suggests the development of strongly alkaline crevice chemistry in this test. Therefore, it is reasonable to try to explain the insensitivity of the crevice tungsten potentials to the changing chemical conditions within the crevice. As mentioned earlier, the crevice tungsten wire tip was probably placed too far from the tube surface to represent the actual chemistry. Assuming the development of an acidic crevice chemistry, the increase of bulk Na concentration and corresponding decrease in bulk Cl concentration can be interpreted as the result of ion migration. Ion migration would take place to maintain charge neutrality after excess metal cations accumulated in the crevice.

To determine if the tube surface cracked, the tubing was removed from the MB, and a dye penetrant test was performed. Figure 124 shows the tube surface area before application of the dye penetrant. To make sure that no crack had formed on the tube, the hard scales were removed, and the dye penetrant was applied, as shown in Figure 125. No cracks had formed underneath the hard scale. The black hard scale shown in Figure 124 seems to be magnetite because it stuck to a magnet. The source of the magnetite is likely the inner surface of the MB secondary chamber made of SS. The solution pH of the current test is slightly acidic, which can enhance the dissolution of magnetite from the SS surfaces and increase the bulk Fe ion concentration.



Figure 122.
Top of the crevice ring after removal of the Inconel foam and retaining ring, which shows the diamond dust was secure inside the crevice.

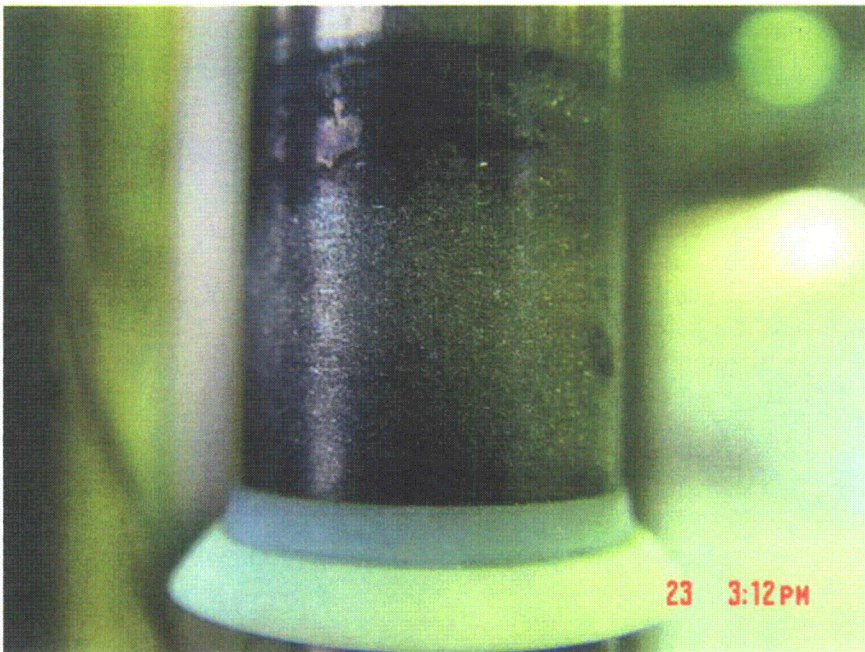


Figure 123.
Alloy 690 TT tubing surface after removal of the crevice ring and diamond dust showing gouging in the crevice region.



Figure 124.
Bare alloy 690 TT tubing
surface (left: crevice top,
right: crevice bottom).

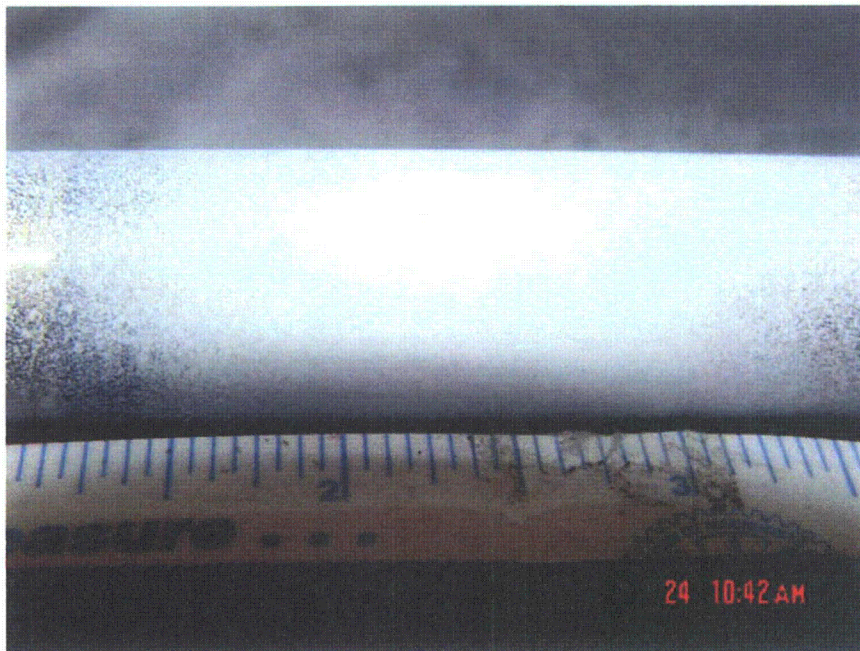


Figure 125.
Dye penetrant test results
after removal of the hard
scale underneath the SS
back ferrule showing no
visible cracks in the
crevice region.

5.3.6 Discussion

Potential and pH Analysis

In Figure 126, the tungsten and Ta potentials in the crevice and bulk solution are plotted as a function of pH. The pH was estimated from the solution sample chemistry using MULTEQ. The sampling time correction was applied to all data. The tungsten potentials in the bulk solution show very good linearity with respect to pH, but the Ta potentials exhibit scatter in a narrow pH range of 4-5. The potential/pH slope of the tungsten electrode is much less than the Nernstian slope of -106 mV/pH . There is no available data for Fe or Ni ion concentration in the bulk water, but the magnetite deposits observed in the crevice region suggest the presence of significant metal ions in the bulk water, which can increase the solution pH but could not be considered in Figure 126. If Fe and Ni concentration data is available and estimated bulk pH shifts in the alkaline direction by the effect of dissolved metal ions, the potential/pH slope will become steeper and closer to the Nernstian value. The W/ WO_x electrode is more appropriate in NaCl solution than the Ta/ TaO_x electrode as a pH sensor because the tungsten potential changes more substantially with respect to the bulk pH change. Neither the tungsten nor Ta potentials in the crevice varied significantly which is inconsistent with the pH change estimated from the crevice samples.

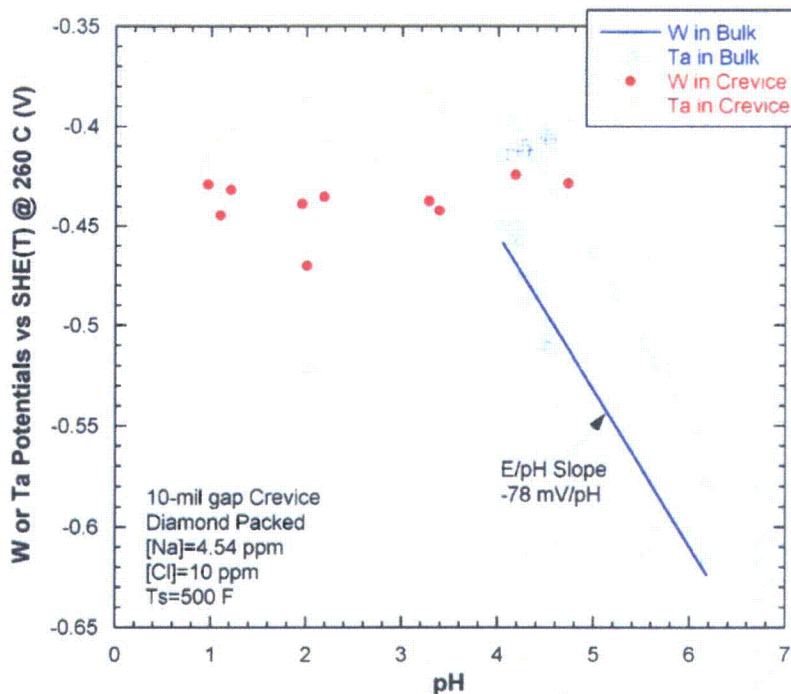


Figure 126. Tungsten and Ta potentials in bulk and crevice as a function of pH estimated from the solution samples by MULTEQ (initial MR=0.7; NaCl-05).

In Figure 127, the measured data in NaCl-05 are compared with the previous NaCl and NaOH test data. The tungsten potential data for the bulk solution in the present test are consistent with the previous data. The crevice tungsten potential data in this test are within the same range as the previous data, but the crevice potentials are again insensitive to crevice sample pH in this test. As discussed earlier, because the crevice tungsten wire tip was not close enough to the tube surface, the crevice tungsten potentials appear to be insensitive to the pH change and indicate only weakly acidic crevice chemistry. The effect of the crevice tungsten wire tip location is discussed again in the next test (NaCl-06). A dashed line designated

by 'Kriksunov et al.' denotes a measured potential of tungsten oxide electrode as a function of pH at 250°C by Kriksunov and Macdonald²⁹.

Figure 128 shows the MR variation in the bulk and crevice samples with time for NaCl-05. The bulk MR was in the range of 0.6-0.8, and the crevice MR was higher than the bulk MR at most times but still less than unity. At $\Delta T=40^\circ\text{F}$ and 60°F , the bulk and crevice MRs tend to vary in opposite directions, which is an expected result because the model boiler system is a closed one so that mass balance should be maintained between bulk and crevice. But at $\Delta T=80^\circ\text{F}$ the crevice MR follows the bulk MR. These results suggest that at lower ΔT the crevice samples represent actual crevice chemistry, but at higher ΔT the crevice samples are mixed with bulk solution so that the crevice MR becomes similar to the bulk MR.

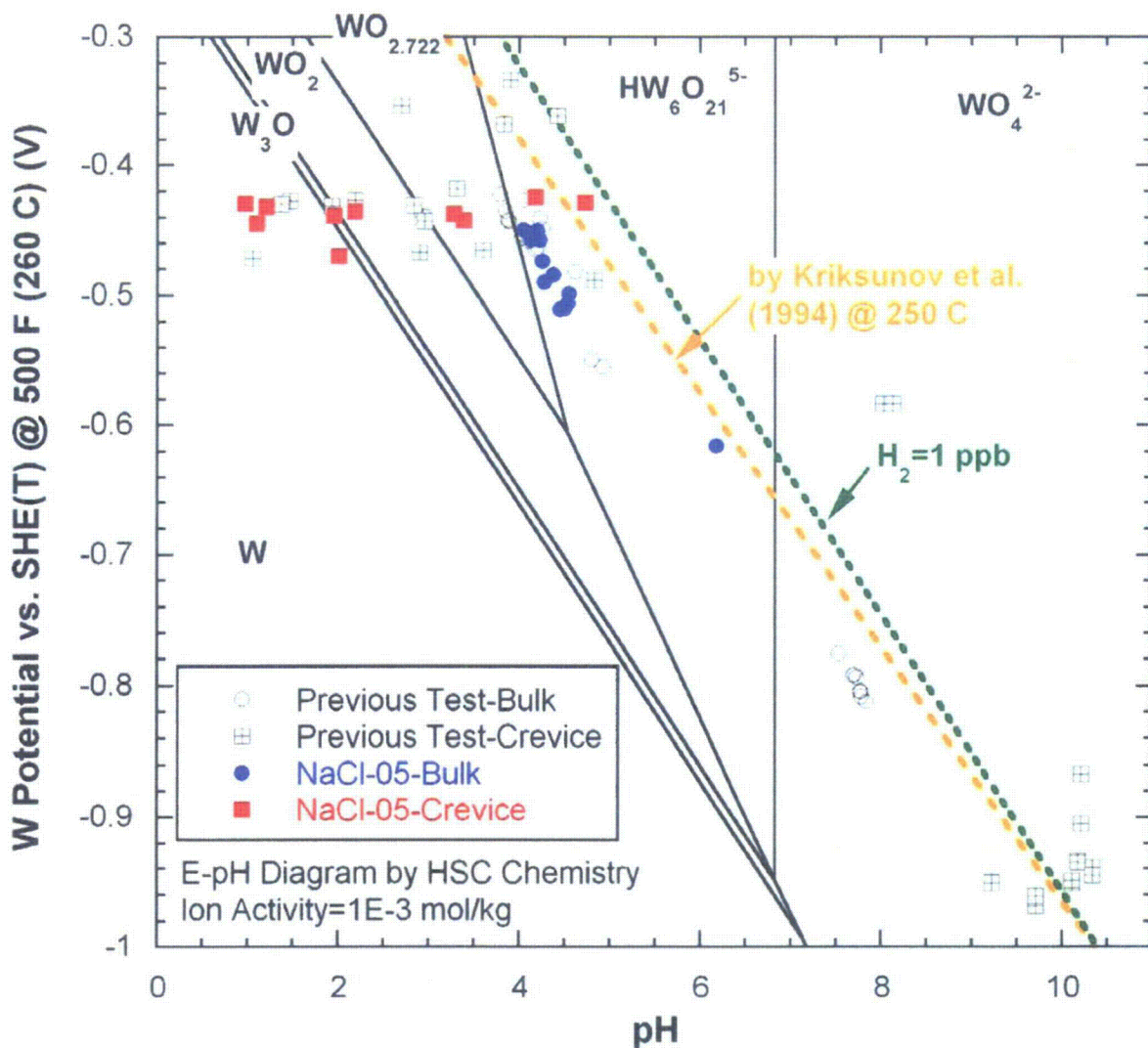


Figure 127. Tungsten potentials measured during NaCl-05 compared to the data from previous tests plotted in a phase diagram of W-H₂O system predicted by the thermodynamic code HSC Chemistry.

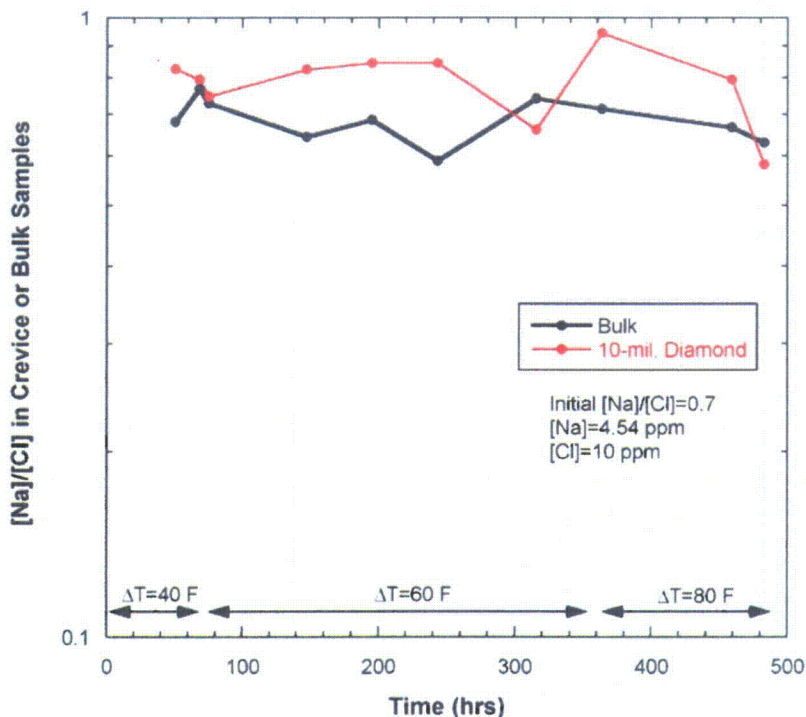


Figure 128.
Molar ratio variations in bulk and crevice samples with time (NaCl-05).

Mass Balance Analysis

Figure 129 shows the total mass of Na and Cl in the crevice as a function of time, which is estimated from the analysis results for the bulk samples. As was done in the analysis of the NaOH-03 test data, we considered the mass losses by the crevice and bulk sampling. The Na and Cl masses before the ΔT change from 40 to 60°F are relatively small. At a given ΔT , an impurity concentration limit in the crevice can be determined thermodynamically, which is called a thermodynamic limit. If the thermodynamic limit is larger than a solubility limit, the solubility limit becomes an effective limit. The estimated thermodynamic limit by MULTEQ at $\Delta T=40^\circ\text{F}$ is 28.9 mg for Na and 44.5 mg for Cl, and these limits are much higher than the measured crevice Na and Cl masses. Therefore, the crevice did not reach the thermodynamic limit at $\Delta T=40^\circ\text{F}$. However, after the ΔT was changed from 40°F to 60°F, significant Na and Cl hideout occurred. In Figure 129 the solubility limits of Na and Cl are also plotted. The Na and Cl masses became saturated much above the Na and Cl solubility limit calculated by MULTEQ. At $\Delta T=60^\circ\text{F}$ the precipitated NaCl on the tube surfaces and the concentrated liquid appear to coexist because the hideout masses of Na and Cl exceeded the solubility limit. To determine the variation of the Na-to-Cl molar ratio, the Na and Cl hideout amounts were plotted on a molar basis instead of mass, as shown in Figure 130. Except at $\Delta T=40^\circ\text{F}$ and the early part of $\Delta T=60^\circ\text{F}$, the Na-to-Cl molar ratio was less than one. If the total amounts of Na and Cl in Figure 129 or 130 are used as input values for MULTEQ, the predicted crevice pH is less than 1.0, which means strong acid chemistry developed inside the crevice.

To compare test results obtained from different bulk concentrations, the term "Na or Cl exposure" is introduced, which is defined as the time integration for the variation in bulk concentration. Figure 131 shows the Na and Cl masses as a function of Na and Cl exposures. At $\Delta T=40^\circ\text{F}$ the Na hideout is much

faster than Cl hideout at the same bulk solution exposure, probably because of the volatility effect of Cl. As ΔT increased, Cl hideout became larger. Since Na and Cl have different atomic weights, the comparison with molar quantity is better suited to evaluating the Na or Cl preferential concentration in the crevice. Figure 132 shows the total moles of Na and Cl in the crevice as a function of Na and Cl exposures. The results in Figure 132 still indicate that, at lower ΔT , Na tends to accumulate preferentially in the crevice, but at higher ΔT , Cl hideout becomes more efficient under the diamond-packed crevice condition and $MR=0.7$. At $\Delta T=60^\circ\text{F}$ the Cl hideout rate was almost the same as the Na hideout rate. This finding suggests that the volatility effect of Cl became less significant, probably because the formerly present Na-rich liquid phase caused a boiling point elevation and decreased the boiling rate. As discussed earlier, the results in Figure 129 suggest that the metal cations in the crevice drive Cl⁻ ions into the crevice at $\Delta T=60^\circ\text{F}$.

In Figure 133, Na mass variations in the crevice obtained from the NaOH-03 test are compared with those from the NaCl-05 test. In the NaCl-05 test, the Na mass before changing ΔT from 40 to 60°F was much lower than the steady state value of the NaOH-03 test at $\Delta T=40^\circ\text{F}$. But at $\Delta T=60^\circ\text{F}$, significant Na hideout occurred in the NaCl-05 test. The discrepancy of Na hideout in the two tests may be interpreted as due to the bulk chemistry difference ($\Delta T=60^\circ\text{F}$) and exposure time difference ($\Delta T=40^\circ\text{F}$). If NaCl has a similar solubility limit to NaOH, the steady-state Na mass at $\Delta T=60^\circ\text{F}$ will be smaller and closer to that of the NaOH-03 test. However, NaCl has a much lower solubility than NaOH, which could result in NaCl precipitation. The crevice at $\Delta T=60^\circ\text{F}$ in the NaCl-05 test appears to be composed of NaCl precipitation and saturated NaCl solution because the Na and Cl hideout mass observed at $\Delta T=60^\circ\text{F}$ exceeded the NaCl solubility limit. Additional tests could confirm whether the low Na mass at $\Delta T=40^\circ\text{F}$ in the NaCl-05 test, as compared with the NaOH-03 test, was caused by the bulk chemistry difference or shorter exposure time. Assuming the whole crevice areas reached the NaCl solubility limit, the maximum Na mass is 33 mg with the given crevice porosity. If unoccupied space in the crevice is completely filled with NaCl precipitation, the maximum Na mass is 94 mg. By using the two limiting values, we estimated how much volume of crevice is filled with NaCl precipitates. At $\Delta T=60^\circ\text{F}$, 40 % of the unoccupied space in the crevice is filled with NaCl precipitates, and 50 % is filled at $\Delta T=80^\circ\text{F}$. The top area of the crevice near the mouth should have lower concentration because of the concentration gradient between the bulk solution and crevice. Therefore, the actual fraction of crevice area filled with NaCl precipitates is larger than the estimated value.

Appendix B presents a mass balance analysis for the NaCl-05 test with a simple analytical method applicable to a closed system like the MB.

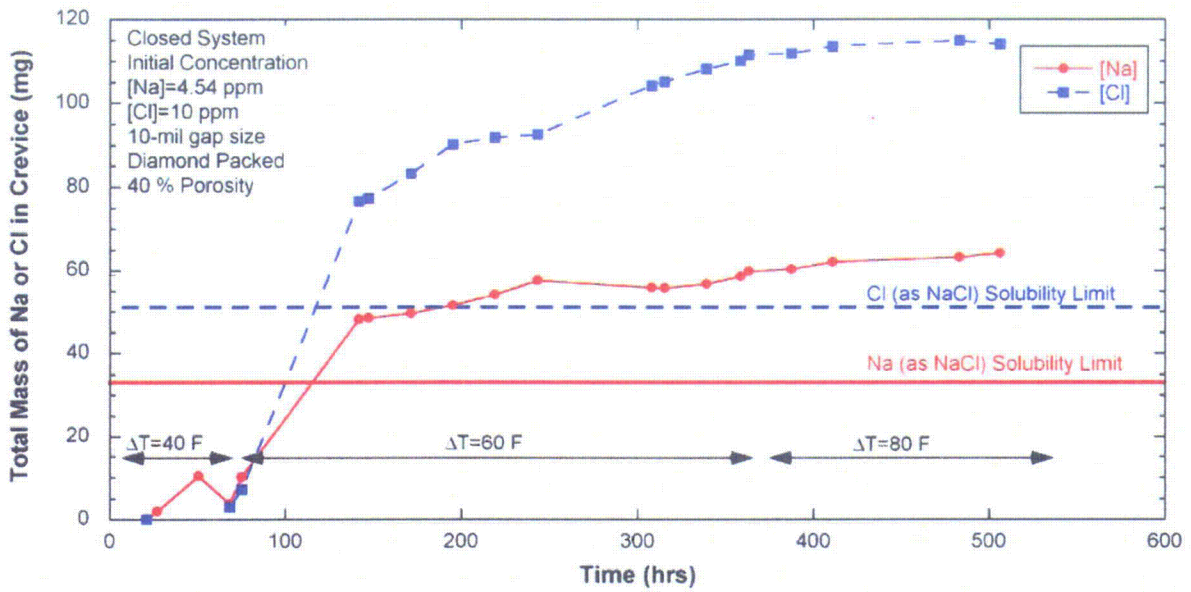


Figure 129. Total mass of Na and Cl in crevice as a function of time for the previous MR=0.7 test with single diamond-packed crevice (estimates from the analysis of bulk samples; NaCl-05).

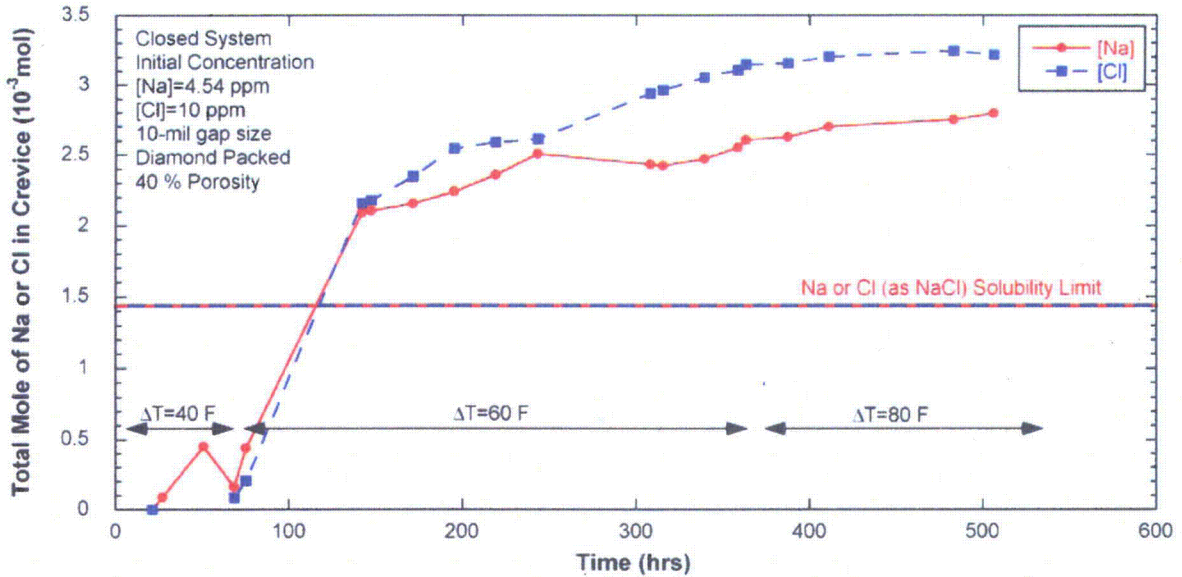


Figure 130. Total moles of Na and Cl in crevice as a function of time for the previous MR=0.7 test with single diamond-packed crevice (estimates from the analysis of bulk samples; NaCl-05).

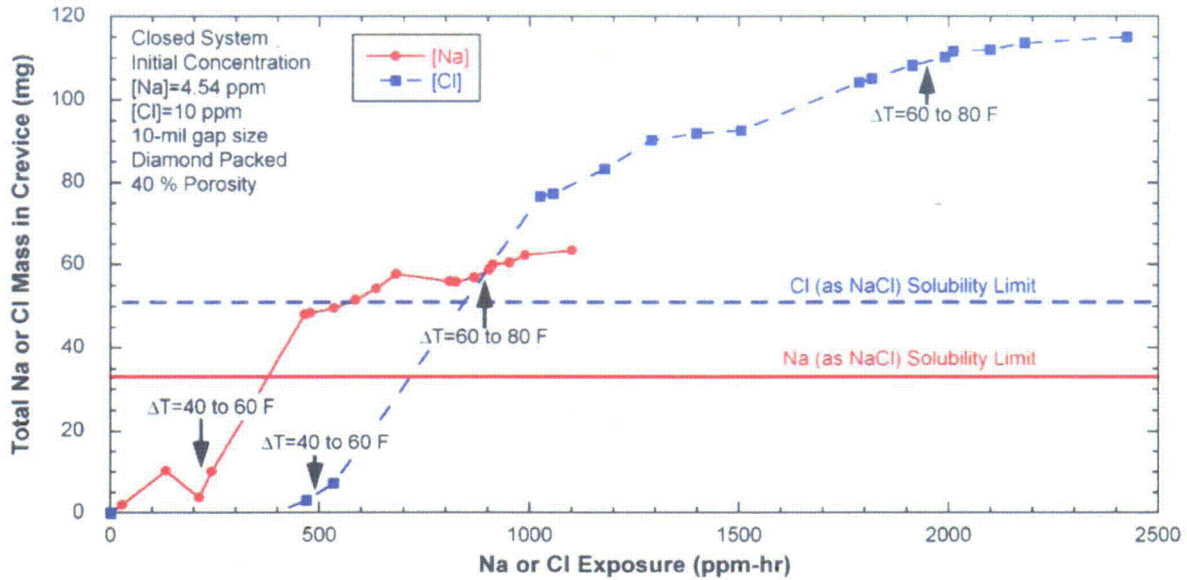


Figure 131. Total mass of Na or Cl in crevice as a function of bulk Na or Cl exposure for the previous MR=0.7 test with single diamond-packed crevice (estimates from the analysis of bulk samples; NaCl-05).

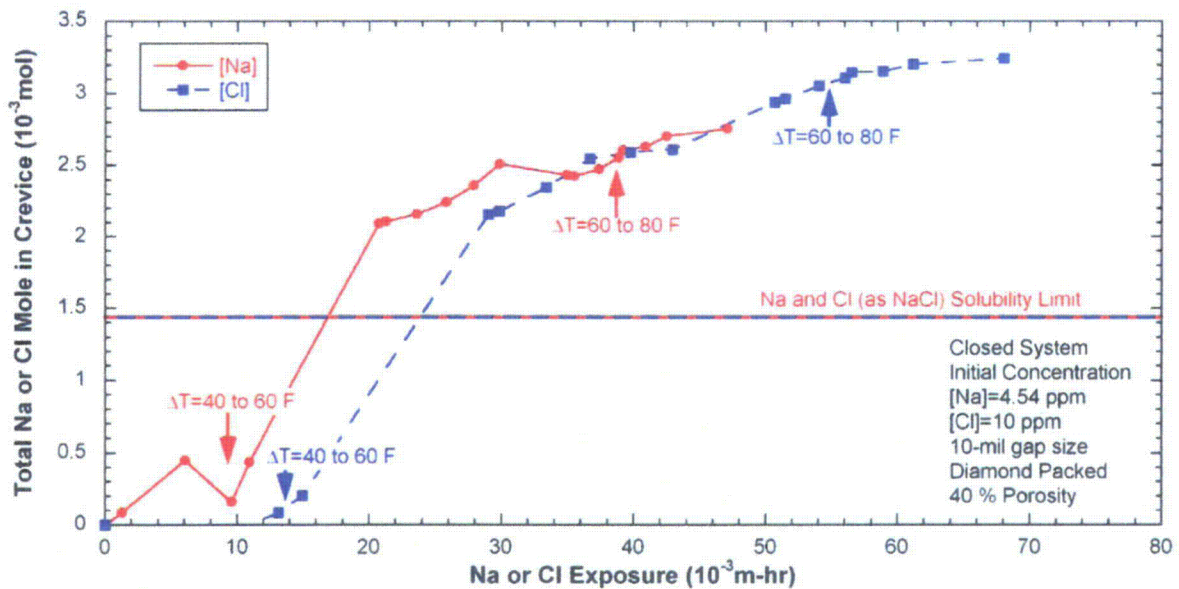


Figure 132. Total moles of Na or Cl in crevice as a function of bulk Na or Cl exposure for the previous MR=0.7 test with single diamond-packed crevice (estimates from the analysis of bulk samples; NaCl-05).

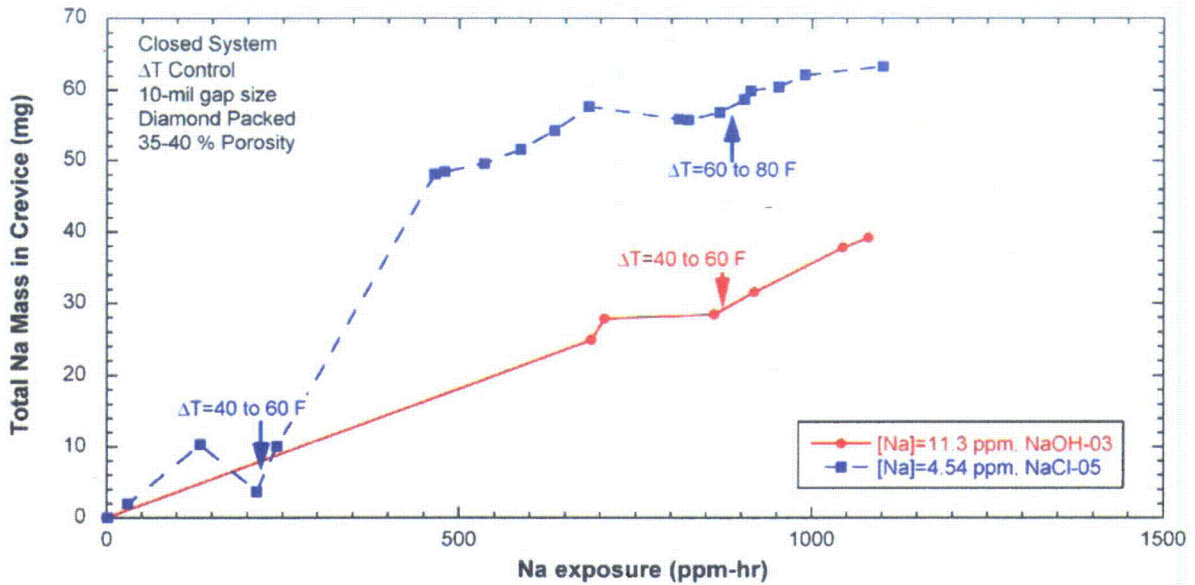


Figure 133. Total Na mass variation in crevice with Na exposure for two tests: NaOH-03 and NaCl-05 with a Na-to-Cl molar ratio of 0.7.

5.3.7 Summary

A NaCl solution test has been conducted with a single crevice packed with diamond and having a bulk MR of 0.7. As seen in the previous NaCl tests, the crevice tungsten potentials indicated that, at the beginning of crevice boiling, the crevice pH became alkaline but then changed to acidic, followed by pH stabilization at the weakly acidic condition. Based on the mass balance analysis, Na was preferentially concentrated in the diamond-packed crevice at lower ΔT , which indicates the volatility effect of Cl. However, at higher ΔT , Na and Cl hideout results were comparable, and sometimes Cl was preferentially concentrated; this concentration appears to have been caused by ion migration due to the excess metal cations formed by severe corrosion in the crevice. Post-test examination showed that severe gouging occurred on the alloy 690 TT tube surfaces. It indicates that strongly acidic crevice chemistry developed on the tube surfaces. The dye penetrant test showed no surface cracks. It appears that it is more difficult to cause stress corrosion cracking in alloy 600 or 690 tubing with a strong acid than with a strong base.

5.4 NaCl-06: NaCl (MR=0.7) Test with Magnetite Packing

5.4.1 Background

Another NaCl test has been conducted with only one crevice simulator packed with magnetite. The crevice was intentionally packed more tightly than in past tests with magnetite to evaluate the influence of packing on flow permeability and hideout. The crevice in NaCl-06 was packed with high-purity magnetite powder, and the porosity of the packed crevice was 54 %, which is much lower than the porosity of the previous magnetite-packed crevice (78 %) and higher than that of the previous diamond-packed crevice (40 %). Test results, data analysis, and post-test examination results are discussed.

5.4.2 Temperature Data

Figure 134 shows the crevice temperature variation with time in NaCl-06. Three thermocouples were installed to monitor crevice temperature. Thermocouples T2 and T4 are located 0.57 in. below the crevice top opening and they were fixed by soft Teflon ferrules, as described in Section 2.3.2. The third thermocouple labeled “Near Electrodes” is located near a crevice electrode assembly so that it monitors the temperature at the electrode tip. To obtain reference data on crevice behavior, the secondary chamber was initially run with pure water at primary/secondary temperatures of 540/500°F. After a period of time, NaCl was injected into the secondary chamber while maintaining the initial temperature. After steady state was reached as indicated by crevice temperatures and chemistry data, the primary temperature T_p was further increased in stages; each time waiting for a “steady state” to be reached. The overall test lasted for 720 hours without any cracking in the alloy 690 tube. Table 6 shows the test temperatures and dwell times for each test period.

Table 6. Test conditions and dwell times for each test period of the NaCl-06 test.

Test Period #	Water Chemistry	Secondary Temperature (°F)	Max Crevice Temperature (°F)	Primary Temperature (°F)	Dwell Time (hr)
1	High purity water	493	500.5	540	15
2	NaCl, MR=0.7	500	516.3	540	362
3	NaCl, MR=0.7	500	524.6	560	194
4	NaCl, MR=0.7	500	533.4	580	146

The crevice temperatures under the high purity water were around 500°F, which is about 6-7°F higher than the secondary saturation temperature at the same time period. For comparison, in the diamond-packed crevice testing, the crevice temperatures with high purity water were about 10°F higher than the saturation temperature due to the high thermal conductivity of diamond. The crevice temperature quickly increased after the NaCl solution injection, as shown in Figure 134. The abrupt temperature change after the solution injection did not occur in the previous tests with the diamond packing or the tests with less-loaded magnetite packing. This difference in behavior might be attributed to the increase in the secondary water temperature of about 7°F after the NaCl solution injection. The thermocouple labeled “Near Electrodes” showed a higher temperature than the two others because its location is deeper in the crevice. Another sudden temperature increase of this thermocouple occurred at 100 hours and is attributed to contact with Na-rich liquid phase, based on the crevice tungsten potential data described in Section 5.4.4. When more stable crevice conditions were achieved after many hours, the “Near Electrode”

thermocouple showed similar temperature to T2 at $\Delta T=40^\circ\text{F}$. The T4 thermocouple data were almost identical to T2 until 120 hours. Under the stable condition at $\Delta T=40^\circ\text{F}$ the deviation between T2 and T4 was about 3°F . This temperature deviation appears to indicate that, in a highly packed magnetite crevice, the local temperature variation increases as the crevice solution concentration proceeds. After ΔT was increased from 40 to 60°F , the three thermocouples quickly responded, but the “Near Electrodes” thermocouple was the most sensitive to the ΔT change. Based on these observations, we inferred that the boundary between the steam-dominant and concentrated liquid-dominant regions was located somewhere between the two crevice depth levels of “Near Electrodes” and T2 or T4 at $\Delta T=60^\circ\text{F}$. The temperature increase and stabilization of the “Near Electrodes” thermocouple suggests that the steam phase was dominant, and the boiling point elevation by the concentrated liquid phase could not occur around the “Near Electrodes” area. The two other thermocouples indicate a gradual temperature elevation due to impurity hideout. The T2 temperature increased and stabilized at 1°F lower temperature than the “Near Electrodes” temperature, but it decreased again and even became lower than T4. Thermocouple T4 showed a sudden temperature increase, as was observed in the “Near Electrodes” thermocouple at $\Delta T=40^\circ\text{F}$. This temperature increase can be attributed to the boiling point elevation due to impurity hideout. However, the temperature decrease suggests that the chemical condition in a highly packed crevice can become locally unstable, or consolidation and redistribution of magnetite particles near the tube wall can affect the thermal conditions. The post-test examination revealed that hard scales had formed on the tube wall. After ΔT was increased from 60°F to 80°F , all three thermocouple readings exhibited a rapid increase, suggesting that at higher ΔT the steam phase is more dominant in highly packed magnetite crevice, especially at the “Near Electrodes” area. Since the T2 temperature was gradually increasing when the MB shut-down was initiated, we concluded that thermal stabilization in the crevice was not achieved after 146 hours of operating at $\Delta T=80^\circ\text{F}$.

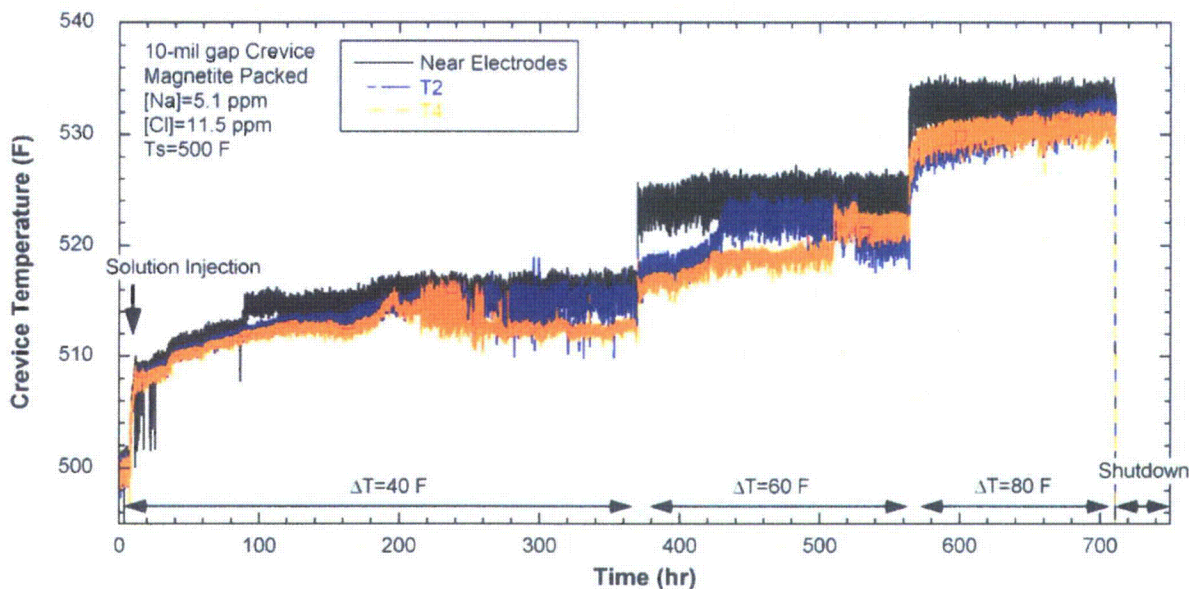


Figure 134. Crevice temperatures as a function of time for the magnetite-packed crevice and secondary water chemistry at Na-to-Cl molar ratio of 0.7 (NaCl-06).

Figure 135 shows the variation in normalized crevice temperature with time for NaCl-06; the crevice temperatures minus the bulk secondary temperature are normalized by the bulk primary-to-secondary temperature difference. The temperature oscillation of T4 observed at $\Delta T=40^\circ\text{F}$ can possibly be explained as follows: The concentrated liquid phase became dominant at the region surrounding T4,

which raised the temperature. The subsequent temperature decrease might be attributed to a local chemistry change. The “Near Electrodes” thermocouple did not show a significant change after ΔT was increased from 40°F to 60°F. However, the normalized temperatures of T2 and T4 slightly decreased, indicating that the boiling heat transfer dominates over single-phase conduction heat transfer. If the single-phase conduction heat transfer is dominant, the normalized temperature remains almost the same value regardless of the ΔT change as observed for the “Near Electrodes” thermocouple. At about 500 hours T4 suddenly increased to the same temperature as T2. Apparently, the tip area of T4 was suddenly surrounded by a concentrated liquid phase, as was observed at $\Delta T=40^\circ\text{F}$. After this abrupt increase of temperature, the normalized T4 temperature did not change significantly, even after the increase of ΔT from 60°F to 80°F. After the increase in ΔT from 40°F to 60°F, T2 started to increase slowly and about 60 hours later T2 became stabilized, followed by a temperature decrease. The observed temperature oscillation for T2 at $\Delta T=60^\circ\text{F}$ looks similar to that observed at $\Delta T=40^\circ\text{F}$ for T4. The temperature increase can be explained by the impurity hideout and boiling point elevation, and the temperature decrease, by the movement or consolidation and redistribution of magnetite particles near the tube wall. After the ΔT increase from 60°F to 80°F, the normalized temperatures were almost the same as before. This finding indicates that the ratio between steam and liquid phase was not much different after the ΔT change. The gradual increase of T2 indicates the gradual replacement of steam phase with concentrated liquid. We concluded from these results that there is much spatial variation within the crevice in that zones of steam or water change location randomly as different paths of boiling-induced expulsion and ingress of secondary bulk water occur.

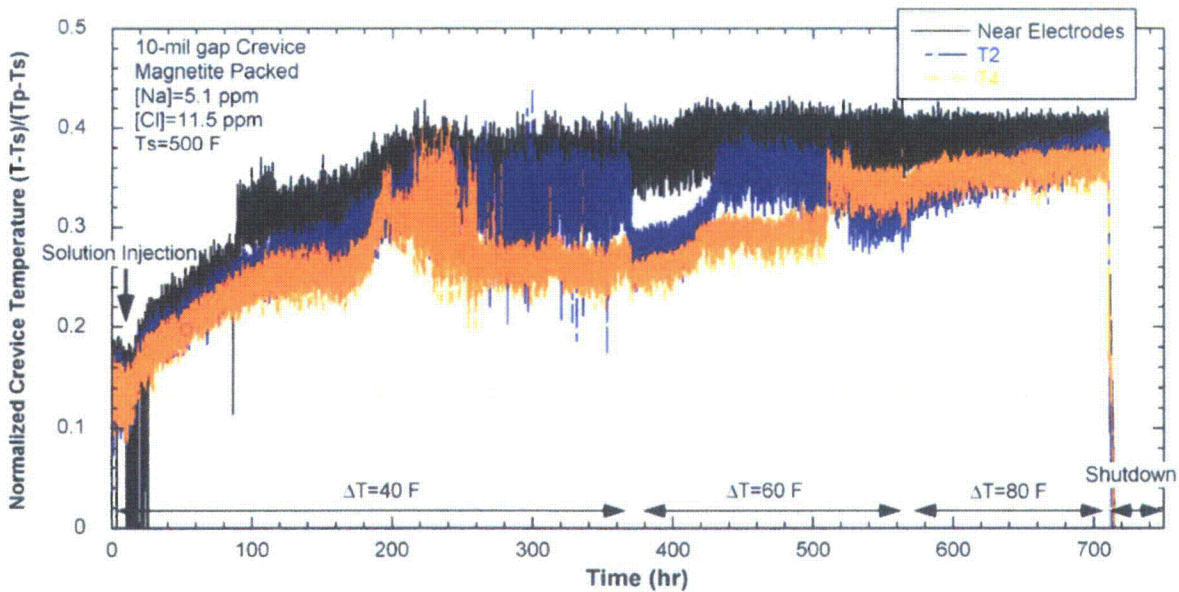


Figure 135. Normalized crevice temperatures as a function of time for the magnetite-packed crevice and secondary water chemistry at Na-to-Cl molar ratio of 0.7 (NaCl-06).

5.4.3 Bulk and Crevice Chemistry

Bulk conductivity and the secondary chemistry variations with time are shown in Figure 136, as measured by an *in situ* conductivity probe and ICP/OES of bulk water samples extracted during the NaCl-06 test. At $\Delta T=40^\circ\text{F}$ the bulk water conductivity stabilized about 200 hours after the NaCl solution injection. The samples analysis indicates that the bulk Na and Cl concentrations behave in a very complex

manner as hideout progresses. Apparently, Na and Cl concentrated in the crevice in a different manner because of the volatility effect of Cl. This issue is discussed again in Section 5.4.6. At $\Delta T=60^\circ\text{F}$ the rate of bulk conductivity reduction is similar to that at $\Delta T=40^\circ\text{F}$. The bulk conductivity quasi-stabilized for a period but it then started to decrease again. The bulk conductivity showed continuous hideout of impurity after the ΔT change from 60°F to 80°F . The chemical analysis for bulk samples at $\Delta T=60^\circ\text{F}$ and 80°F also indicated the continuous hideout of Na and Cl in the crevice. The MB was shut down before a steady state was reached at $\Delta T=80^\circ\text{F}$ because the test time was limited.

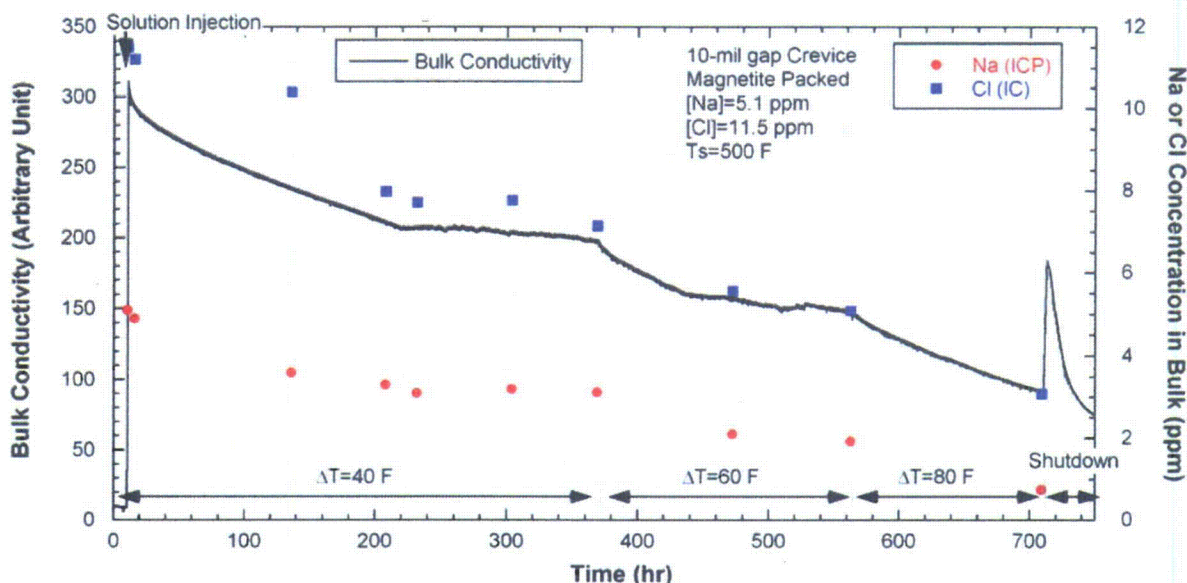


Figure 136. Bulk conductivity as a function of time for the magnetite-packed crevice and secondary water chemistry at Na-to-Cl molar ratio of 0.7 (NaCl-06).

Figure 137 shows the crevice and bulk conductivity versus time. At 100 hours the crevice conductivity suddenly increased and became stable, followed by a gradual decrease. It appears that, initially, the area around the conductivity probes was steam-blanketed or the fraction of concentrated liquid phase was relatively small. As concentrated liquid phase penetrated into the crevice, steam in the crevice pores was replaced by the concentrated liquid, causing the local conductivity to rapidly increase. As compared with the diamond-packed crevice conductivity shown in Figure 118 for NaCl-05, it took much longer for a liquid path to occur between the two conductivity probes. Even though the porosity of magnetite packing is higher than that of diamond packing, the smaller particle size of magnetite likely made the flow between crevice pores more restrictive and caused the time delay. The subsequent gradual decrease of the crevice conductivity is unexpected; NaCl precipitation is impossible at $\Delta T=40^\circ\text{F}$ because it can only occur above $\Delta T=46^\circ\text{F}$, which is the highest obtainable boiling point elevation corresponding to the solubility limit of NaCl at 500°F predicted by MULTEQ. Therefore, we cannot confidently explain the conductivity decrease. It might be caused by the return of steam domination around the probe location.

After ΔT was increased from 40°F to 60°F , the crevice conductivity signal became noisy, but the conductivity value did not increase much. Occasionally, the conductivity signal showed a spike, but it quickly returned to the original value because of a momentary increase of single-phase liquid. The increase of ΔT from 60°F to 80°F made the crevice conductivity signal even more noisy, followed by very low signal, possibly indicating steam blanketing or local dryout. The NaCl precipitation in this zone

may have increased the flow resistance of the packing, resulting in local dryout around the conductivity probe. Even though the liquid path between two probe wires was lost, a thin liquid film may have formed on the tip area of the conductivity probes or the crevice electrodes, which would still have permitted measurement of the crevice electrode potentials even at $\Delta T=80^{\circ}\text{F}$.

The normalized bulk conductivity as a function of ΔT is plotted in Figure 138. All conductivity data for each ΔT test were normalized with the initial conductivity value immediately after the ΔT change. The reduction rate appears to increase with the increase of ΔT , except for the beginning of testing at $\Delta T=40^{\circ}\text{F}$. The relatively high rate of bulk conductivity reduction at the beginning of $\Delta T=40^{\circ}\text{F}$ may indicate the initial adsorption of Cl to the magnetite particles, which is supported by the chemical analysis of bulk samples shown in Figure 136. Figure 139 shows the bulk conductivity variation for the magnetite-packed crevice in comparison with previous data from the diamond-packed crevice test. As shown in Figure 139, the rate of bulk conductivity reduction is much higher for the diamond-packed crevice, which suggests that the impurity hideout rate is much higher in a diamond-packed crevice than in a magnetite-packed crevice. The impurity hideout rate is proportional to various factors like heat flux, liquid penetration depth related to total nucleate boiling area, etc. As compared with the magnetite-packed crevice, the diamond-packed crevice has a deeper liquid penetration depth because it is more permeable, and this condition provides more nucleate boiling area. Greater boiling area will eventually cause faster hideout of bulk impurity if the heat flux is the same. The impurity hideout rate can be increased by not only the higher permeability of the diamond packing, but also the higher thermal conductivity of the diamond powder in the area adjacent to the tube surface, which can serve as an additional site for bubble nucleation and increase the nucleate boiling area. However, due to its lower thermal conductivity, we do not expect that the magnetite powder can provide additional bubble nucleation sites and increase the boiling area near the tube surface.

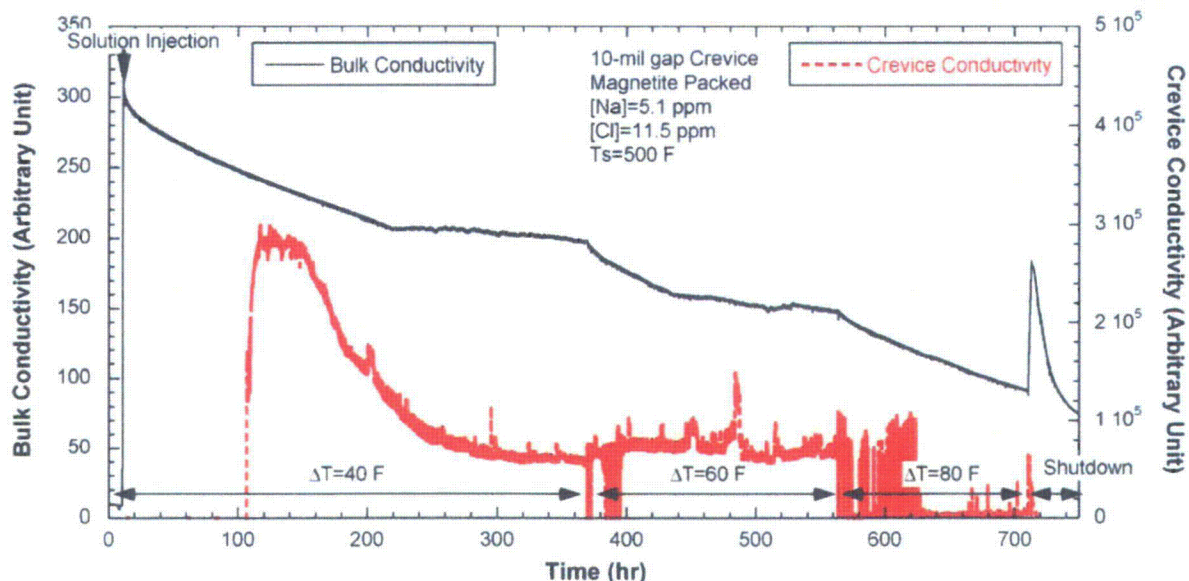


Figure 137. Crevice and bulk conductivities as a function of time for the magnetite-packed crevice and secondary water chemistry at Na-to-Cl molar ratio of 0.7 (NaCl-06).

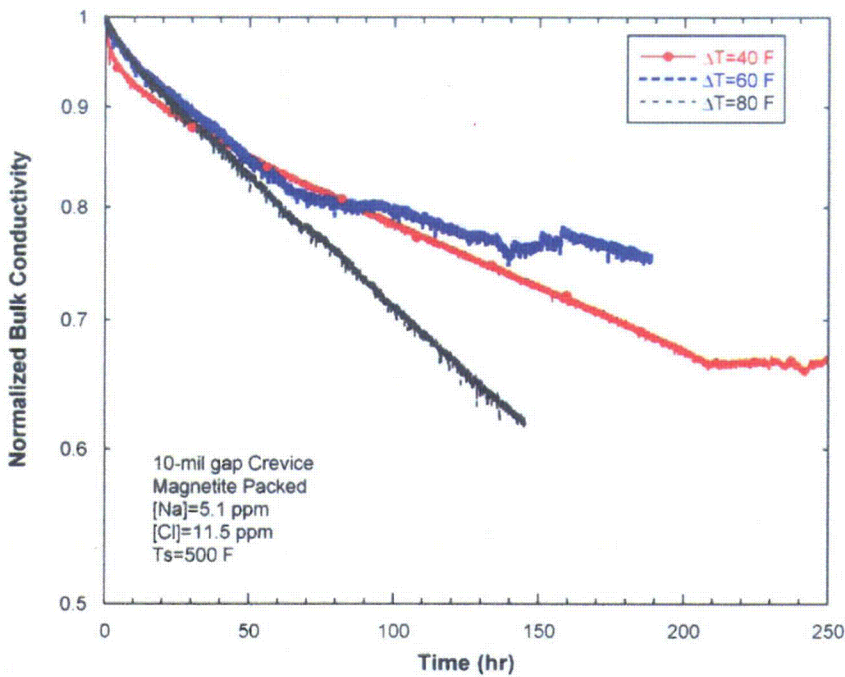


Figure 138. Normalized bulk conductivity variation as a function of ΔT for the magnetite-packed crevice and secondary water chemistry at Na-to-Cl molar ratio of 0.7 (NaCl-06).

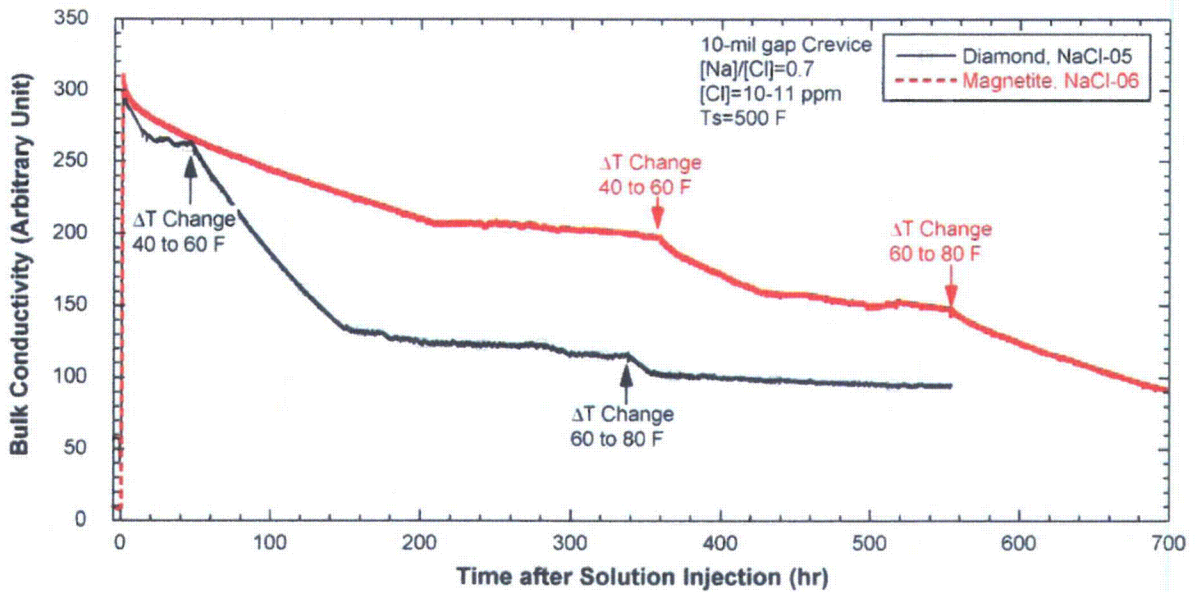


Figure 139. Bulk conductivity variation for the magnetite-packed crevice in comparison of that for the diamond-packed crevice.

5.4.4 ECP Measurement

Figure 140 shows the tungsten electrode potential variations for the bulk water and crevice (electrodes A1 and A2) after the initial NaCl injection into the secondary chamber. The overall decrease of bulk tungsten potential from the start to $\Delta T=60^{\circ}\text{F}$ was caused by the decrease of total bulk concentration rather than the Na-to-Cl molar ratio change, as shown in Figure 44. The bulk tungsten potential changed very slowly after ΔT changed from 60°F to 80°F , even though the bulk conductivity was still decreasing. Two tungsten crevice electrodes were installed 30 degree apart at the same level. As shown in Figure 140, the two crevice tungsten potentials (A1 and A2) show significant differences. Crevice A1 does not vary much except in the initial 50 hours, and A2 does not indicate electric contact until 90 hours after the solution injection. The curve for A1 indicates the development of a weakly acidic crevice throughout the test periods. The region around A2 may have become steam-blanketed before becoming wetted. The time when the potential signal indicated wetting corresponds to the time when the crevice conductivity started to increase drastically, as described earlier. Although it is difficult to determine quantitatively, but the electrode tip of A2 was closer to the tube surface than that of A1. Therefore, the potential discrepancy between the two tungsten electrodes suggests a radial pH gradient in the magnetite-packed crevice. Based on the results in Figure 140 for A2, we inferred that pH variation becomes more dynamic closer to the tube surface. Near the tube surface the pH is likely initially alkaline, which would result in preferential Na hideout around the tube surface because of the volatility effect of Cl. As the test proceeds, the pH near the tube surfaces becomes more acidic, and the radial pH difference becomes smaller because of the preferential Cl hideout. Since the boiling point elevation causes a reduction of boiling rate at the tube surfaces, the volatility effect of Cl may become less significant. Eventually, the steady-state potentials of the two tungsten electrodes become very close to each other near the end of the test time at $\Delta T=40^{\circ}\text{F}$, and this indicates the development of a slightly acidic crevice. Before reaching the steady-state potential at $\Delta T=40^{\circ}\text{F}$, the crevice A2 potential decreased from -400 mV to -450 mV (with respect to an Ag/AgCl reference electrode) during the test period of 220-300 hours, even though bulk chemistry showed no significant change. During this time period, the crevice temperatures and conductivity still varied. Inside the highly packed magnetite crevice, thermal-hydraulic and chemical changes appear to occur without altering the bulk chemistry. This result shows the limitation of estimating the crevice behavior from the bulk solution data and supports the importance of direct crevice chemistry monitoring. Another possibility to explain the crevice A2 potential decrease is the dissolution of magnetite. At a slightly acidic condition, the solubility of magnetite increases, as does the concentration of Fe cation. To retain the charge neutrality, anion concentration like OH^- or Cl^- needs to increase. Among the previous tests with diamond packing, NaCl-03 and NaCl-05 clearly showed evidence of an electromigration effect by the simultaneous decrease of Cl and increase of Na in bulk solution. But during the test period of 220-300 hours, the concentration of these two ions in the bulk solution did not show any significant variation. The magnetite packing is more flow restrictive and less permeable than the diamond packing, which makes it more difficult for ions to move into and out of the crevice. Therefore, the migration of Cl^- is not likely. Another way for the charge neutrality to be retained is an increase of OH^- ion concentration and decrease of H^+ ion; this condition leads to an increase of crevice solution pH and a decrease of the crevice tungsten potential.

Crevice A2 responded quickly to the change of ΔT from 40°F to 60°F , but A1 was not sensitive to the temperature change. The results shown in Figure 140 indicate that the pH near the tube surfaces became more acidic when ΔT was increased. A pH increase near the tube surfaces was anticipated after the increase of ΔT because of the volatility effect of Cl, but the measured pH became slightly more acidic. This inconsistency might occur because the location of A2, which was closer to the tube wall than A1, still was not close enough to the tube surfaces to observe the Cl volatilization and pH increase occurring right on the tube wall. After the increase of ΔT from 60°F to 80°F , A1 did not show any significant

change, but A2 became unstable and showed potential fluctuation. The increase of ΔT appears to have produced a steam-dominant condition near the electrode tip area of A2. The noisy signal became quiet about 40 hours later, and the potential became similar to the value before the ΔT was increased.

These results appear to contradict the observation by Baum that pH increased near the tube surface with an increase of ΔT .³⁹ The tungsten potential difference between the magnetite-packed crevice and bulk solution in Baum's test is plotted as a function of ΔT in Figure 141. The bulk concentration is $[Cl]=2.7$ ppm, lower than our test condition of $[Cl]=10$ ppm. At $\Delta T=22^\circ C$ ($40^\circ F$), the tungsten potential at the tube surface gradually increased, indicating crevice acidification. Overall, the potential variation at $\Delta T=22^\circ C$ ($40^\circ F$) looks very similar to the observed tungsten potentials in our test, designated as A2 in Figure 140. Our test results showed that the minimum crevice tungsten potential was lower than the bulk tungsten potential, but Baum's work indicated that the crevice tungsten potential was always higher than the bulk tungsten potential. This difference can be attributed to the total Na bulk concentration being higher than that in Baum's work. Explaining the discrepancy of the crevice tungsten potential variation at higher ΔT in our work and Baum's is difficult, but it should be noted that in our test the crevice tungsten wire tip was not located on the tube surface as in Baum's work, and our total exposure time before changing ΔT from $40^\circ F$ to $60^\circ F$ was more than two times longer.

Figure 142 shows the tungsten potentials in the bulk and crevice after the MB shut-down. After shut-down of the primary and secondary heater power, the tungsten potential for A1 decreased while that for A2 quickly increased. This behavior means that A1 became slightly alkaline and A2 moved in the acidic direction, even though there were large potential fluctuations followed by stabilization. After the shut-down, Cl ion might have moved toward the tube surface; this condition would cause a decrease of pH near the tube surface and a slight increase of pH away from the tube surface. Crevice A1 returned to the bulk potential value at room temperature, while A2 did not. Furthermore, A2 was about 80 mV higher than the tungsten bulk potential at room temperature. These findings suggest that even though the shut-down produced chemical homogenization in most of the crevice, the near surface area labeled A2 maintains the acidity probably because of Cl ions adsorbed to the magnetite particles on the surface.

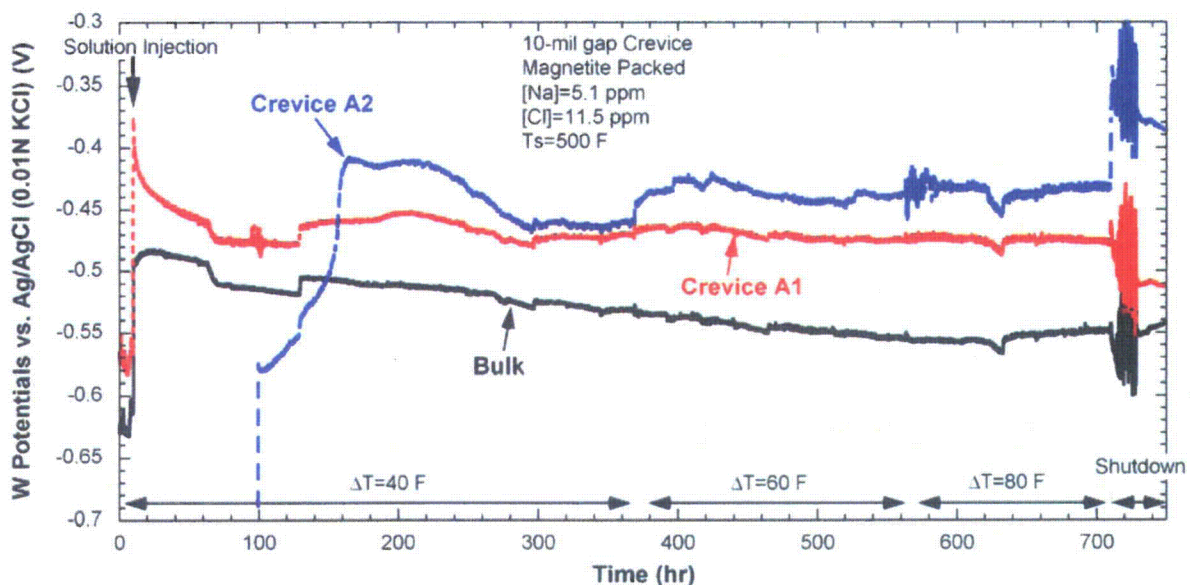


Figure 140. W/WO_x potentials measured at bulk and crevice as a function of time for the magnetite-packed crevice and secondary water chemistry at Na-to-Cl molar ratio of 0.7 (NaCl-06).

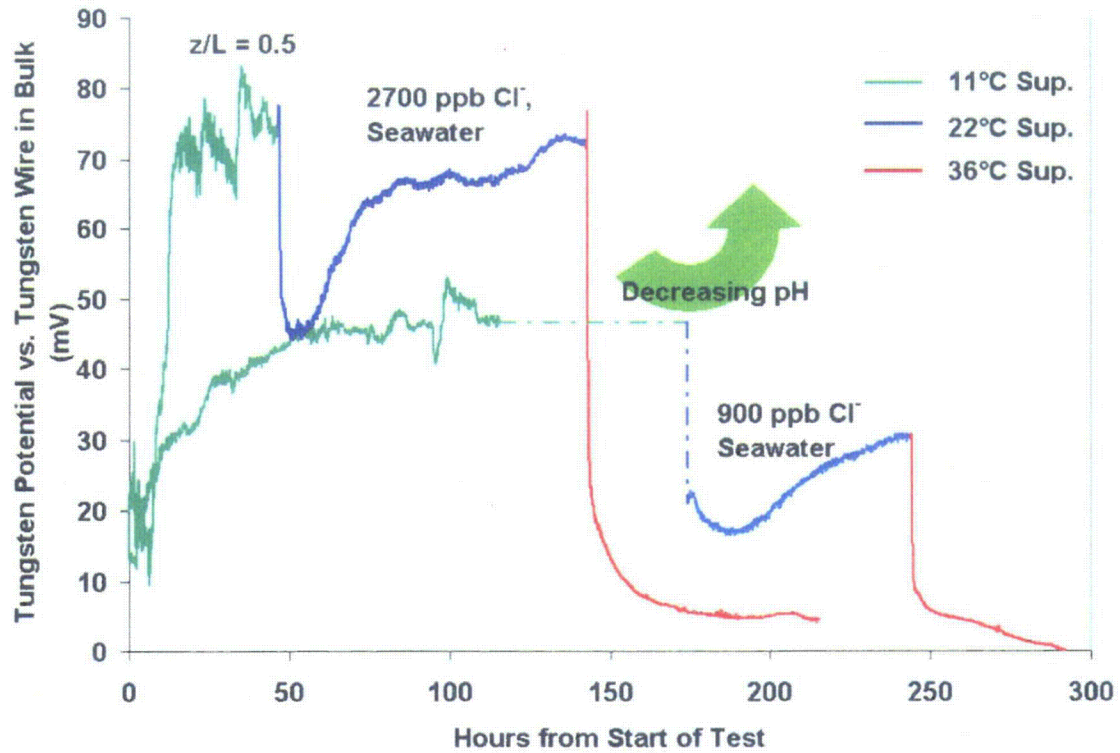


Figure 141. Tungsten potential difference variations as a function of ΔT in seawater addition testing (from Baum).³⁹

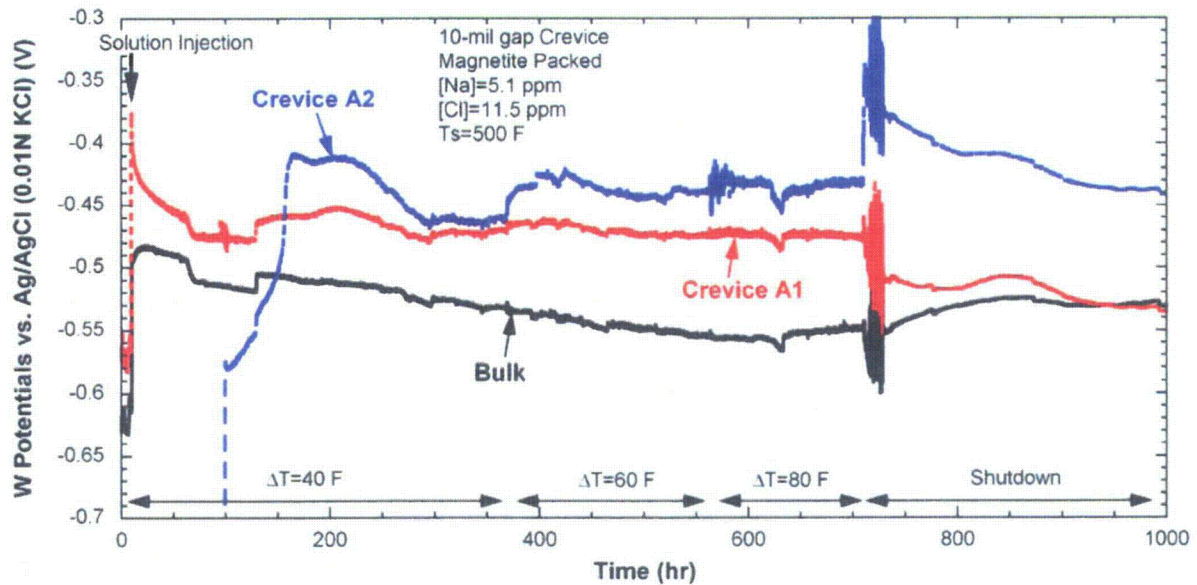


Figure 142. WWO_x potentials measured at bulk and crevice after the MB shut-down (NaCl-06).

Figure 143 shows the Pt electrode potentials in the bulk water and crevice as a function of time. The crevice Pt potentials showed no significant change with the increased ΔT . A Ta/Ta oxide electrode was also used as a pH electrode as in the previous test, NaCl-05. Figure 144 shows the variations in Ta electrode potential with time. The Ta electrode potentials in the crevice did not show any significant change with the increase of ΔT . The insensitivity of the Pt and Ta electrodes in the crevice, as observed for A1 in Figure 141, is attributed to their not being close enough to the tube wall to represent the chemical change on the tube surface. The Ta electrode potentials for the bulk solution gradually increased, indicating the acidification of the bulk water if the Ta electrode was behaving as a pH electrode. However, the tungsten electrode potentials and the calculated pH from bulk samples suggest the pH of the bulk water increased with time. More experimental study could lead insights on using a Ta/Ta oxide electrode as a pH electrode.

Figure 145 shows the alloy 600 electrode potentials in the crevice as a function of time. About 20 hours after the NaCl solution was injected, the crevice potential indicated the wetting of the alloy 600 wire tip area. The alloy 600 potentials abruptly decreased almost at the same time as the crevice tungsten potentials indicated the wetting. From the alloy 600 and tungsten potential behaviors, we inferred that, initially, alkaline chemistry developed on the tube surfaces due to the volatility effect of Cl, and as impurity hideout proceeded, the Na-rich concentrated liquid film expanded further in the axial and radial direction and touched the tips of the tungsten and alloy 600 electrodes.

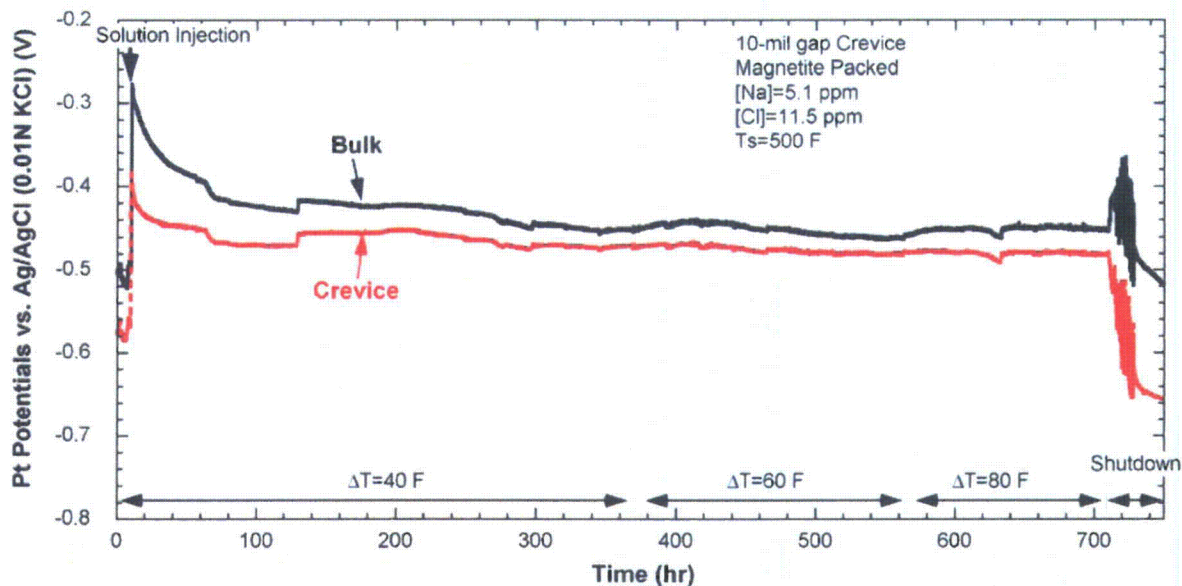


Figure 143. Pt potentials measured at bulk and crevice as a function of time for the magnetite-packed crevice and secondary water chemistry at Na-to-Cl molar ratio of 0.7 (NaCl-06).

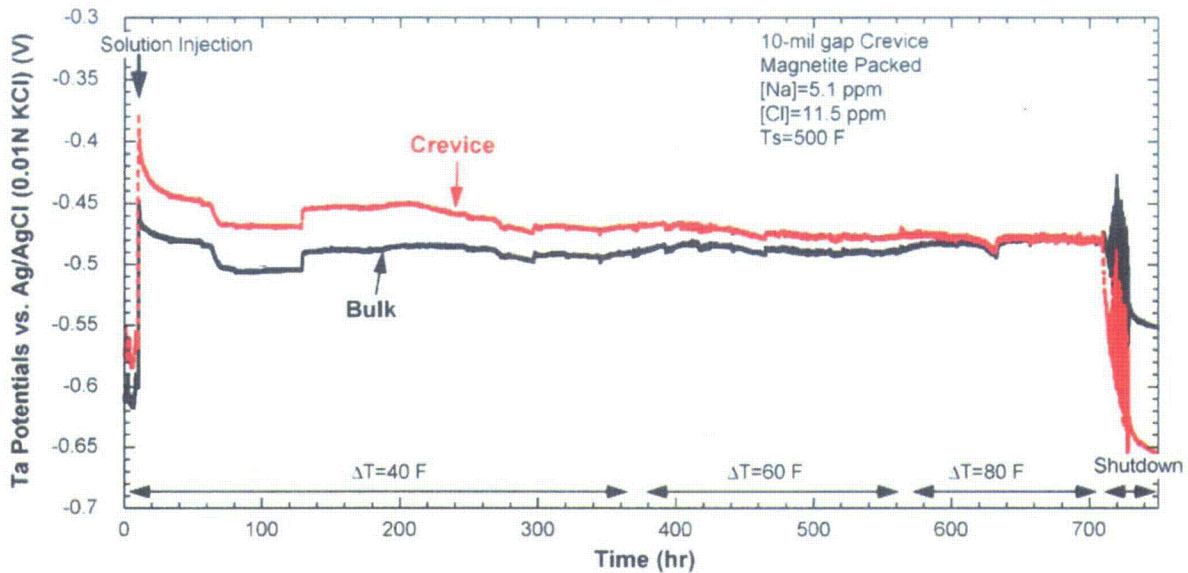


Figure 144. Ta potentials measured at bulk and crevice as a function of time for the magnetite-packed crevice and secondary water chemistry at Na-to-Cl molar ratio of 0.7 (NaCl-06).

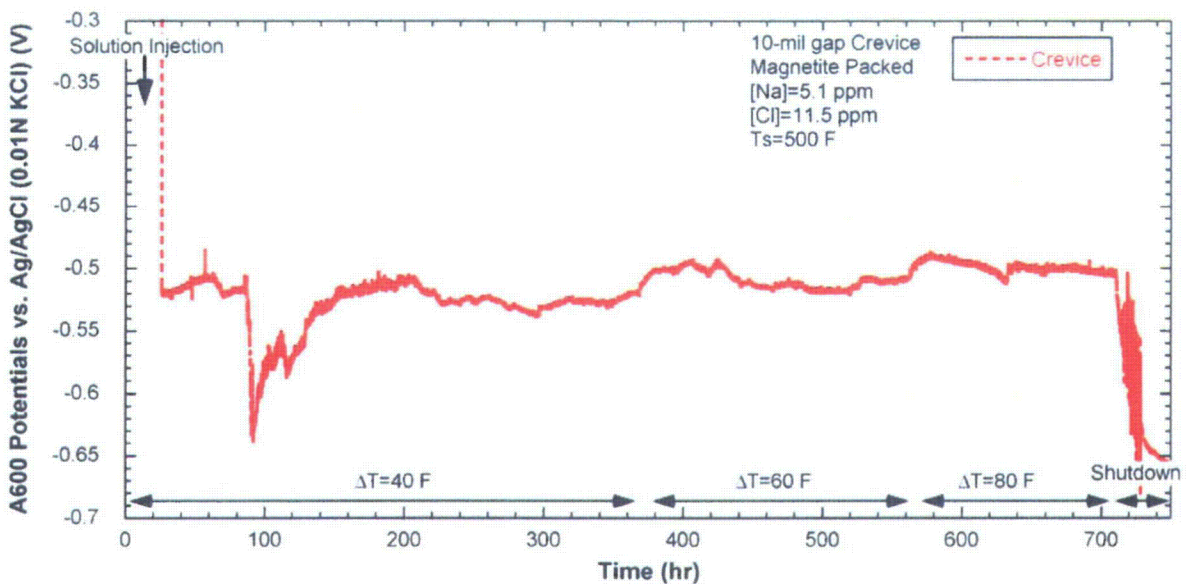


Figure 145. Alloy 600 potentials measured at crevice as a function of time for the magnetite-packed crevice and secondary water chemistry at Na-to-Cl molar ratio of 0.7 (NaCl-06).

In Figure 146, the crevice electrode potentials are compared with the crevice temperature variation. When the tungsten and alloy 600 potentials began to indicate alkaline crevice, the crevice temperature labeled "Near Electrode" increased. The sudden temperature increase can be explained by the contact of the Na-rich liquid phase with the thermocouple tip area. After the sudden potential decreases, the tungsten electrode (WA2), which was installed more closely to the tube surface, and the alloy 600 electrode showed similar behavior.

Figure 147 shows the tungsten potentials for the magnetite- and the diamond-packed crevice with the same Na-to-Cl molar ratio of 0.7. Based on the steady-state potentials, the magnetite-packed crevice appears to be more acidic than the diamond-packed crevice at all ΔT conditions. This result indicates that the magnetite-packed crevice is more flow restrictive, making it more difficult to completely mix the liquid and vapor phases. The initial potential variations after the solution injection are also different. In the diamond-packed crevice, the potential quickly decreased, indicating preferential Na concentration due to the volatility effect of Cl. This decrease was followed by rapid potential increase and stabilization. However, in the magnetite-packed crevice, the pH remained slightly acidic at the location away from the tube surface (WA1). Near the tube surface (WA2), the crevice pH indicated alkaline solution, but it became gradually acidified. With the diamond-packed crevice, the tungsten potential appears to be independent of ΔT , but in the magnetite-packed crevice, the tungsten potential near the tube surface indicated acidification with an increase of ΔT . Based on these tungsten potentials, we concluded that the independence of the tungsten potential in the diamond-packed crevice on ΔT was due to the location of tungsten electrode away from the tube surfaces combined with relatively vigorous mixing inside the crevice as compared with the magnetite-packed crevice.

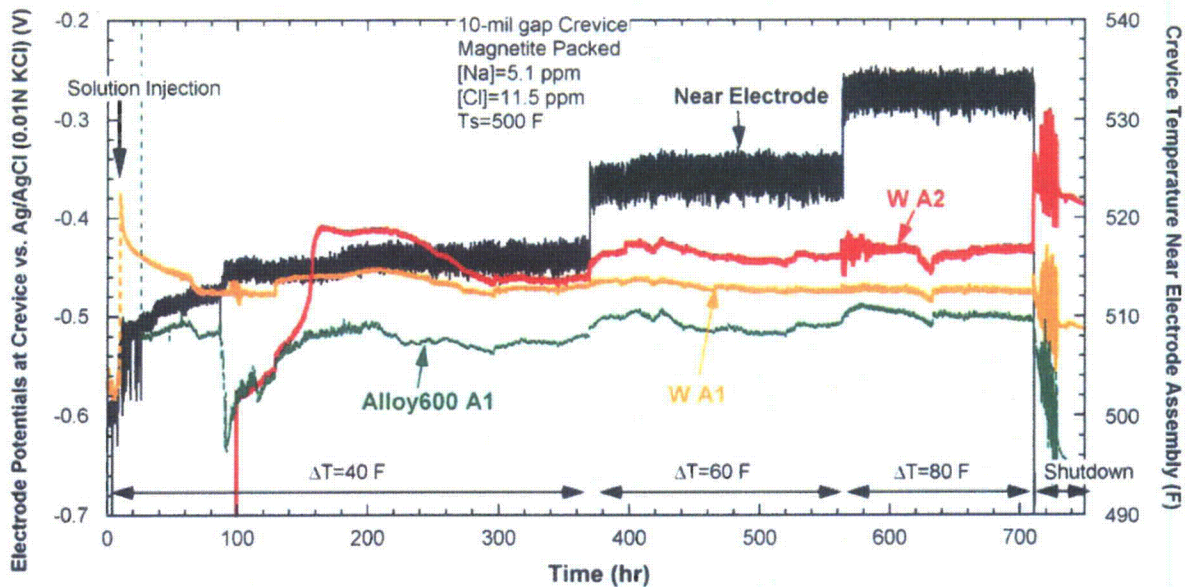


Figure 146. Crevice electrode potentials in comparison of the crevice temperature at the magnetite-packed crevice with the Na-to-Cl molar ratio of 0.7 (NaCl-06).

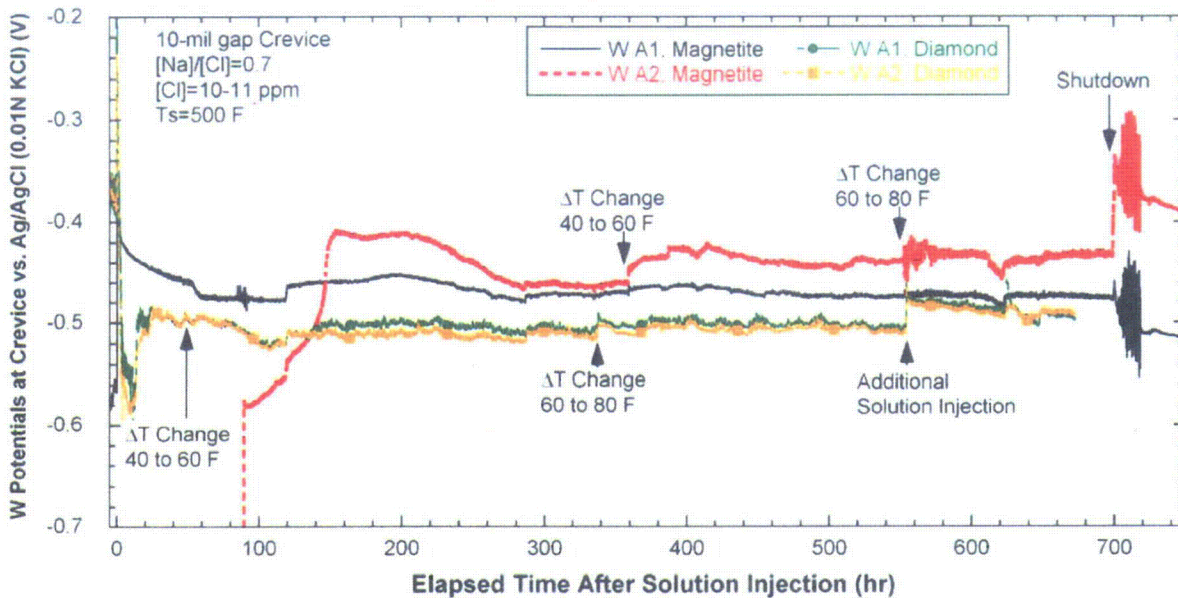


Figure 147. Crevice tungsten potentials measured at the magnetite-packed crevice compared with crevice tungsten potentials at the diamond-packed crevice with the same Na-to-Cl molar ratio of 0.7 (NaCl-06).

5.4.5 Post-Test Examination

The crevice assembly and magnetite powder inside the crevice for NaCl-06 were examined after opening the MB. Figure 148 shows the top area of the crevice assembly, and Figure 149 shows the same area as in Figure 148 but after the top retainer had been removed. These two pictures indicate that the magnetite packing powder remained inside the crevice throughout the test period of 720 hours. Figure 148 also shows two high-pressure fittings welded to the outer wall of the crevice simulator. Visual examination confirmed that the thermocouples installed in the crevice were tight and did not slip throughout the test. Figure 150 shows the crevice mouth area after removal of the foam retaining mesh. Some deposits appear on the crevice ring area, but almost all the magnetite powder was in the crevice. Figure 151 shows the crevice area after we removed the crevice simulator ring. Some magnetite powder was detached from the surface during this removal. With unaided visual observation, we did not find any other deposit except black magnetite powder.

Figure 152 shows that hard scale formed on the alloy 690 tube surfaces underneath the loosely attached magnetite powder. As shown in Figure 152, the area without scale was shiny. Pitting was not evident on the surface except for very small local areas. The tubing under the hard scale regions was not likely damaged. The shiny tube surfaces indicate that tube corrosion was not severe in the magnetite-packed crevice as compared with the diamond-packed crevice. As shown in Figure 153, severe gouging/pitting did occur on the tube surfaces with the diamond-packed crevice in the NaCl-05 test even though the bulk water chemistry and the total exposure time were similar to the NaCl-06. This discrepancy is attributed to the fact that, as shown in Figure 139, the hideout kinetics was much faster in the diamond-packed crevice test, so that the tube corrosion might start earlier than in the magnetite-packed crevice. However, if the NaCl-06 test had been exposed to NaCl water chemistry for a longer time, we expect that similar corrosion phenomena would occur on the tube surfaces. Since the post-test

examination of the tube/crevice as shown in Figure 152 did not show any significant corrosion, an electromigration effect caused by the metal corrosion does not appear to occur in the NaCl-06. Therefore, the preferential Cl hideout in the NaCl-06 test cannot be explained by the electromigration effect. The NaCl-06 test showed that hard scale consisting of magnetite can form on the tube wall in a relatively short time. Similarly, soft magnetite particles can attach and consolidate on the tube surface under the prototypic SG thermal condition.

To detect any crack formed on tube surface for NaCl-06, a dye penetrant test was performed. Figure 154 shows the dye penetrant results for the area shown in Figure 152. The red areas are from the deposit. No cracks were visible on the tube surface except for the regions under the scaly particles shown in Figure 152. We did not inspect underneath the scaly particles but crack is not likely to be present underneath them.

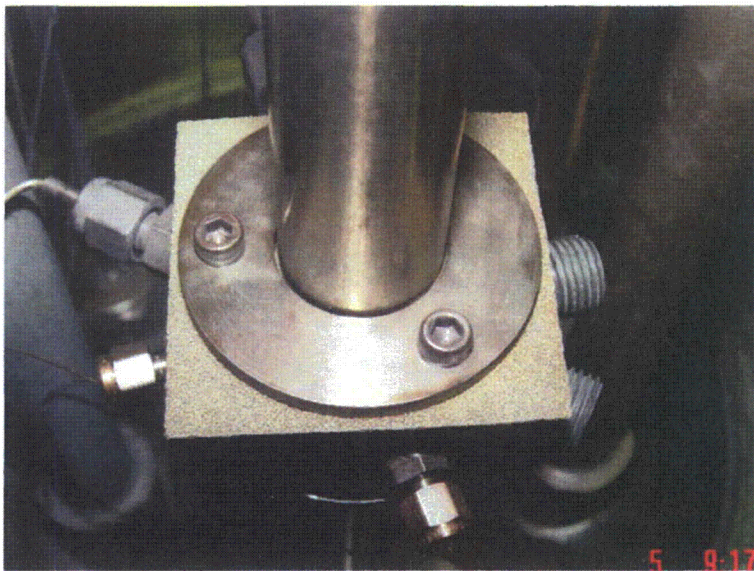


Figure 148.
Top area of crevice
assembly exposed to the
test solution with MR=0.7 for
720 hours at 500°F (260°C).

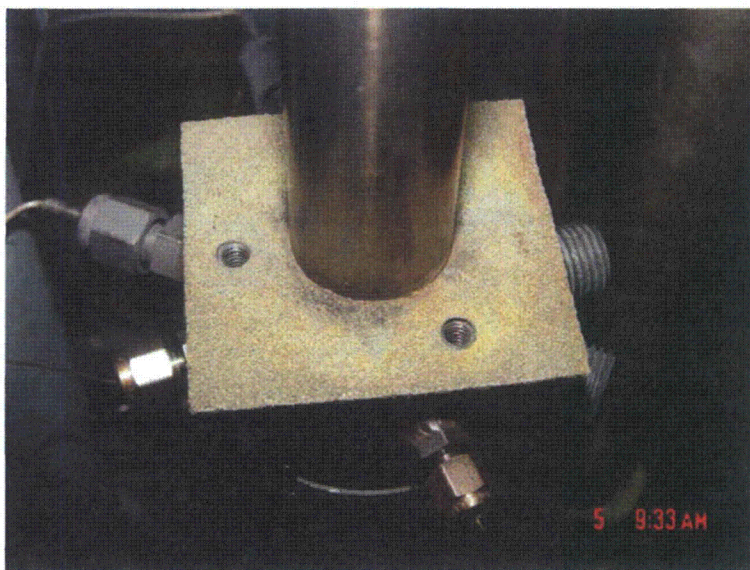


Figure 149.
Top area of crevice assembly
after removal of a top retainer
exposed to the test solution
with MR=0.7 for 720 hours at
500°F (260°C).



Figure 150.
Crevice mouth after removal
of a foam mesh showing that
magnetite powder remains in
place.

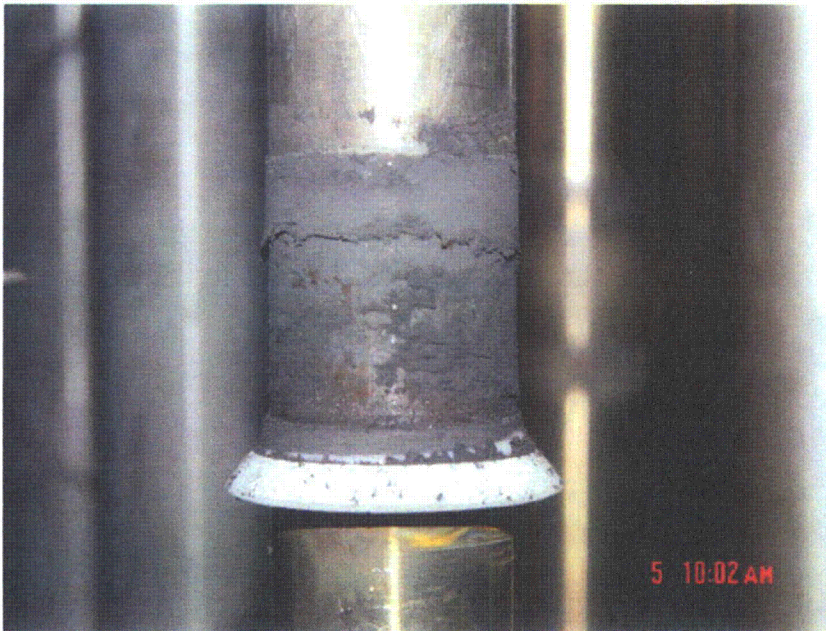


Figure 151.
Magnetite powder clinging to
the alloy 690 tubing surfaces
after removal of the crevice
ring.

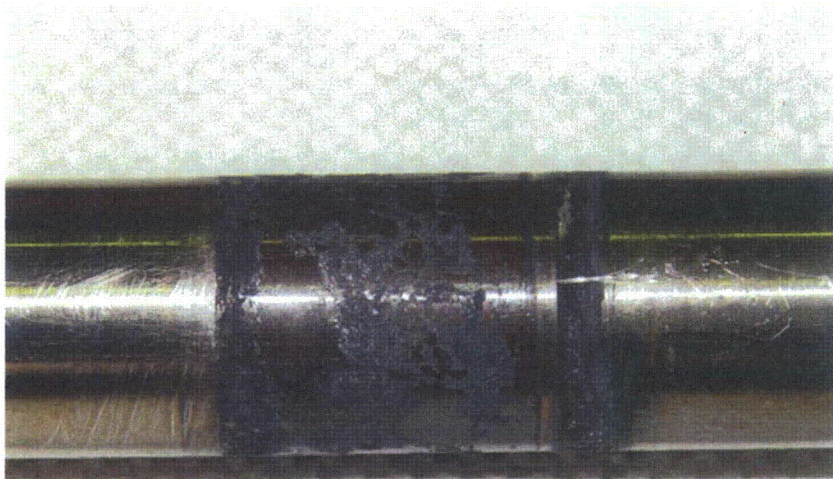


Figure 152.
Hard scale formed on alloy 690 tube surface exposed to the NaCl-06 test solution with MR=0.7 and magnetite packing for 720 hours at 500°F (260°C) (crevice top: left; crevice bottom: right).

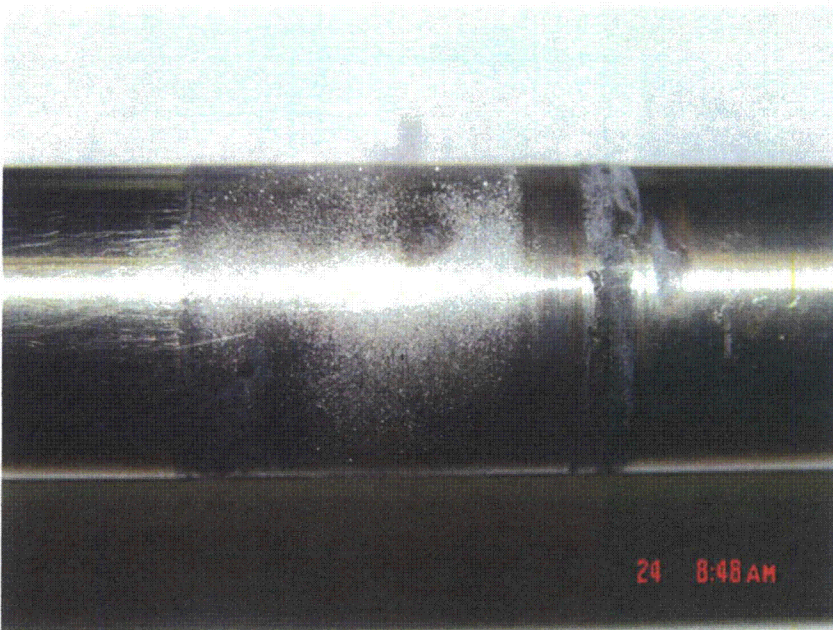


Figure 153.
Alloy 690 tube surface exposed to the test solution of NaCl-05 with MR=0.7 for 700 hours at 500°F (260°C) and diamond-packed crevice (crevice top: left; crevice bottom: right).

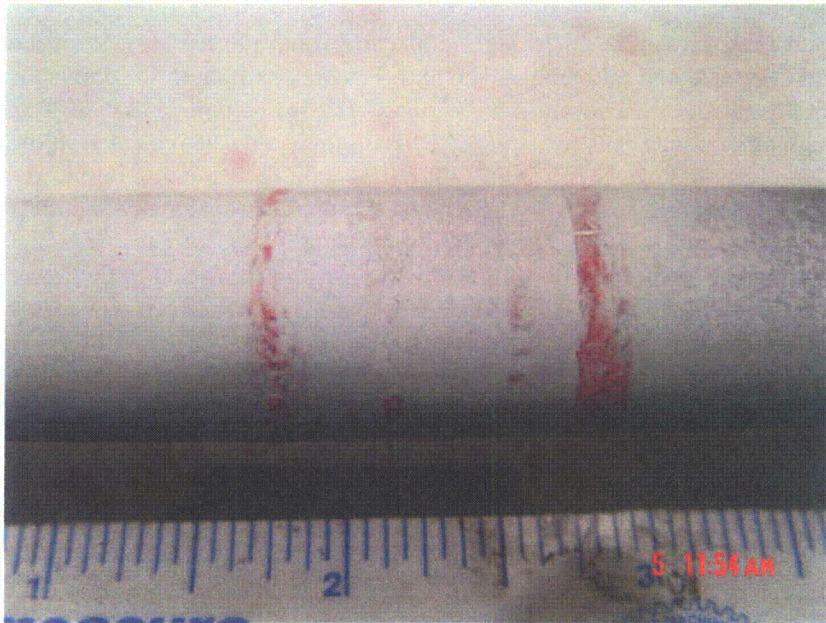


Figure 154.
Dye penetrant test results in
the same area as shown in
Figure 152 (crevice top: left;
crevice bottom: right).

5.4.6 Discussion

Analysis for ECP and pH Data

Samples were taken from the crevice and bulk solution of NaCl-06 and analyzed by ICP/OES and IC for Na and Cl, respectively. As observed in the previous tests, the crevice samples showed a time delay effect because the volume in the sampling line and shutoff valve is comparable with that of the crevice solution sample. The bulk solution sample size is sufficiently large to overcome the sampling volume issue. In this test, to minimize the time delay effect and evaluate crevice concentration more accurately, crevice samples were taken only before changing ΔT . Sampling procedures are composed of three steps: first, 2-drop sampling; second, 2-drop sampling; and third, 5-drop crevice flushing. The volume of the 2-drop sample is roughly equivalent to the dead volume of the sampling line, 90 μL . Therefore, the first 2-drop sample will be the stagnant solution in the sampling line, and the second 2-drop sample will represent the actual crevice solution. After the second step, remaining concentrated crevice solution may still be in the sampling line because the total available crevice volume, excluding the space occupied by magnetite particles, is 250 μL in this test. The third step, a 5-drop sampling, is intended to flush all crevice solution in the sampling line. We anticipated that the first 2-drop sample would show relatively low impurity concentration, and the second 2-drop sample would show high concentration. Since the Na and Cl in the first 2-drop sample, if there is, eventually come from the crevice solution by diffusion, the concentrations are adjusted by the summation of the first and second 2-drop samples to account for the dilution effect. Assuming the first sample's volume is the same as the second sample's one, no other volume correction is necessary. Table 7 shows the Na and Cl concentration for the first and second 2-drop samples. "Adjusted Conc." means the summation of the first and second samples' concentrations. The first samples showed lower concentrations than the second samples for both Na and Cl, except for $\Delta T=40^\circ\text{F}$. At this ΔT , the concentrated liquid phase appears to have been dominant around the sampling port so that the diffusion of Na and Cl ions was easier. At higher ΔT , the steam phase became more dominant so that ionic diffusion through the liquid phase was limited. The decrease in total concentration with the increase in ΔT can also be attributed to the steam phase growing with the increase in ΔT .

The dissolved Fe and Ni concentrations are summarized in Table 7. The bulk concentrations of Fe and Ni were about 0.7 and 0.2 ppm, respectively, which might come from the internal surface of the secondary chamber and partly from alloy 600 and 690 tubing. The high Fe concentration in the crevice is partially attributed to the presence of magnetite. The molar ratio of the crevice sample at $\Delta T=80^\circ\text{F}$ is much lower than before. This difference might be caused by two effects: dilution and steam condensation. The extracted samples from the crevice could have been mixed and diluted with bulk solution during the sampling procedures. This dilution effect by bulk solution is difficult to avoid unless the crevice mouth is shut off so that the bulk liquid cannot penetrate into the crevice during the sampling procedure. At higher ΔT , more steam may be sampled and the concentration of Na and Cl in the steam may result in the lower MR. The crevice samples at higher ΔT should be analyzed carefully because of these two effects (i.e. the dilution effect or steam condensation).

Table 7. Na and Cl concentration results for crevice samples and adjusted Fe and Ni concentrations in the same crevice samples.

#	Sample Description	1 st 2 Drops (ppm)		2 nd 2 Drops (ppm)		Adjusted Conc. (ppm)		[Na]/[Cl]	Adjusted Fe Conc. (ppm)	Adjusted Ni Conc. (ppm)
		Na	Cl	Na	Cl	Na	Cl			
1	$\Delta T= 40^\circ\text{F}$ after 362 hr	1514	2984	516	975	2030	3959	0.79	202.4	16.6
2	$\Delta T= 60^\circ\text{F}$ after 194 hr	14.2	59.5	738	1599	752.2	1658.5	0.70	190.5	26.8
3	$\Delta T= 80^\circ\text{F}$ after 146 hr	0.0	28.0	7.7	165	28.0	172.7	0.25	59.5	6.6

Figure 155 shows the tungsten potentials measured in the bulk water and crevice as a function of pH calculated from the solution sample analysis. In previous tests, only Na and Cl were considered as impurities, but in this analysis dissolved Fe and Ni were included as well. As shown in Figure 155, Fe and Ni tend to increase the solution pH. Additional metal cations need additional anions to maintain charge neutrality. Therefore, when metal cations are introduced in the bulk solution, the concentration of OH^- ions increases and the solution pH increases. The slopes of the bulk tungsten potential data with respect to bulk solution pH were dependent on the presence of Fe and Ni. When dissolved Fe and Ni are considered, the bulk potential/pH slope of -88 mV/pH is closer to the Nernstian slope of -106 mV/pH at 500°F than when Fe and Ni are not considered. The two bulk data sets with and without considering Fe and Ni are sensitive to the solution pH change, suggesting that the W/WO_x electrode can behave as a pH electrode in dilute NaCl solution with $\text{MR}=0.7$ at 500°F . However, a decreasing trend of the potential with the increase of pH is not apparent for crevice tungsten potentials even after the pH correction using Fe and Ni concentration. However, the crevice tungsten potentials are always higher than the bulk tungsten potentials; this finding is consistent with the crevice solution pH always being lower than the bulk solution pH.

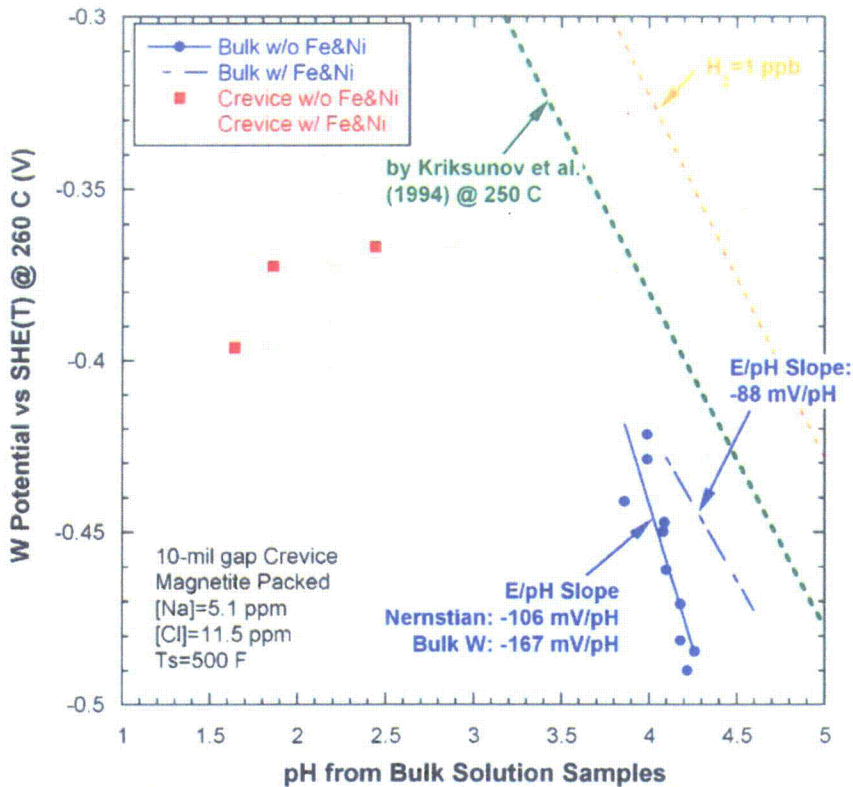


Figure 155. Tungsten potentials in bulk and crevice as a function of pH calculated from solution sample analysis with and without Fe and Ni (NaCl-06).

In Figure 156 the potential data for the crevice and bulk solution are compared with the previous test results in a W-H₂O phase diagram. The bulk solution data are slightly shifted toward the alkaline direction as compared with earlier data, and this shift is attributed to including the dissolved Fe and Ni ions. In earlier ICP/OES analysis, Fe and Ni were not included. If Fe and Ni ions had been considered for the previous bulk solution data, the tungsten potential data would have likely fit a single line. If we consider only the bulk solution data in this test (NaCl-06) and the previous alkaline data (NaOH-03), for which the pH is higher than 6, the potential/pH slope is -103 mV/pH, which is very close to the Nernstian value of -106 mV/pH at 500°F. These results are consistent with the earlier work done by Kriksunov et al.²⁹ They reported that the W/WO_x electrode followed the Nernstian slope in the pH range of 2-11 at high temperature. In Figure 156, the Kriksunov et al. test results are plotted. Considering the test temperature of the earlier work is 250°C (482°F), the results from NaCl-06 appear to be consistent with the earlier work. The crevice tungsten potential data of this test is 30-60 mV higher than the previous NaCl test data. This discrepancy appears to be attributed to two changes: the location of tungsten wire tip and packing materials. As indicated by Figure 140, in the NaCl-06 test, one crevice tungsten wire tip located closer to the tube surface than the other represented the active chemistry change near the tube surface area, which caused different crevice potentials from the previous crevice potential data at the same crevice sample pH. This test (NaCl-06) used magnetite powder as packing materials, which caused lower permeability and less volatility effect of Cl than diamond powder. Therefore, the magnetite-packed crevice might maintain acidity more efficiently than the diamond-packed crevice, which led to higher crevice W/WO_x electrode potentials.

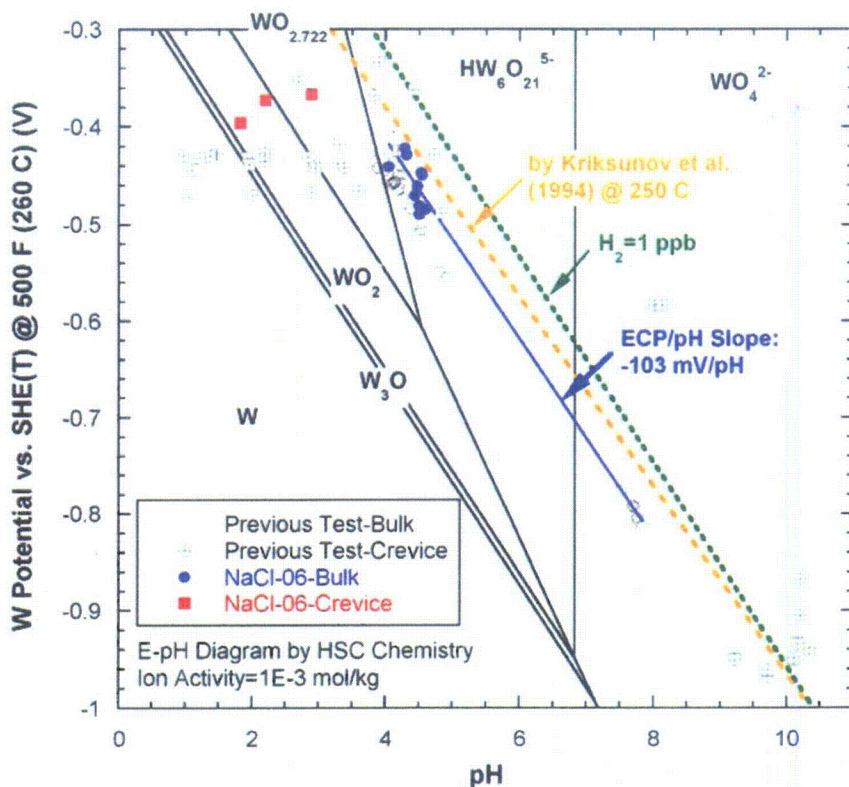


Figure 156. Measured tungsten potentials in the NaCl-06 test in comparison with the previously measured tungsten potentials in a W-H₂O phase diagram predicted by the thermodynamic code HSC Chemistry.

The plateau in the crevice tungsten potential data with respect to solution pH may be caused by a metal-to-metal cation reaction. However, as shown in Figure 156, the tungsten-to-tungsten cation reaction is not thermodynamically stable at 500°F, but tungsten oxides are stable in the low pH region. Therefore, the insensitivity of crevice tungsten potential data to crevice pH cannot be attributed to the metal-to-metal cation reaction. Instead, as discussed before, the tungsten wire tip location relative to the tube wall should be considered.

Mass Balance Analysis

One advantage of a closed MB system is that the impurity amount in a crevice can be estimated from the changes of bulk impurity concentration. Based on the analysis for Na and Cl concentration in the secondary bulk samples, we estimated the total accumulated Na and Cl masses in the crevice at corresponding points of time. Figure 157 shows the total mass of Na and Cl in the crevice as a function of time. Figure 158 shows the same results in terms of total moles. Since Na and Cl have different atomic mass, mole units are better than mass units for evaluating and comparing each ion's hideout. At the very beginning of the concentration process, the accumulated Na and Cl moles were the same. However, Na was initially concentrated preferentially, and then Cl started to be concentrated as the Na concentration became saturated at $\Delta T=40^\circ\text{F}$. In the time period when Cl was preferentially concentrated in the crevice, the crevice tungsten potential near the tube surface also indicated the acidification of the crevice, as shown in Figure 140. Possible explanations for this behavior are as follows. Preferential concentration of Na indicates the volatility effect of Cl in the crevice, and the subsequent preferential concentration of Cl might be caused by the boiling rate reduction due to the boiling point elevation by Na concentration and the resultant reduction of the volatility effect. Also, if metal corrosion occurred in the crevice, the metal cations can drive the Na ion out and the Cl ion into the crevice to maintain charge neutrality, which is

called the “electromigration effect.” However, from the post-test examination discussed in the previous section, the tube corrosion in the crevice was not significant. After steady state was reached at almost 200 hours, the total mole of Cl was higher than that of Na, indicating the development of an acidic crevice. Preferential concentration of Na or Cl was not evident at $\Delta T=60^\circ\text{F}$ and 80°F . The test was stopped prior to the crevice reached a saturation condition at $\Delta T=80^\circ\text{F}$.

Using MULTEQ[®], a thermodynamic concentration limit was calculated for Na or Cl at $\Delta T=40^\circ\text{F}$, assuming that all unoccupied empty space in the crevice was filled with concentrated solution. The calculation indicated that the Na concentration was close to the thermodynamic limit at the given conditions, and the Cl concentration was a little higher than the limit. In a highly packed magnetite crevice, the Na concentration process appears to be thermodynamically limited, but this is only a hypothesis. Actually, the Cl concentration was expected to be lower than the thermodynamic limit due to the volatility effect. The higher Cl concentration than the thermodynamic limit at $\Delta T=40^\circ\text{F}$ might be attributed to the adsorption of Cl to magnetite particles. The adsorption can occur as long as adsorption sites are available regardless of ΔT . At $\Delta T=60$ and 80°F , the Na and Cl concentrations exceeded their solubility limit as NaCl, and NaCl precipitation might have occurred. The NaCl solubility is dependent on temperature but the solubility limits at $\Delta T=60$ and 80°F are identical because the bulk saturation temperature is constant (500°F). Note that the results in Figures 157 and 158 show only the average crevice concentration, not the local variation in crevice chemistry, which would actually be large due to the significant variations in boiling and flow path behavior in the crevice introduced by the packing.

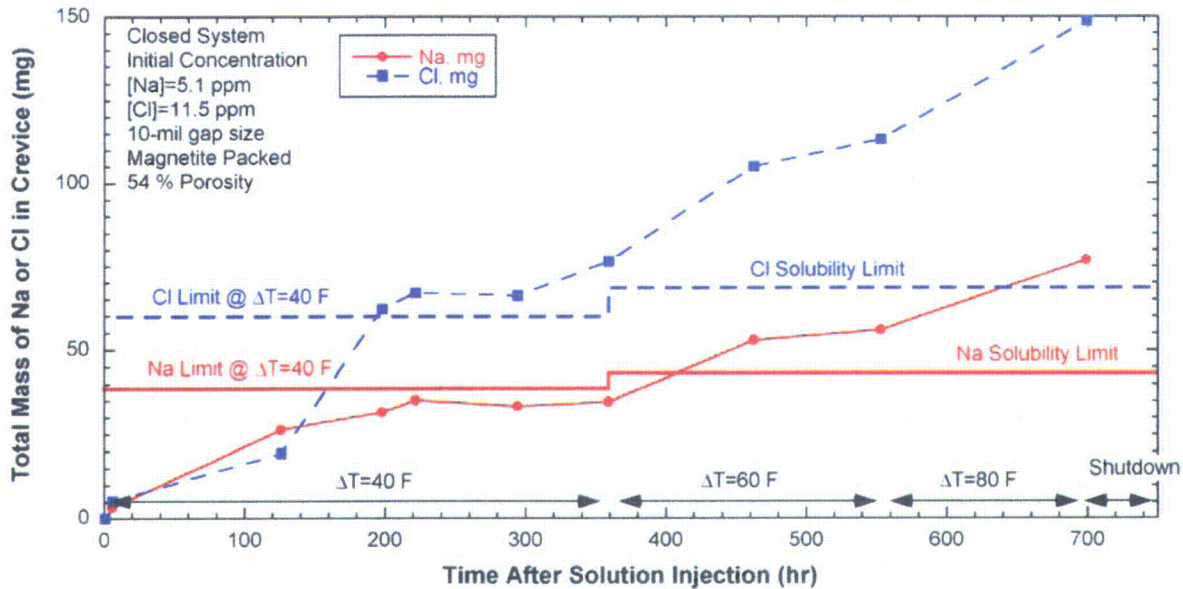


Figure 157. Total mass of Na and Cl accumulated in the crevice as a function of time based on the results of bulk solution analysis (NaCl-06).

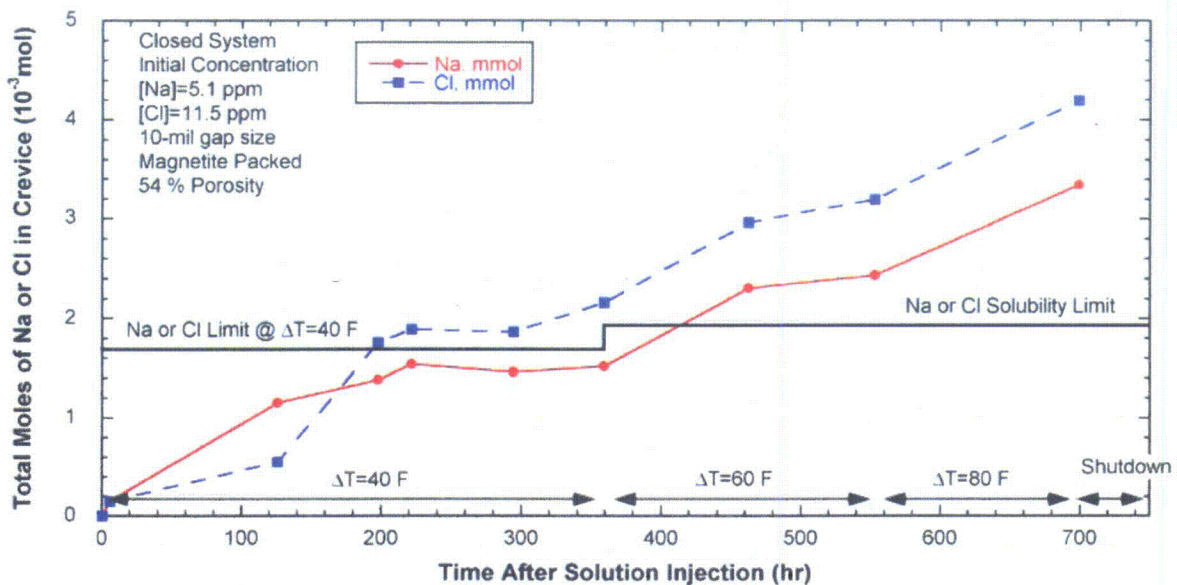


Figure 158. Total moles of Na and Cl accumulated in the crevice as a function of time based on the results of bulk solution analysis (NaCl-06).

The results shown in Figures 157 and 158 do not account for the bulk concentration difference between Na and Cl. To account for this effect, "exposure" was introduced. As mentioned earlier, "exposure" is defined as the time integration for the variation in bulk impurity concentration. Figure 159 shows the total mass of Na and Cl as a function of exposure. If the bulk concentrations are the same for Na and Cl, it is expected that Na will reach steady state before Cl at a given ΔT . Since Na and Cl have different atomic mass, the total moles of Na and Cl with respect to molal exposure were plotted, as shown in Figure 160. The "molal exposure" means the time integration for the bulk impurity concentration in a molal unit instead of ppm unit. The preferential Na concentration in the crevice at the early stage of testing is clear. The hideout kinetics of Na is faster than that of Cl under the same molal exposure at $\Delta T=60^\circ\text{F}$ and 80°F . The Na hideout rates are proportional to ΔT and the Cl hideout rates also appear to depend on ΔT except for the delayed preferential Cl concentration at $\Delta T=40^\circ\text{F}$. The delayed preferential Cl concentration, as discussed before, is attributed to the adsorption of Cl on magnetite particles or the reduced volatility of Cl due to the boiling point elevation and the resultant steam-phase reduction.

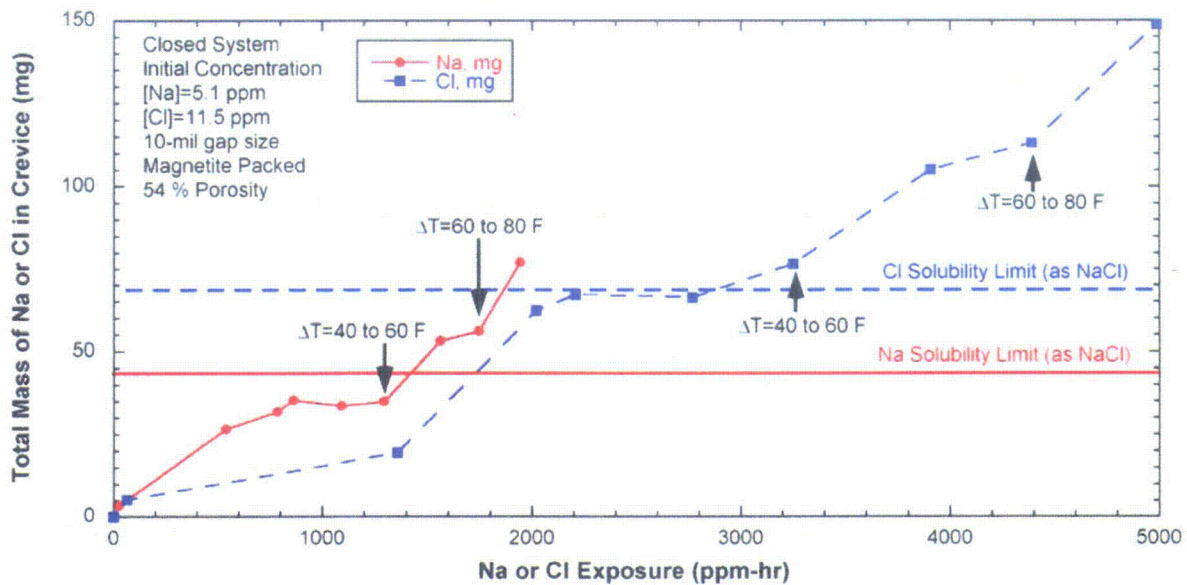


Figure 159. Total mass of Na and Cl accumulated in the crevice as a function of exposure based on the results of bulk solution analysis (NaCl-06).

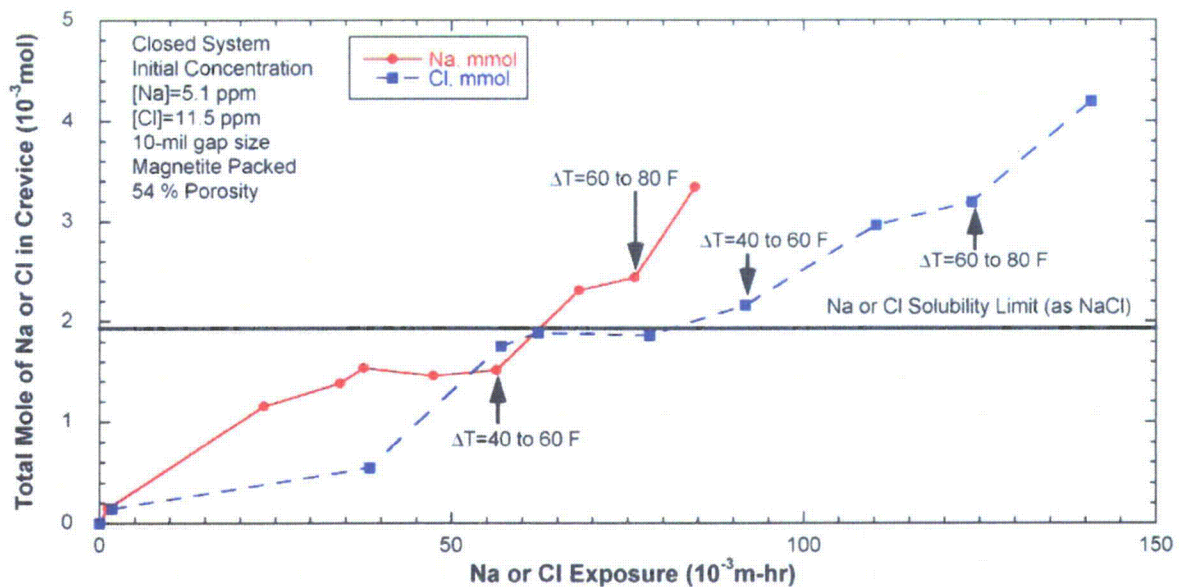


Figure 160. Total moles of Na and Cl accumulated in the crevice as a function of molal exposure based on the results of bulk solution analysis (NaCl-06).

Figure 161 shows the Na-to-Cl MR variation in the bulk and crevice for NaCl-06. The crevice MR was calculated from the total accumulated amount of Na and Cl estimated from bulk-sample chemical analysis. The initial MR was 0.7 in the bulk solution, but this MR decreased as the crevice MR increased up to 2. As the bulk MR increased, the crevice MR decreased and stabilized at MR=0.8, which is higher than the initial MR=0.7 but still lower than 1.0. This finding suggests that the magnetite-packed crevice became initially alkaline due to the volatility effect of Cl but then acidified due to the delayed preferential Cl concentration. The decrease of bulk MR with the increase of ΔT also suggests that the preferential Na

concentration occurred at higher ΔT as well as at 40°F because the volatility effect of Cl became more significant at higher ΔT ; this is consistent with earlier Baum's test results³. However, the crevice MR did not significantly increase, and the crevice tungsten potential also indicated slight acidification rather than alkalization. Prior to the ΔT change from 60°F to 80°F the formerly accumulated impurity levels may have been so high, as compared with the newly accumulated impurity amount, that the impact of changing ΔT was not significant. If the temperature condition had started with $\Delta T=60^\circ\text{F}$ or 80°F , initial large preferential Na hideout is expected and probably would be followed by a delayed preferential Cl hideout.

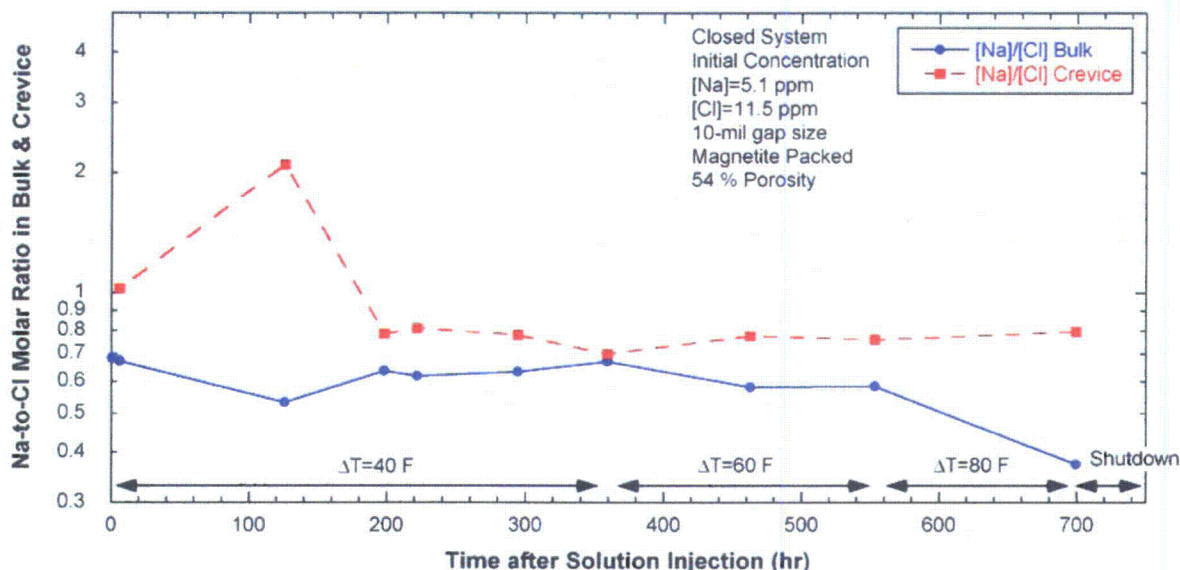


Figure 161. Na-to-Cl molar ratio variation of bulk samples and estimated crevice concentration from bulk chemical analysis (NaCl-06).

To evaluate the dependency of Na concentration on choice of packing material, we compared the Na concentration from two tests (NaCl-05 and NaCl-06) as a function of Na exposure, as shown in Figure 162. To account for the porosity difference in each test, the total accumulated Na mass was divided by the total available unoccupied space in the crevice, which was defined by the integrated-volume average Na concentration. The concentration of the NaCl-05 prior to the ΔT change (40°F \rightarrow 60°F) is much lower than that of the NaCl-06. In the NaCl-05 test, the test duration at $\Delta T=40^\circ\text{F}$ was much shorter than the NaCl-06. Although the bulk solution conductivity data showed stabilized behavior, as indicated in Figure 117, we might have increased ΔT from 40°F to 60°F too early. The Na concentration rate in the NaCl-05 test was highest at $\Delta T=60^\circ\text{F}$. At $\Delta T=60^\circ\text{F}$, the maximum concentration rate in NaCl-05 was 3.5 times higher than that in NaCl-06, and the saturation concentration of the NaCl-05 is about two times higher than that of the NaCl-06. This discrepancy suggests that the difference in packing materials can affect the Na concentration at $\Delta T=60^\circ\text{F}$; the magnetite-packed crevice appears to be thermodynamically limited while the diamond-packed crevice is not thermodynamically limited because of NaCl precipitation which could increase the saturated Na concentration above the thermodynamic limit. At $\Delta T=80^\circ\text{F}$, the Na concentration in NaCl-05 was readily saturated, probably because significant NaCl precipitation had occurred at $\Delta T=60^\circ\text{F}$. The Na concentration in NaCl-06 did not saturate as it did for NaCl-05. Further Na hideout would be expected if NaCl-06 was run longer at a $\Delta T=80^\circ\text{F}$.

Figure 163 shows the Cl concentration behavior in the diamond- and magnetite-packed crevice tests (NaCl-05 and NaCl-06 tests). Figure 163 clearly shows the effect of packing materials on Cl concentration. The Cl concentration of NaCl-05 (diamond-packed) prior to the ΔT change (40°F→ 60°F) is much lower than that of NaCl-06 (magnetite-packed). A longer-term test for the diamond-packed crevice $\Delta T=40^\circ\text{F}$ could determine whether this is attributed to the shorter exposure time or the discrepancy of packing materials (diamond vs. magnetite). At $\Delta T=60^\circ\text{F}$, the maximum Cl concentration rate in NaCl-05 is 4.4 times higher than that in NaCl-06. At $\Delta T=80^\circ\text{F}$, the final Cl concentration of NaCl-06 is slightly lower than that of NaCl-05. It is expected that if the NaCl-06 test was run longer, the Cl concentration would have increased further and might be saturated at a similar level to that of NaCl-05.

The hideout rate depends on the heat flux and the total area where the nucleate boiling can occur. The heat flux difference on the tube surface between diamond and magnetite would not be significant. The total area for the boiling is expected to be much different. The magnetite-packed crevice is less permeable so that the liquid phase cannot penetrate as deep into the crevice as it can when the crevice is packed with diamond powder. Based on the temperature data shown in Figures 134 and 135, at $\Delta T=60^\circ\text{F}$ the liquid phase appears to penetrate at least 50 % of the depth of the magnetite-packed crevice. Assuming that the whole crevice tube surface was wetted in the diamond-packed crevice at $\Delta T=60^\circ\text{F}$, the difference in the hideout rates between the diamond- and magnetite-packed crevices should not exceed a factor of two. The present results suggest another source of the difference. The diamond has very high thermal conductivity so that the diamond surface itself near the tube wall may be able to behave as the boiling site. In this case, the total boiling area is increased more than two times.

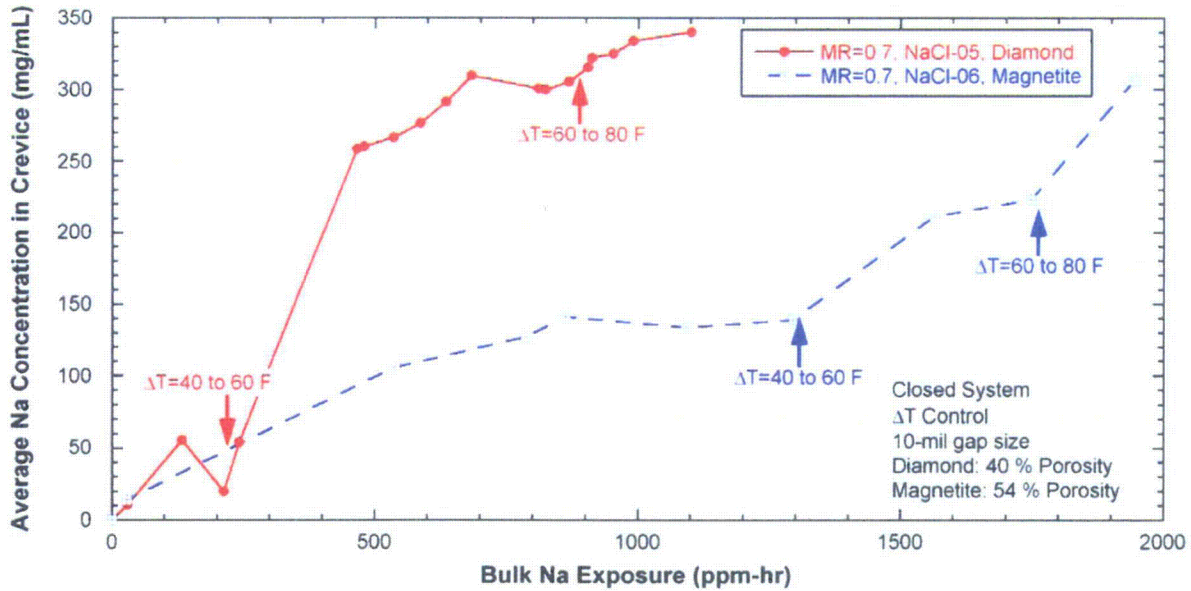


Figure 162. Integrated-volume average Na concentration variations with exposure for NaCl-05 and NaCl-06 tests.

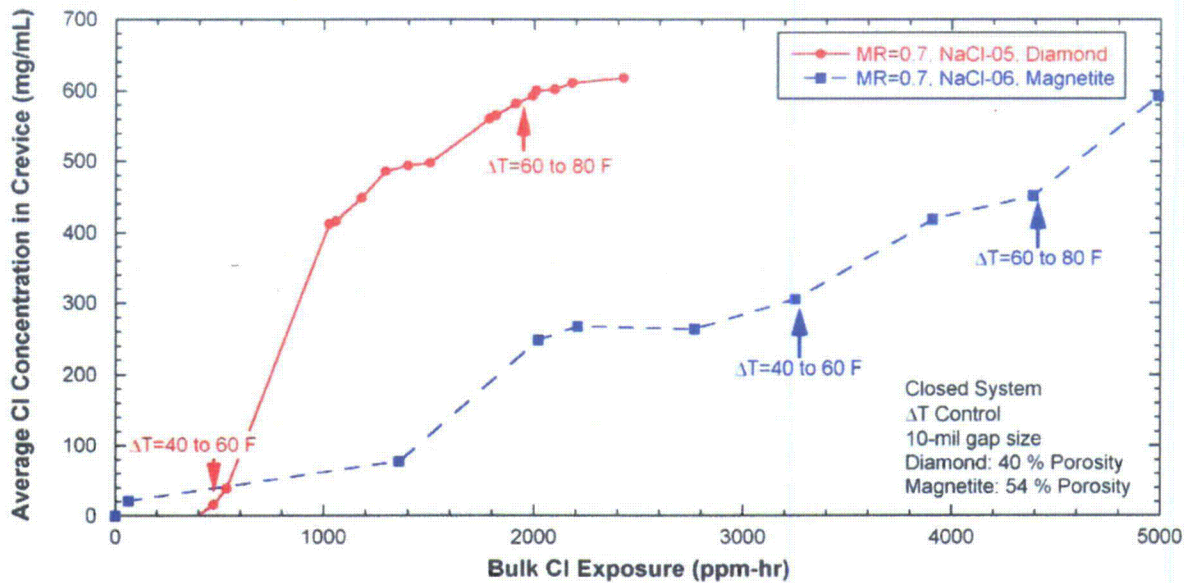


Figure 163. Integrated-volume average Cl concentration variations with exposure for NaCl-05 and NaCl-06 tests.

Permeability

Porosity and permeability are measures of restriction to flow into and out of the crevice packing. Our test results show that these factors are important with regard to crevice hideout behavior and strongly relate to how rapidly stable conditions are achieved in the crevice. Figure 164 shows the permeability of our diamond-packed and magnetite-packed crevices as predicted by the Carman-Kozeny equation⁴⁰:

$$k = \frac{D_p^2 \varepsilon^3}{72\tau(1 - \varepsilon)^2}$$

where k = permeability, m^2

D_p = particle diameter, m^2 .

ε = porosity

τ = tortuosity

(6)

Eq. (6) is valid for a uniform porous material packed with spheres having the same diameter. As shown in Figure 164, the mean diameter of our diamond particles is 146 μm , and the porosity is 40 %. The estimated permeability for the diamond-packed crevice is 44 Darcy units. One Darcy unit is equivalent to $9.87 \times 10^{-13} m^2$. The tortuosity of the diamond-packed crevice was derived from the estimated value for a carbon fiber-filled crevice by Millett.¹⁹ The tortuosity is a measure of how much the flow path wanders or turns in a packed crevice as compared with the non-packed condition and strongly influences effective flow resistance. Millett estimated the tortuosity for carbon fiber-filled crevice and synthetic magnetite-filled crevices. He also established the reference permeability value for the magnetite-packed crevice, which is 0.1 Darcy. Therefore, the permeability difference between diamond- and magnetite-packed crevices is almost three orders of magnitude, as shown in Figure 164. For a low-permeable crevice, the liquid and steam flow into and out of the crevice is slow and limited, and mixing inside the

crevice becomes more difficult, producing spatial variations both thermally and chemically. For a low-permeability crevice, it takes longer to reach steady state.

A low-permeability crevice can have a different crevice chemistry compared with a high-permeability crevice at given bulk chemistry and thermal conditions. The mixing between liquid and steam phases and Cl escaping from the heat transfer tube surface become harder in a low-permeability crevice. The two effects (induced mixing and Cl escaping) result in a decrease in pH (acidification) on the tube surface.

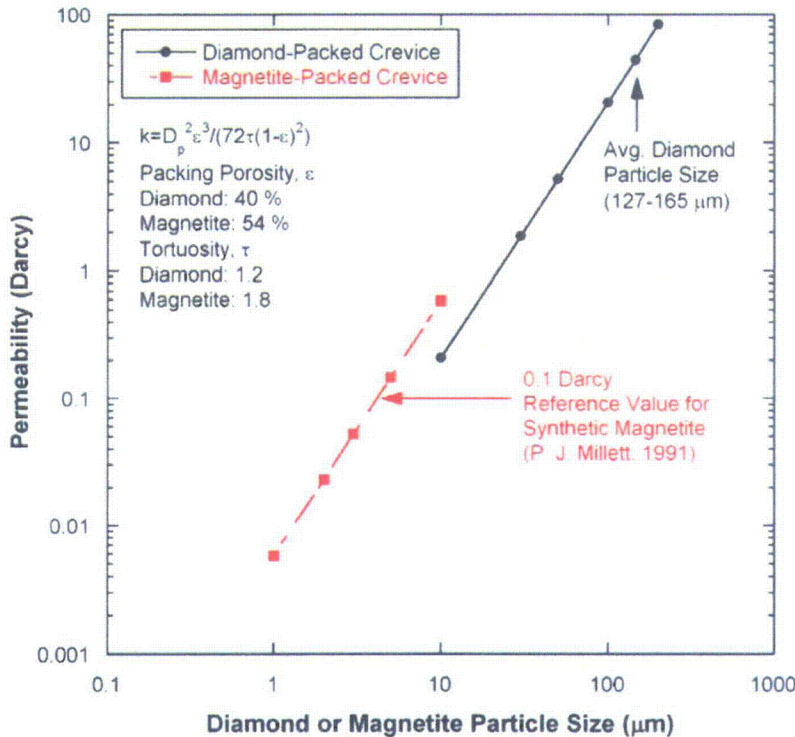
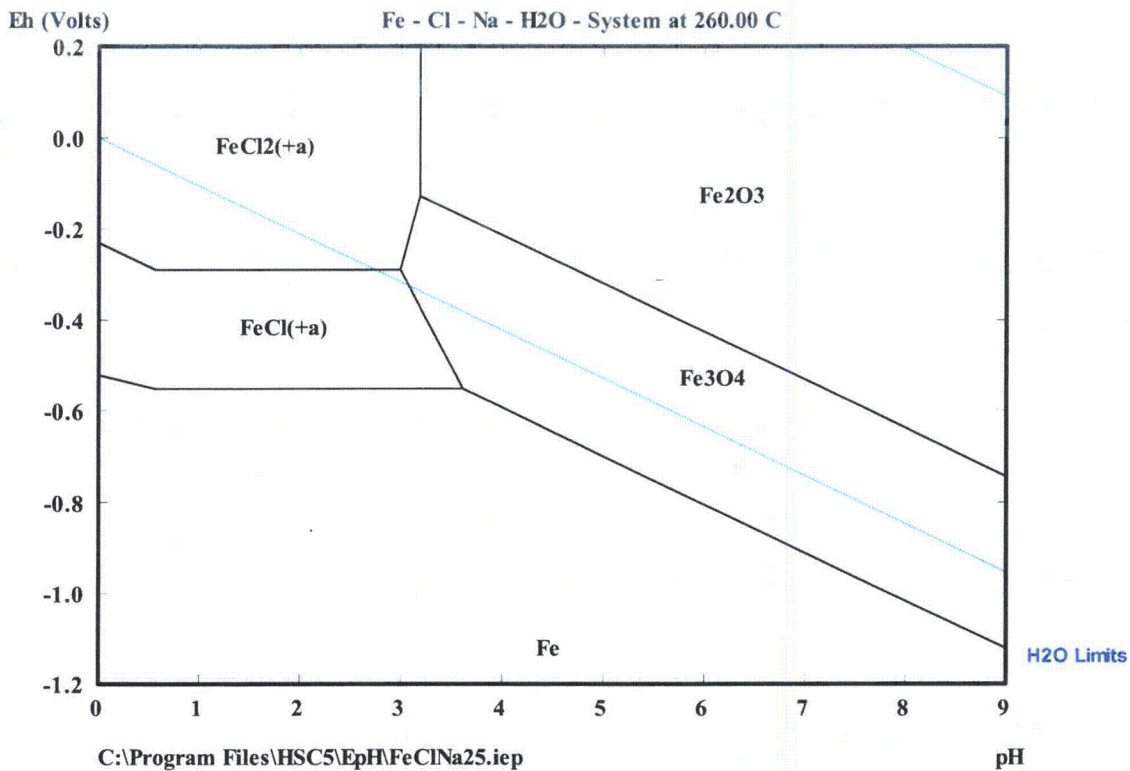


Figure 164. Permeability of single-crevice tests for diamond- and magnetite-packed crevices predicted by Carman-Kozeny equation (1 Darcy = $9.86923 \times 10^{-13} \text{ m}^2$).

Magnetite Dissolution

Diamond powder is inert under highly acidic or caustic chemistry, but magnetite's solubility depends on the pH. If the chemistry in a magnetite-packed crevice becomes strong acid or alkaline, consideration should be given to the dissolution of packed magnetite and its effect on the solution chemistry. Figure 165 shows a potential-pH diagram of Fe in water that contains Na and Cl ions of 0.1 mol/kg at 500 °F, predicted by the thermodynamic code HSC Chemistry. In deaerated acid solution FeCl^+ is a predominant ion. If an acidic crevice is formed in a magnetite-packed crevice, dissolved ferrous ions from the magnetite react with chloride ions and form FeCl^+ . The formation of FeCl^+ will increase the solution pH. This prediction is supported by the pH estimation by MULTEQ shown in Figure 155. We can expect that if a magnetite-packed crevice becomes acidic by the chloride ions, dissolved ferrous ions react with the chloride ions so that the crevice pH becomes less acidic to some extent. However, the quantitative estimation of the pH variation due to magnetite dissolution could benefit from additional study.



ELEMENTS	Molality	Pressure
Fe	1.000E-01	4.628E+01
Cl	1.000E-01	4.628E+01
Na	1.000E-01	4.628E+01

Figure 165. Potential-pH diagram of Fe-Cl-Na-H₂O system at 260°C (500°F) predicted by the thermodynamic code HSC Chemistry.

5.4.7 Summary

The NaCl-06 test at $\Delta T=40$ °F took about 300 hours to reach a steady state in the magnetite-packed crevice. This duration means the kinetics are slower than in the previous diamond-packed crevice test (NaCl-05) because of the lower permeability and higher flow restriction with the magnetite packing. We inferred from the crevice conductivity and tungsten potential that initially, at the deep crevice region, pores were filled mainly with steam and then replaced by the Na-rich liquid phase as the process continued. Crevice tungsten potential measurements indicated the presence of a radial pH gradient near the tube wall. While the tungsten potential located away from the tube surface was not much changed, the potential closer to the tube surface indicated larger fluctuation of crevice pH. At $\Delta T=40$ °F, an initially alkaline pH solution developed near the tube surface but gradually became acidified, which was supported by the bulk solution analysis. The preferential concentration of Na in the crevice will cause a boiling point elevation, which will decrease the steam phase at the tube surface and will make the volatility effect of Cl less significant. The crevice tungsten potential near the tube surface maintained the acidity with the further increase of ΔT from 40 °F to 60 °F and 80 °F, which contradicts the results of earlier literature. However, the molar ratio of bulk samples indicated that the volatility of Cl became more

significant with increasing in ΔT , which is consistent with earlier literature. During the same time period the diamond-packed crevice will result in more severe corrosion of the tube than the magnetite-packed crevice at $\Delta T=60$ °F or higher because of the faster impurity hideout kinetics.

6. Overall Discussion

6.1 Comparison with Literature Data

6.1.1 NaOH Test

Lumsden⁴¹ performed crevice hideout tests with a diamond-packed crevice and NaOH bulk chemistry. Figure 166 shows the total mass of Na in the crevice as a function of time. The bulk Na concentration for each test is specified in the figure. A constant heat flux was applied during the test instead of the ΔT control used in our test. A ΔT control test is considered to be closer to the thermal conditions in SGs than a constant heat flux test. The porosity in the crevice after packing with diamond powder was 52 %. The radial gap size and depth of the crevice were 0.25 mm (10 mil) and 25 mm (1 in.), respectively.¹² The crevice geometry of Lumsden's test is almost identical to ours. A feed/bleed system was used to try to maintain the secondary water chemistry at constant condition.

Lumsden's data were recalculated to the "exposure" base and compared with our single-packed crevice data from NaOH-03, as shown in Figure 167. Considering the differences of the primary heating method and crevice porosities, the hideout rate for the NaOH-03 test appears to be consistent with Lumsden's data for the 20 ppm and 2 ppm bulk Na tests. Lumsden's data show similar behavior in an "exposure" scale, suggesting that the Na hideout rate is directly proportional to the bulk Na concentration. In Figure 167 the Na concentration limits calculated by MULTEQ were specified as parallel lines for each ΔT . Since NaOH has a very high solubility limit, the Na concentration in the crevice is expected to be thermodynamically limited by available superheat if the crevice packing has enough flow restriction. At $\Delta T=40^\circ\text{F}$, the saturation Na mass is slightly higher than the thermodynamic limit. When the crevice gap is being filled with diamond powder, some excess diamond powder usually remains at the crevice mouth, and this condition may result in an overestimate of the crevice porosity. If the crevice becomes more porous, the thermodynamic limit of the total Na mass becomes higher due to the larger crevice volume. From the data in Figure 167, we inferred that the crevice was fully wetted, and the steady-state crevice concentration was thermodynamically limited for the diamond-packed crevice and NaOH bulk chemistry; this behavior is expected in the case of highly soluble solutes like NaOH.

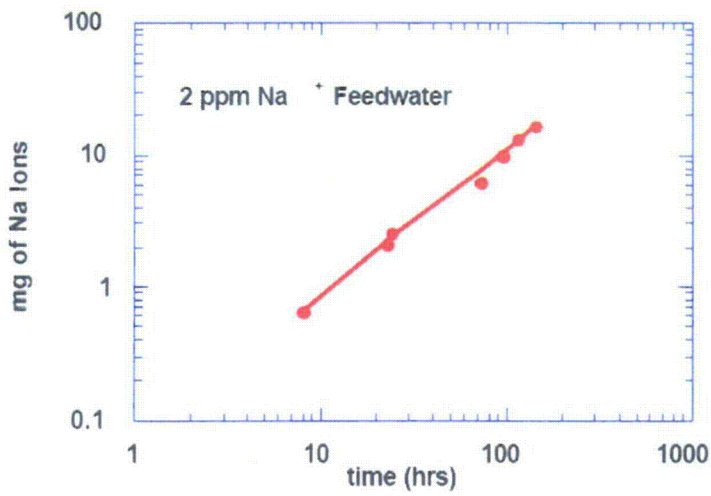
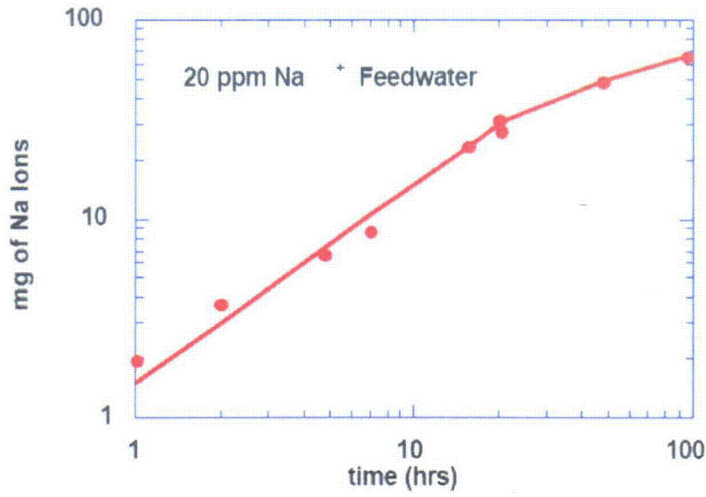


Figure 166.
 Total Na mass in crevice as a function time with two bulk Na concentrations: 20 ppm Na for upper figure and 2 ppm Na for lower figure. Test conditions are as follows: constant heat flux, diamond packed (52 % porosity), $T_{\text{sat}}=280^{\circ}\text{C}$.⁴¹

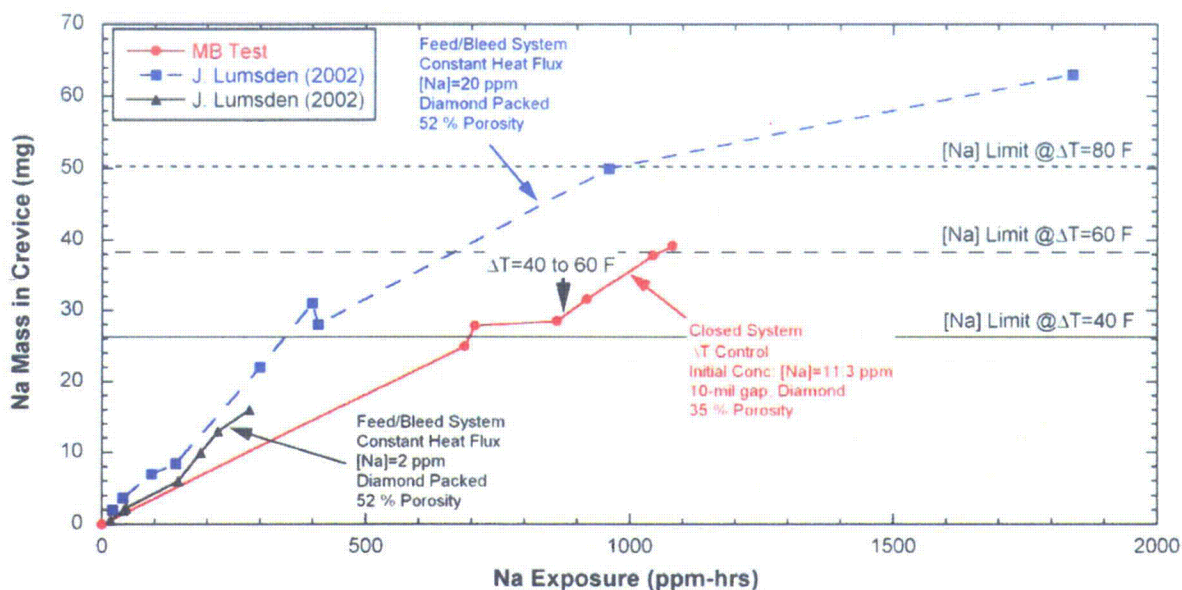


Figure 167. Comparison of 20 ppm NaOH ([Na]=11.3 ppm) test results with available NaOH test data from Lumsden's earlier work⁴¹ (Note: Lumsden's data are the same as shown in Figure 166).

6.1.2 NaCl Test

Mann and Castle performed NaCl hideout tests with carbon-fiber packed crevices.² The porosity of the carbon-fiber packed crevice was 51 %, and its permeability was 43 Darcy. Mann and Castle's data were compared with our crevice test results. The measured permeability is very close to the estimated permeability of our diamond-packed crevice shown in Figure 164. In Figure 168 the total NaCl hideout mass as a function of Cl exposure is compared with our test results for NaCl water chemistry: NaCl-02, -05 and -06. The NaCl-02 test had a molar ratio of 1.0, and NaCl-05 and -06 had a molar ratio of 0.7. Even though there are experimental differences like ΔT and porosity, the initial hideout rate of NaCl-02 is very similar to that of literature data. The NaCl-05 and -06 results differ from the literature data, probably because of the different molar ratio and ΔT conditions. The NaCl-06 test also has a lower permeability than that of Mann and Castle's test. To evaluate the hideout rate of diamond- and magnetite-packed crevices at a certain ΔT , a test such as NaCl-05 or -06 that increases ΔT stepwise is not appropriate. A NaCl hideout test in which ΔT remains constant is more appropriate and would permit this evaluation.

Figure 169 shows the steady-state NaCl mass in the crevice as a function of ΔT . Mann and Castle's test results were obtained with the same crevice geometries and experimental conditions as given in Figure 168. The absolute NaCl masses from our tests cannot be compared with the literature data due to the difference in experimental parameters. Figure 169 plots the overall dependency of the steady-state mass on ΔT . Mann and Castle's test shows the results at MR=1.0, and our tests show the steady-state NaCl mass at MR=0.7. The NaCl-05 test results show an irregular variation with the increase of ΔT . The NaCl-05 test underwent electromigration, which might have affected the steady-state concentration in the crevice. Even though a steady state was not reached at $\Delta T=60^\circ\text{F}$ and 80°F in the NaCl-06 test, the NaCl mass shows a similar variation to Mann and Castle's test.

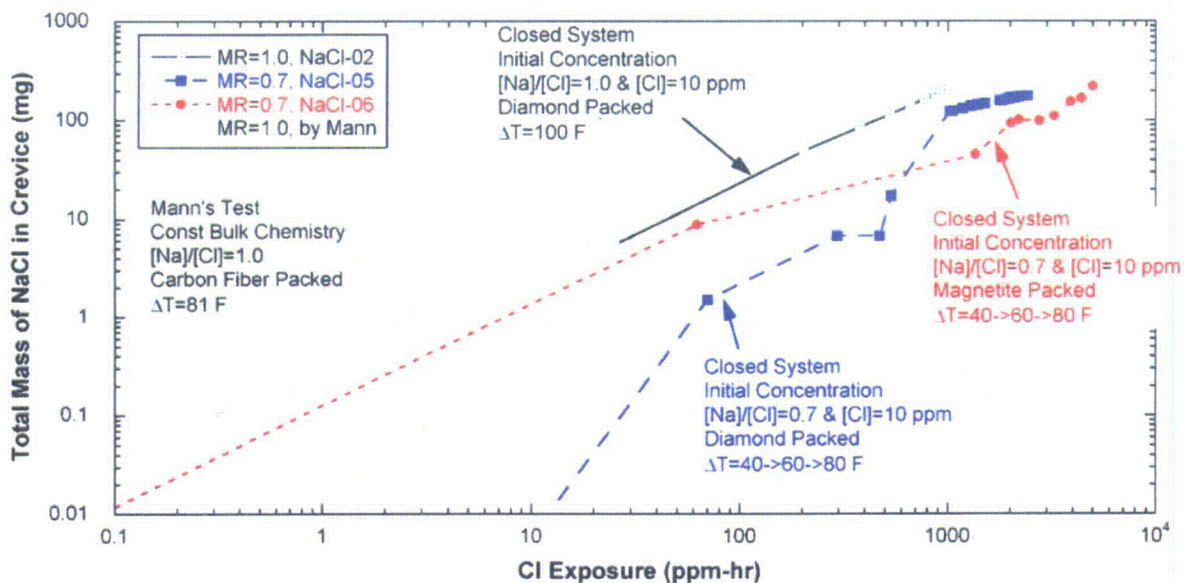


Figure 168. Comparison of NaCl hideout mass as a function of Cl exposure determined by Mann and Castle² and our test results for molar ratios of 1.0 (NaCl-02) and 0.7 (NaCl-05 and -06).

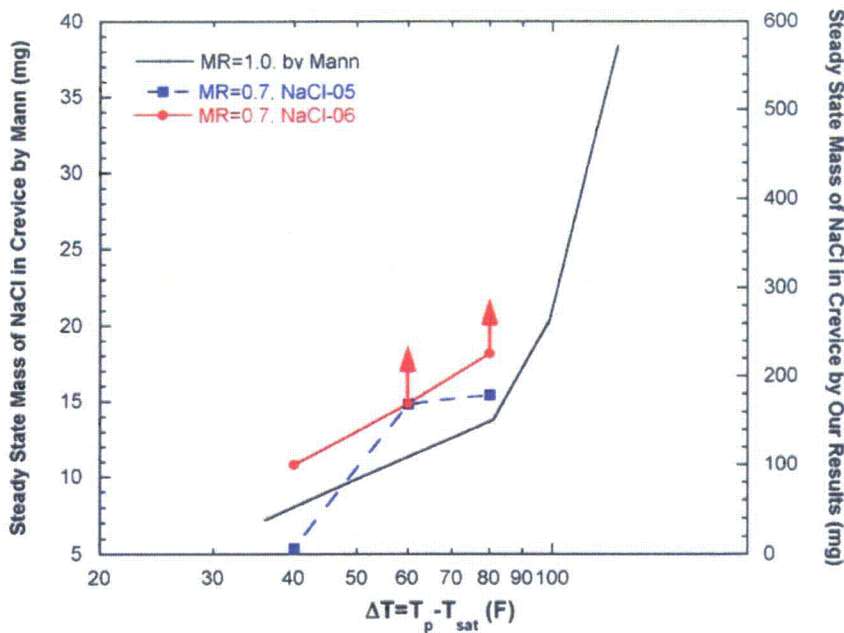


Figure 169. Comparison of the steady-state NaCl mass in the crevice as a function of ΔT from NaCl-05 and -06 tests and tests by Mann and Castle.²

Figure 170 shows the results of NaCl hideout as a function of Cl exposure in the corroded carbon-fiber packed crevice of Mann and Castle² and the magnetite-packed crevice of NaCl-06. In Mann and Castle's test the carbon-fiber filled crevice was exposed to acidic bulk chemistry, which caused corrosion of a tube support plate and formation of magnetite inside the crevice region. Therefore, the corroded crevice of Mann and Castle's test may be considered to be packed with a mixture of carbon fiber and magnetite. The crevice packing permeability in Mann and Castle's test was about 100 times lower than that in NaCl-06, which is expected to result in a lower hideout rate. As compared with the hideout rate at $\Delta T=80^\circ\text{F}$ in NaCl-06, the hideout rate of Mann and Castle's test with $\Delta T=81^\circ\text{F}$ is about three times lower,

which supports the effect of lower permeability qualitatively. Quantitative effect of permeability on the impurity concentration in the crevice could be evaluated through a modeling work.

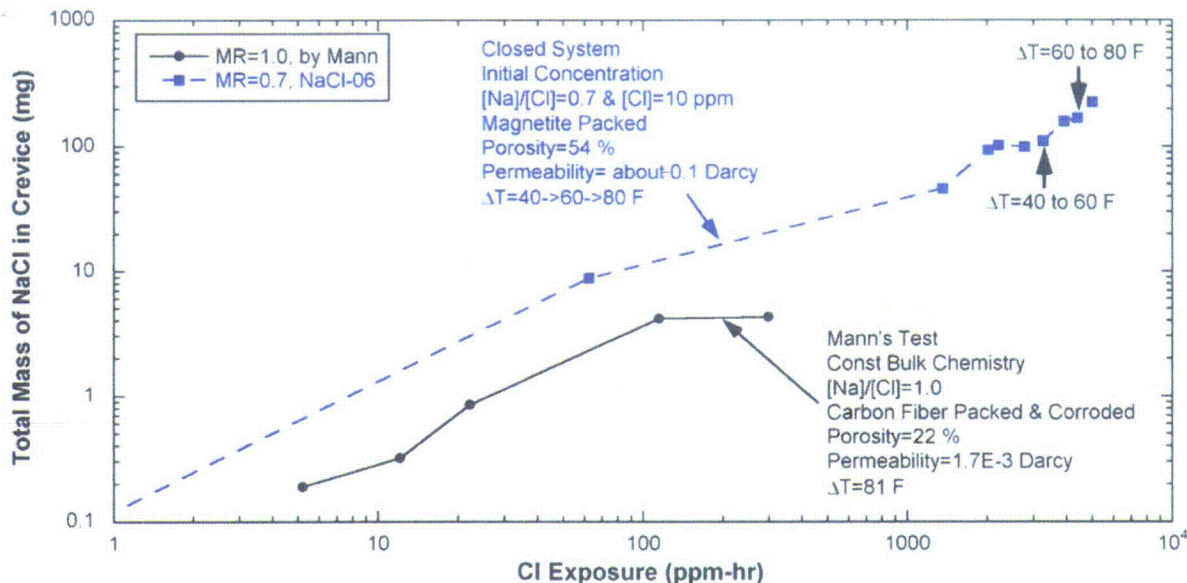
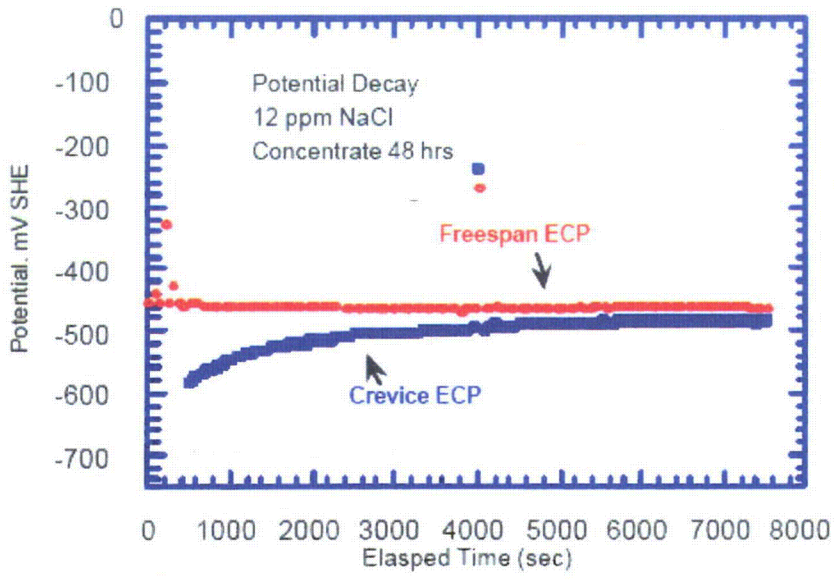


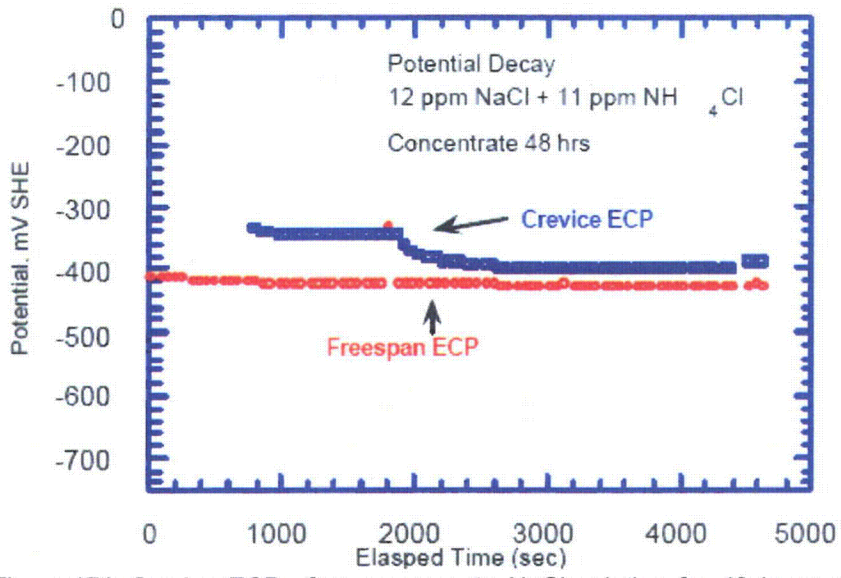
Figure 170. Comparison of NaCl hideout mass as a function of Cl exposure in the corroded carbon-fiber packed crevice of Mann and Castle² and in the magnetite-packed crevice of NaCl-06.

6.1.3 ECP Data Comparison

Figure 171 shows the ECP measurements in the crevice and bulk solution after exposure to the NaCl solution for 48 hours, from a test conducted by Lumsden.⁴¹ Lumsden's test explored the effect of Na-to-Cl molar ratio on crevice ECP. An electric heater inside the primary tubing was turned off after 48 hours, and the crevice ECP variation was monitored. As shown in Figure 171(a), the crevice ECP of alloy 600 was lower than that of the bulk solution at MR=1.0, indicating that crevice pH is more alkaline. At MR=0.2 the crevice ECP was higher than that of the bulk solution, indicating that crevice pH is slightly more acidic, as shown in Figure 171(b). Figure 172 shows the measured crevice and bulk Pt potentials in our MR=1.0 test, NaCl-02. When ΔT was changed from 80°F to 40°F, the crevice Pt potentials quickly dropped and gradually recovered, which is a similar behavior to the results in Figure 171(a). As shown in Figure 59 (NaCl-03, MR=0.3), the crevice pH where the molar ratio was 0.3 was more alkaline at $\Delta T=40^\circ\text{F}$ and the beginning of the $\Delta T=60^\circ\text{F}$ test than the bulk solution, but then the crevice pH became gradually acidic. In our MR=0.7 tests, NaCl-04 and -05, the crevice pH was slightly more acidic than the bulk solution, as shown in Figures 76 and 120. Our crevice ECP results where the molar ratio was less than unity appear to be in reasonable agreement with Lumsden's data shown in Figure 171(b).



(a) [Na]/[Cl]=1.0



(b) [Na]/[Cl]=0.2

Figure 171. Crevice ECP after exposure to NaCl solution for 48 hours when the molar ratios of bulk solution was (a) [Na]/[Cl]=1.0 and (b) [Na]/[Cl]=0.2.⁴¹

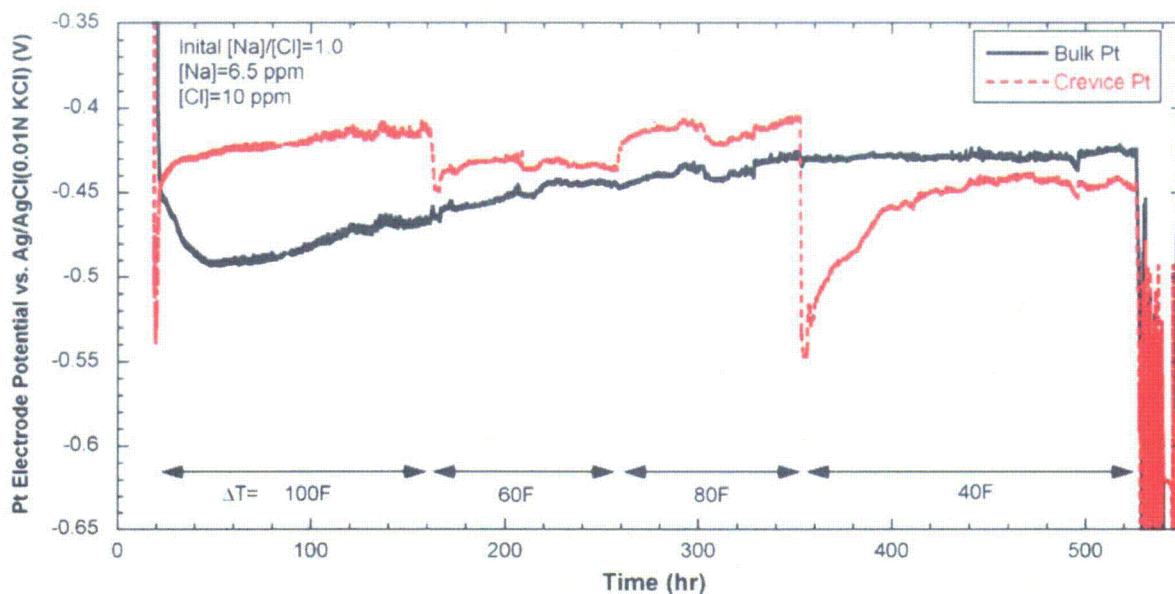


Figure 172. Pt electrode potential variations in bulk and crevice with the molar ratio of 1.0 (NaCl-02 test).

6.2 Comparison with MULTEQ Prediction

The test results for crevice pH and crevice temperature elevation were compared to calculations by the thermodynamic equilibrium code, MULTEQ. Figure 173 shows the crevice pH calculated by the MULTEQ code as a function of boiling point elevation. For the MULTEQ prediction, we assumed that the bulk water chemistry is the same as that in the NaOH-03 test. We selected the “static system” option, which has suboptions: “steam retained” and “steam removed.” It was assumed that precipitates are retained in the system. A static system with “steam retained” means that the liquid phase, the solid precipitates, and the vapor phase stay within the system and no mass exchange occurs through the system boundary.²⁴ It was also assumed that all phases are in thermodynamic equilibrium. In this option, as the calculation step increases, the steam mass fraction increases and the liquid mass fraction decreases. This condition leads to an increase of the impurity concentration in the liquid phase. A static system with “steam removed” is the same system as that with “steam retained” except that the vapor phase formed in each step is removed from the system.²⁴ This system is not closed since vapor can cross the system boundaries. The concentration process is assumed to take place in a series of finite steps, which are specified by the operator. Since this system constitutes a continuous process modeled as finite steps, the final composition is a function of the step size selected by the operator.²⁴ The static system with the “steam removed” models a system with incomplete mixing; the static system with the “steam retained” models a perfectly mixed system. Therefore, if the step size in the “steam removed” option is increased, it is assumed that mixing in the system will become more difficult. Two options can be considered as extreme cases that may occur in actual SG crevices. An actual crevice condition is expected to be somewhere between the two extreme cases. Baum has discussed the crevice pH variation in magnetite-packed crevice as a function of ΔT .³ Figures 173-175 and 178-179 present the calculated results for different options and system conditions.

Figure 173 shows that the calculated crevice pHs with the options of “steam retained” and “steam removed” are the same under the NaOH-03 test condition. The crevice pH increases with increasing

elevation of the boiling point. The largest rate of increase in pH occurs when the boiling point elevation is less than 5°F. The slope of the curve for crevice pH as a function of boiling point elevation is low at relatively high concentrations of Na mainly because the activity coefficient of the Na⁺ ion is lower at higher concentration and soluble NaOH becomes more stable than Na⁺ ion at high Na concentration. The measured crevice pH by the crevice tungsten electrode in the NaOH-03 test as a function of measured crevice boiling point elevation is also plotted in the same figure. The measured boiling point elevation was determined by the difference between the measured crevice temperature and bulk temperature (500°F). The crevice pH becomes close to the prediction results as the boiling point elevation increases and tends to fit with the prediction line. The initial discrepancy at lower elevations in the boiling point appears to be due to the crevice concentration being transient rather than in equilibrium because the lower elevation data in the boiling point were acquired during the transient condition before reaching the saturated state at $\Delta T=40^\circ\text{F}$ and MULTEQ prediction is valid in equilibrium state. Based on the comparison, we inferred that the MULTEQ code prediction and the experimental data at equilibrium state with NaOH bulk chemistry showed a reasonable agreement.

Figure 174 shows the calculated crevice pH as a function of boiling point elevation for a molar ratio of 1.0 and Cl concentration of 10 ppm. As observed in Figure 173, the crevice pH increases with the increase in boiling point elevation, but the crevice pH is about 3 units lower than that of the NaOH-03 test. In Figure 174, the discrepancy between “steam retained” and “steam removed” is not significant but becomes larger as the boiling point elevation increases. This change can be interpreted as the volatility effect of Cl. The NaCl-02 test had a molar ratio of 1.0 but employed no crevice pH electrode. The crevice Pt electrode potential was about 100 mV lower than the bulk Pt potential at $\Delta T=40^\circ\text{F}$, and the bulk pH was 4.4. Assuming the crevice Pt electrode behaves as a hydrogen electrode, the estimated crevice pH is roughly 5.4, and the corresponding crevice temperature elevation is 12°F. The estimated pH from the Pt potentials (pH=5.4) is much lower than the predicted crevice pH (pH=7.5) by MULTEQ at the same temperature elevation. This discrepancy was discussed in Section 4.2.3.

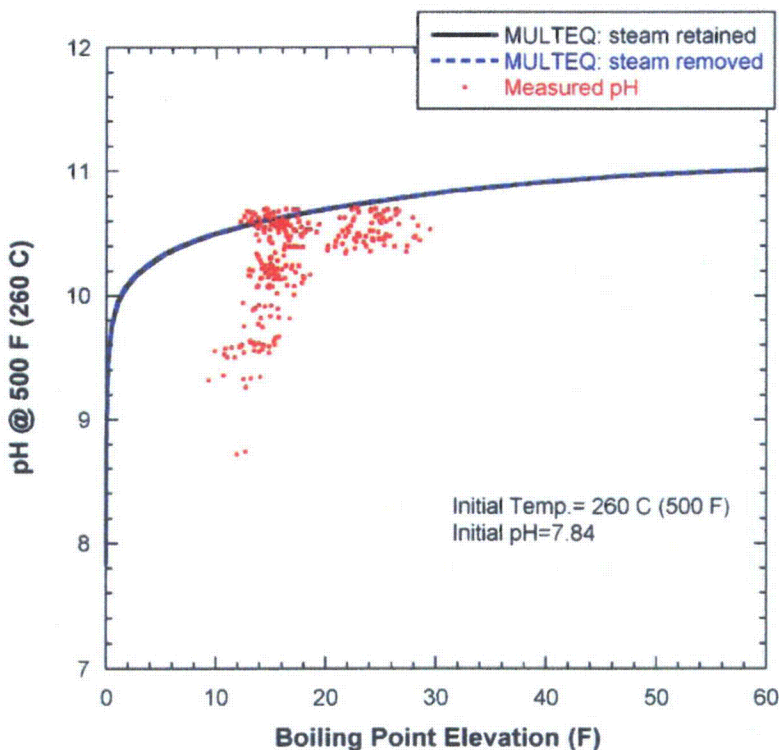


Figure 173.
Calculated crevice pH by MULTEQ as a function of boiling point elevation in comparison to the measured crevice pH based on the crevice tungsten potential data in the NaOH-03 test (nominal [Na]=11.3 ppm and [Cl]=0.6 ppm).

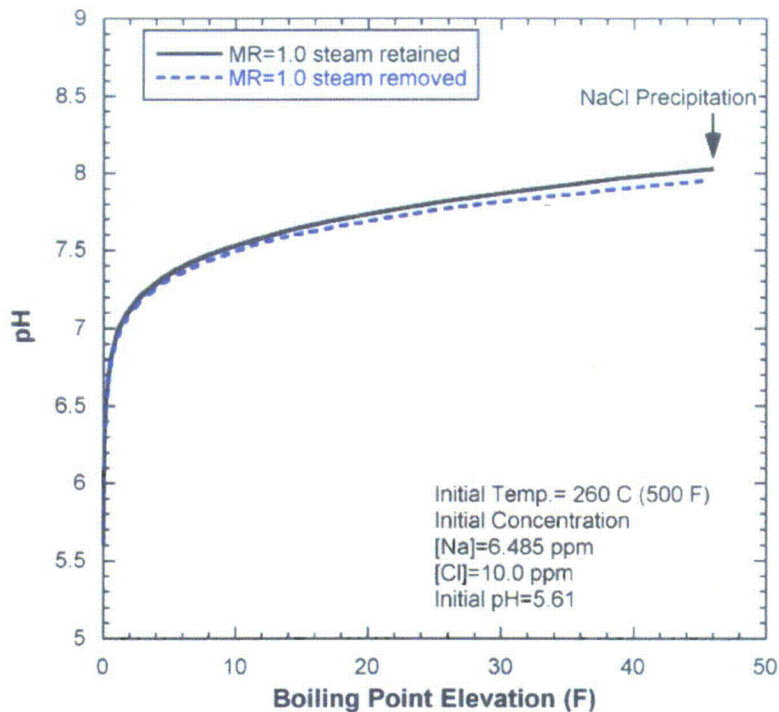


Figure 174.
 Calculated crevice pH by
 MULTEQ as a function of boiling
 point elevation at MR=1.0.

Figure 175 shows the calculated crevice pH by MULTEQ as a function of boiling point elevation for the molar ratio of 0.7 and Cl concentration of 10 ppm. Figure 175 shows a large difference between the two options: “steam retained” and “steam removed.” To interpret the calculation results, each ion’s concentration variation was plotted as a function of concentration factor. The “concentration factor” in MULTEQ is defined as the ratio between the total mass of the system and liquid mass at each calculation step. Figure 176 shows the ion concentration calculation results as a function of concentration factor for the steam retained option. The initial pH decrease can be attributed to the concentration of impurities, as discussed in Figure 44. As the concentration progresses, the molar ratio becomes higher and closer to one due to the volatility of Cl, which makes the crevice pH increase. The further increase of the crevice pH, even though the molar ratio had already reached one, was attributed to the decrease of aqueous HCl concentration. To maintain the equilibrium constant among HCl(aq), H⁺, and Cl⁻, H⁺ should decrease when HCl(aq) decreases because Cl⁻ increases. Figure 177 shows the predicted ion concentrations for the “steam removed” option. The molar ratio becomes close to one at higher concentration factors as compared with the “steam retained” option. This condition makes the crevice pH decrease continuously even at a relatively high concentration factor. The increase in crevice pH can be interpreted as the result of the increase in the molar ratio and the decrease of aqueous HCl concentration. The HCl(aq) concentration in liquid phase with the “steam removed” option is higher than that with the “steam retained” option. In the case of “steam retained”, HCl(aq) should be in equilibrium with the HCl in the vapor phase so that the HCl(aq) concentration cannot be increased continuously. However, in the “steam removed” option, the total mass of the steam phase at each calculation step is much smaller than that of the “steam retained” option. Therefore, the volatilized and lost HCl amount from the liquid phase is smaller, which enables the continuous increase of HCl(aq) concentration as the concentration progresses.

The measured crevice pH as a function of measured crevice boiling point elevation from the NaCl-05 test is also plotted in Figure 175. As was observed for Figure 173, transient phenomena are initially observed at lower boiling point elevations. As the boiling point elevation increases, the crevice pH deviates from the "steam retained" condition. This trend could be attributed to the location of the crevice pH electrode in relation to the tube wall. In the NaCl-05 test the crevice pH electrode was apparently far from the tube wall so that the measured crevice pH does not accurately represent the crevice chemistry on the tube wall.

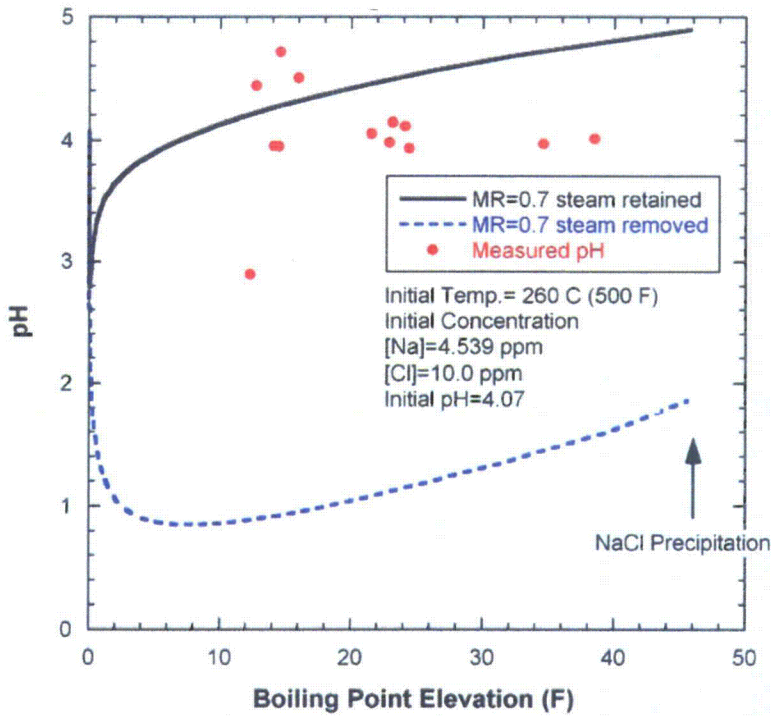


Figure 175. Crevice pH calculated by MULTEQ as a function of boiling point elevation compared to the measured crevice pH based on the crevice tungsten potential data in the NaCl-05 test (MR=0.7).

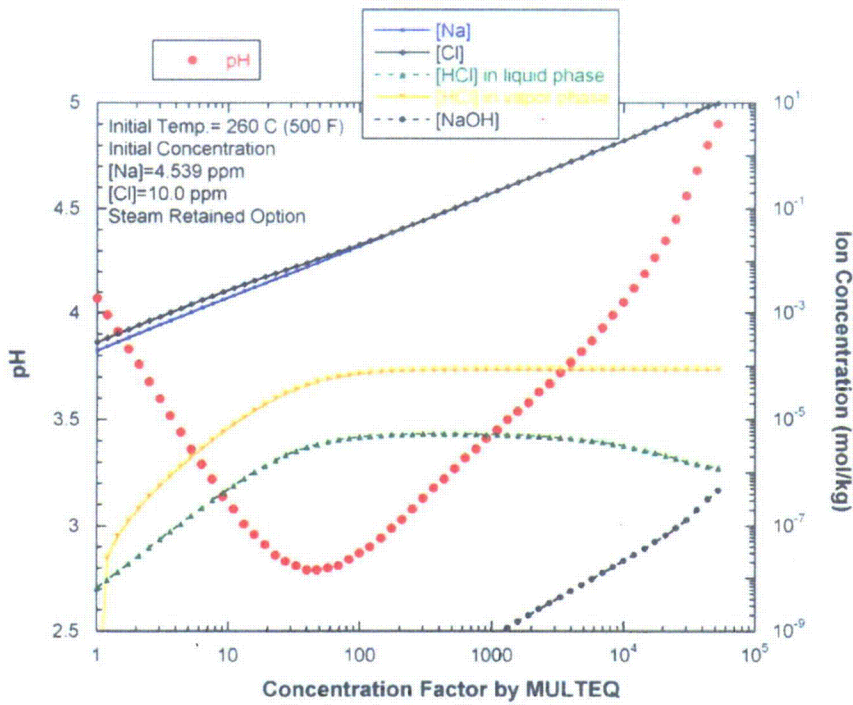


Figure 176. Crevice pH and ion concentration as a function of concentration factor calculated by MULTEQ assuming the "steam retained" condition and MR=0.7.

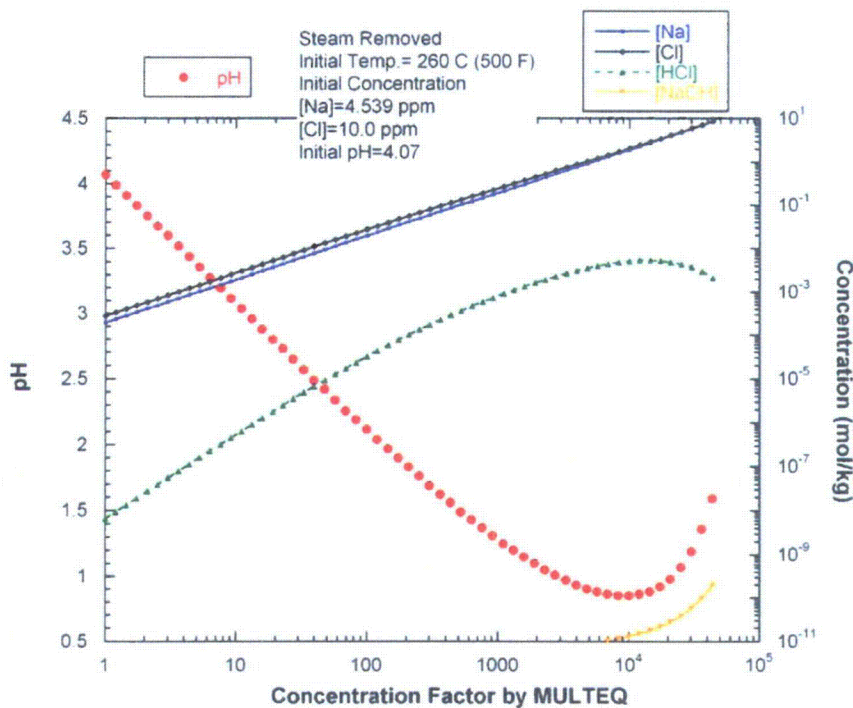


Figure 177. Crevice pH and ion concentration as a function of concentration factor calculated by MULTEQ assuming the "steam removed" condition and MR=0.7.

The crevice pH with respect to the boiling point elevation from the NaCl-06 test is shown in Figure 178. As discussed in Section 5.4.4 and 5.4.6, the crevice pH took a long time to reach steady state because of the complex Na and Cl concentration behavior. The data scatters at lower boiling point elevations

represent the transient crevice condition. The NaCl-06 data show lower crevice pH values than the NaCl-05 data at the same boiling point elevation. This difference appears to be reasonable because the magnetite-packed crevice in NaCl-06 has higher flow restriction and lower permeability than the diamond-packed crevice in NaCl-05, and this condition results in less mixing between liquid and vapor phases, moving the crevice pH closer to the “steam removed” option.

Figure 179 shows the calculated pH as a function of boiling point elevation for a molar ratio of 0.3. The overall pH trend with respect to the boiling point elevation is similar to that with the molar ratio of 0.7 shown in Figure 175, but the absolute pH value is lower at the same boiling point elevation because of the lower Na concentration and molar ratio. The measured crevice pH as a function of the measured boiling point elevation is plotted in the same figure. Even though there is some data scatter, the crevice pH data follow the “steam retained” option curve. Since the diamond-packed crevice in the NaCl-03 test has higher permeability than the magnetite-packed crevice, the measured data were expected to be close to the “steam retained” results. As can be deduced from Figures 176 and 177, the molar ratio does not exceed unity in the MULTEQ calculations. However, the measured or estimated molar ratios in our experiments exceeded unity because of the preferential hideout of Na. Some data located above the line for the steam retained option shown in Figures 178 and 179 may represent more prototypic crevice concentration phenomena. Since these phenomena occur during transient conditions, they are difficult to predict with a chemical equilibrium model like MULTEQ code.

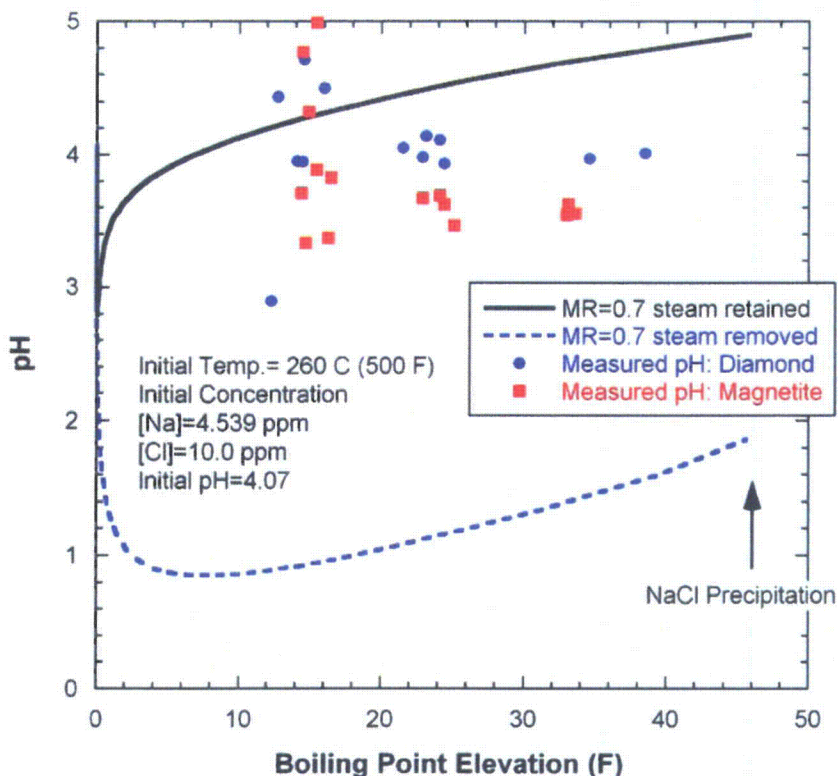


Figure 178.
 Measured crevice pH based on the crevice tungsten potential data in the NaCl-06 test in comparison with the NaCl-05 test and calculated pH by MULTEQ.

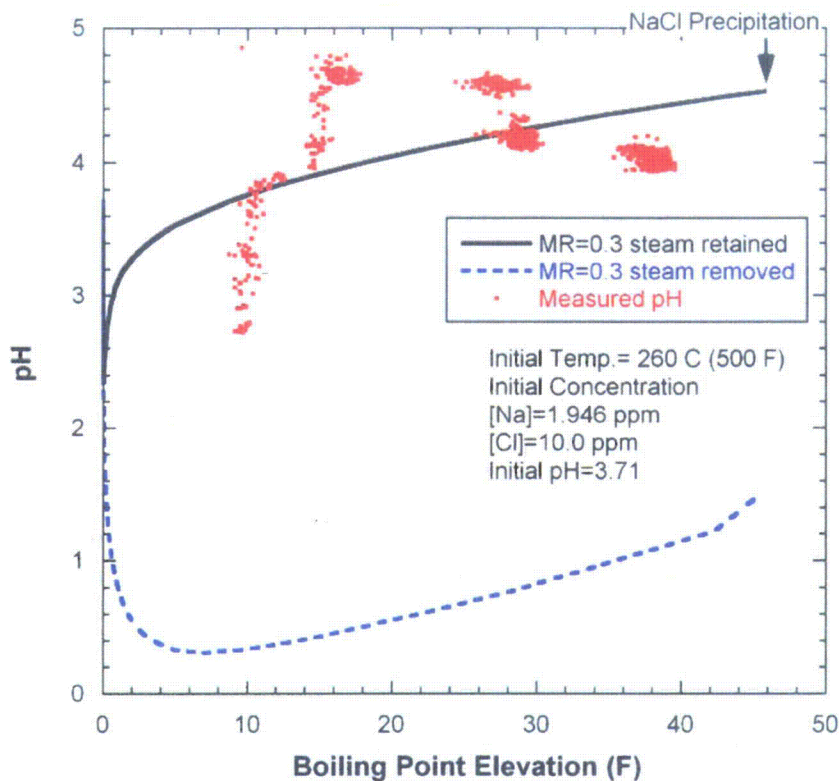


Figure 179. Calculated crevice pH by MULTEQ as a function of boiling point elevation in comparison with measured crevice pH based on the crevice tungsten potential data in the NaCl-03 test.

6.3 Implication of MB Test Results for Operating Steam Generator

6.3.1 Crack Propagation in an Unpacked Crevice

As discussed in Section 5.2.4, we have some preliminary experimental evidence that once a tube crack is formed, the crack itself can act as a crevice that causes, in the presence of NaOH bulk chemistry, the crack to grow even if the sludge or debris is cleaned out of the SG. The alloy 600 tube has been used in the NaOH-01 through NaCl-05 tests. Through-wall cracks in the unpacked crevice were initiated during the NaOH-01 and -02 tests and grew to completely through-wall during the NaOH-03 test which followed the NaCl-01 through NaCl-04 tests. Crack growth under the NaCl-01 and -02 tests where the MR=1.0 was not expected because the 20-mil gap crevice packed with diamond would be in a well-mixed condition, and the molar ratio would be close to a neutral condition. The NaCl-03 and -04 tests where the MR<1.0 may have a chance for crack growth to occur because they had the magnetite-packed crevices which seem to show an initial preference for Na concentration. However, since the initial Na preference was followed by pH neutralization, as observed in the NaCl-06 test, and the magnetite packing porosity of NaCl-03 and -04 was much higher than that of NaCl-06, crack growth in the 20-mil gap crevice did not likely occur during the NaCl-03 and -04 tests. The SCC growth data³⁷ indicated that the crack growth rate at pH=11 is about one order of magnitude higher than that at pH=1 and also suggested that the cracks were more likely to grow in the NaOH test than the NaCl test. However, we did not experimentally confirm that a crack will grow without flow restriction under NaCl rather than NaOH bulk water chemistry. If a crack does not grow in a NaCl solution where there is no restriction to flow, crack growth

would not be expected in an actual SG since the Na-to-Cl MR in most SGs is close to the neutral condition. If a crack does grow under a NaCl solution where there is no restriction to flow, crack growth may occur. It may be worthwhile to grow 50 % through-wall cracks, and then test them in the MB to determine if they will become 100% through-wall without any crevice or packing present under the NaCl and the NaOH bulk water chemistry.

6.3.2 Diamond vs. Magnetite

Diamond has a much higher thermal conductivity than magnetite, which enhances the boiling rate in the crevice and increases the impurity hideout rate. Two parameters characterize packing materials: porosity and permeability. Porosity provides an indication of the available space for liquid to concentrate in the crevice. If the impurity hideout rates are the same, a crevice having lower porosity will reach steady state earlier. Permeability determines how quickly the liquid or vapor phase can penetrate into or escape out of the packed crevice, and how much the liquid and vapor phases can mix in the crevice. The diamond-packed crevices in the MB tests had lower porosity but higher permeability than the magnetite-packed crevice. The diamond-packed crevices can result in an overestimate of the impurity hideout rate. To evaluate the hideout rate realistically, the magnetite-packed crevice test appears to be more appropriate. In one MB test, the packing porosity of the magnetite-packed crevice was 54%, and its permeability was about 0.1 Darcy. The examination of the tubes removed from SGs showed that there was a considerable radial variation in the physical and chemical characteristics of the crevice deposits.⁴ The deposits on the tube side of the crevice were enriched in calcium, magnesium, phosphate, and silicate, while the deposits on the tube support plate side of the crevice were composed of almost 100 % dense (0 % porosity) magnetite. Highly porous magnetite separated the two regions. The tube-side crevice deposits in actual SGs are much denser and have a lower porosity than the magnetite packing in the MB test. The hideout rate in the crevice in actual SGs is expected to be lower than that of our magnetite-packed crevice and the crevice pH is expected to be closer to the prediction result by MULTEQ with the “steam removed” option because of the difficulty in mixing between the liquid and steam phases. These differences suggest that an actual SG crevice compared with our MB test is more acidic at the same ΔT . Further experimental and analytical studies would aid in our understanding of what would occur in actual SG crevices.

6.3.3 Hideout Kinetics Estimation in Actual SG Crevices

In an actual SG crevice packed with magnetite, the kinetics of the impurity concentration will be much slower than experienced in the MB tests because the impurity concentrations in the SG will be much less (i.e. in the ppb range), even if the packing porosity and permeability are assumed to be the same as in the current MB test. Also, the total exposed time in an actual SG crevice will be much longer than that in the MB test. If the exposed time is long enough, however, the crevice impurity concentration in an actual SG crevice can become as high as in the MB test. If the exposed time is not long enough, the actual SG crevice may not reach a steady-state condition after one fuel cycle. Longer-term MB experiments with more dilute impurity concentration in the bulk solution and a theoretical model for predicting the long-term crevice concentration behavior with ppb-range impurity may be useful.

Based on the Na and Cl hideout behavior in the magnetite-packed crevice test, NaCl-06 (Figure 159), the hideout rates of Na and Cl as a function of ΔT were estimated, as shown in Figure 180. The hideout rates of Na are always higher than those of Cl. One data point, labeled “Cl hideout rate after Na saturation,” indicates the measured hideout rate when the delayed preferential Cl concentration occurred at $\Delta T=40^\circ\text{F}$, as shown in Figure 159. This hideout rate data can be used to independently estimate the hideout rate for Na and Cl in an actual SG crevice.

To determine the hideout rate in an actual SG, the physical characteristics in an actual SG crevice must be known. Baum's assumption⁵ for the tube-side deposits was introduced in this estimation; the deposit layer was assumed to extend 38 μm and have 10 % porosity. The total crevice depth was assumed to be 25.4 mm (1 in.). Actual crevice gap size would be larger than 38 μm , but in this estimation we focus on the hideout characteristics of the tube-side deposits. The total pore volume is about 7×10^{-3} mL. The assumed crevice would have a lower permeability than that in the NaCl-06 test, but for a simple estimation, we assumed that the deposits have a similar permeability to that in the NaCl-06 test. Because the bulk impurity concentration in an actual SG is much lower than that of MB tests, it will take more time to reach a certain concentration level for Na or Cl. The ΔT was assumed to be 60°F because this temperature is closer to the ΔT in an actual SG. The bulk solution concentration for Na and Cl was assumed to be 1 and 2 ppb, respectively, to maintain the molar ratio of 0.7 used in NaCl-06 and to represent actual impurity concentrations in SGs. For the Na hideout rate, the measured hideout rate at $\Delta T=60^\circ\text{F}$ was chosen, and the Na concentration was assumed to continuously increase until it reached the thermodynamic limit of NaOH at $\Delta T=60^\circ\text{F}$. For the initial Cl hideout rate, the measured Cl hideout rate at $\Delta T=40^\circ\text{F}$ was used instead of that at $\Delta T=60^\circ\text{F}$. Baum noted that the loss of acidity on the tube wall becomes more significant with the increase in ΔT ,³ and NaCl-06 started with a ΔT of 40°F, which was increased 362 hours later to 60°F. Therefore, the measured Cl hideout rate at $\Delta T=60^\circ\text{F}$ is expected to be affected by the test results at $\Delta T=40^\circ\text{F}$. If the ΔT starts at 60°F, the Cl hideout rate is expected to be similar or even lower than the one measured at 40°F in the NaCl-06 test. The Cl hideout rate is assumed to change when the Na concentration reaches the thermodynamic limit at $\Delta T=60^\circ\text{F}$. Based on the results at $\Delta T=40^\circ\text{F}$ in the NaCl-06 test, the Cl concentration started to increase rapidly when the Na concentration reached about 80 % of the saturation level, and the Na hideout rate became lower. In this estimation, the hideout behavior of an actual SG crevice is determined qualitatively rather than quantitatively, so that a simple assumption for the Cl hideout rate change was introduced.

Figure 181 shows a schematic of Na and Cl hideout mass variations in the assumed crevice deposits as a function of time. Even after a typical fuel cycle (approximately 15 months or 10,800 hours), the Na concentration did not reach the solubility limit at $\Delta T=60^\circ\text{F}$. The average Na-to-Cl molar ratio in the crevice always remains higher than one, indicating the development of an alkaline crevice during one fuel cycle. If the actual hideout rate in a SG crevice is lower than the estimated value, which is a credible assumption because the crevice deposits in a SG would have lower permeability than that in the MB test, the actual crevice condition could be more likely in an alkaline condition during one fuel cycle. Even though the assumptions for this estimation introduce uncertainties, the estimated concentrations in the actual SG crevice deposits near the tube wall indicate that the crevice concentration is likely to be in a transient condition during a typical fuel cycle. It is also expected that the crevice pH near the tube wall remains alkaline for this time period. Therefore, to lead additional insights into the behavior of an actual SG crevice, it may be more important to focus on the kinetics of impurity hideout rather than the steady-state conditions. However, this estimation assumes that impurity in the actual SG crevice is not present at the beginning of a fuel cycle, which may not be true. Some of impurities accumulated during a typical fuel cycle may remain in the crevice after shutdown rather than return to the bulk water. These remaining impurities can affect the crevice chemistry for the next fuel cycle.

A magnetite-packed crevice test having low bulk impurity concentration could be conducted for a relatively long time. The total exposure of Na or Cl under actual SG conditions during one fuel cycle is less than 100 ppm-hr. If the bulk concentration in a laboratory test is 1 ppm, the total test time should be more than 100 hours to simulate one fuel cycle. Whether or not the ppm-range bulk concentration test results can be extrapolated to the ppb range is a different issue. Baum suggested that the acidity loss is likely to become more significant with a decrease in bulk concentration, which will make the crevice pH more alkaline.³ To evaluate how the remaining impurities in the crevice after shutdown affect the crevice

chemistry for the next fuel cycle, the test can be stopped after 100 ppm-hr operation and resumed without opening the MB secondary chamber.

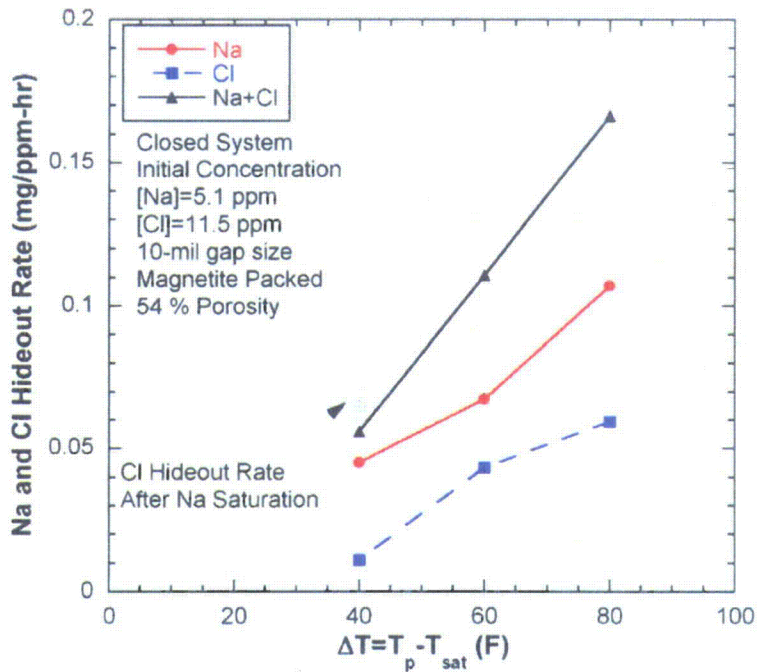


Figure 180. Initial Na and Cl hideout rates as a function of the temperature difference between primary and secondary saturation temperatures (NaCl-06).

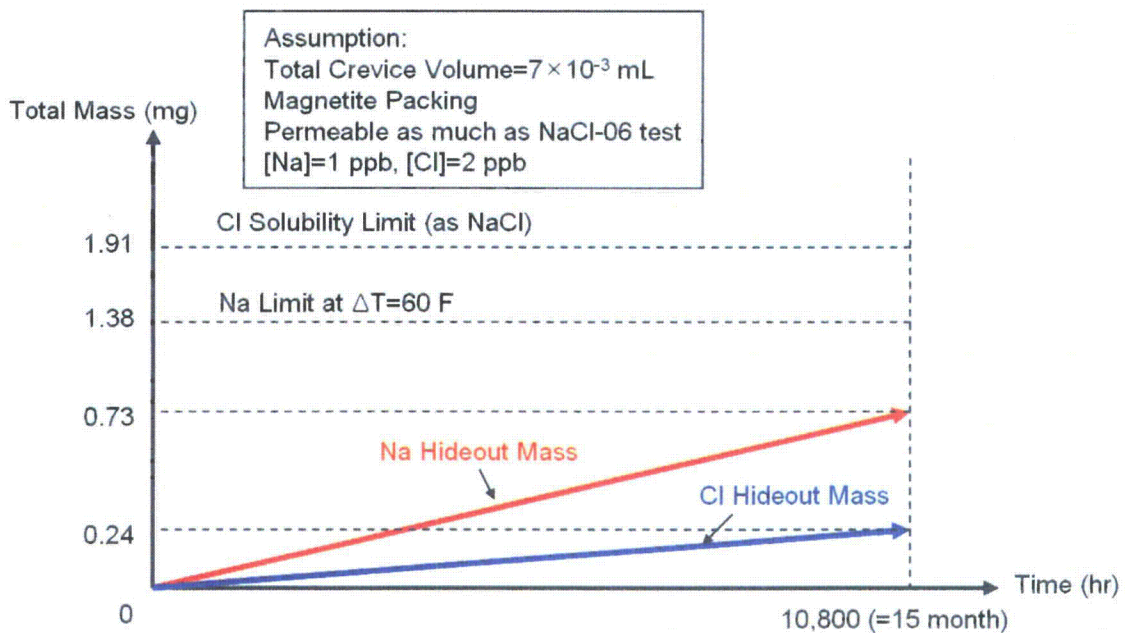


Figure 181. Schematic of Na and Cl hideout mass variations as a function of time in a crevice where the porosity and secondary impurity level are assumed to be similar to those in actual SGs.

6.3.4 Dependency of Cl Volatility Effect on Molar Ratio

The dependency of the Cl volatility effect on bulk concentration and ΔT was discussed by Baum.³ Lower bulk concentration and higher ΔT tends to make the volatility effect of Cl more significant. The dependency of the Cl volatility effect on the Na-to-Cl molar ratio has not been discussed before. This issue is discussed from two points of view here: molar ratio and crevice and bulk tungsten potentials.

Figure 182 shows the molar ratios in crevice samples with respect to those in bulk samples for the diamond-packed crevices. The crevice MRs decrease with the decrease of bulk MRs. The crevice MR data for MR=1.0 is scattered, depending on ΔT . If the Cl volatility effect does not depend on molar ratio, all data points should fit on a single line parallel to the solid line in the figure representing a 1:1 correlation line. In Figure 182, as the bulk MR decreases, the crevice MR tends to deviate from the 1:1 line; this deviance suggests that the Cl volatility effect becomes more significant with the decrease in the bulk MR. If experimental data are acquired for a bulk solution MR of 0.1 or 0.2, the data trend should become clearer.

Figure 183 shows the molar ratio of crevice samples as a function of the MR in the bulk sample for a magnetite-packed crevice. As compared with the diamond-packed crevice data, the number of data points is relatively small with regard to deriving a firm conclusion. One clear difference from the results shown in Figure 182 is that the crevice MRs are close to the bulk MRs, and some data show even lower values than the bulk MRs. This finding needs to be carefully interpreted because all these data were obtained at $\Delta T=80^\circ\text{F}$. At high ΔT a less permeable crevice like a magnetite-packed crevice tends to be filled with steam, and the extracted samples from this crevice show higher Cl concentrations because the steam contains HCl which is condensed and extracted from the crevice. In the magnetite-packed crevice, as discussed in Section 6.3.3, the crevice chemistry is dependent on the exposure time. The crevice data used in Figure 183 represent only the data under a saturated state at each ΔT . Although the data sets are limited, we concluded that, as compared with a relatively permeable crevice like the diamond-packed crevice, the Cl volatility effect in the magnetite-packed crevice is less significant at a saturated state because it becomes more difficult for Cl to escape from the heated tube-wall surface in less permeable packing. Baum also mentioned that the acidity loss on the tube wall becomes less significant with a decrease in packing porosity.³ To further evaluate the dependency of Cl volatility on the molar ratio in the magnetite-packed crevice quantitatively, additional tests should be considered.

We evaluated the dependency of Cl volatility on the molar ratio from the crevice and bulk ECPs. At a molar ratio of 0.3, as shown in Figure 59, the crevice tungsten potentials were lower than the bulk tungsten potentials at $\Delta T=40^\circ\text{F}$ and were mixed (some higher, some lower) at $\Delta T=60^\circ\text{F}$. When the bulk MR was 0.7, the NaCl-04 and -05 test results showed that, during most of the test time, the crevice tungsten potentials did not deviate much from the bulk tungsten potentials, as shown in Figures 76 and 120, respectively. At a bulk MR of 1.0, as shown in Figure 43, the Pt potentials indicated alkaline crevice chemistry at low ΔT . The crevice tungsten potentials in the diamond-packed crevices are reasonably consistent with the results from the molar ratio analysis shown in Figure 182. Since we conducted only one highly packed crevice test with magnetite, we cannot reach a firm conclusion about the Cl volatility dependency on molar ratios. For the magnetite-packed crevice, it is more important to focus on the effect of molar ratio on the hideout kinetics rather than the saturation condition in the crevice as a function of molar ratio.

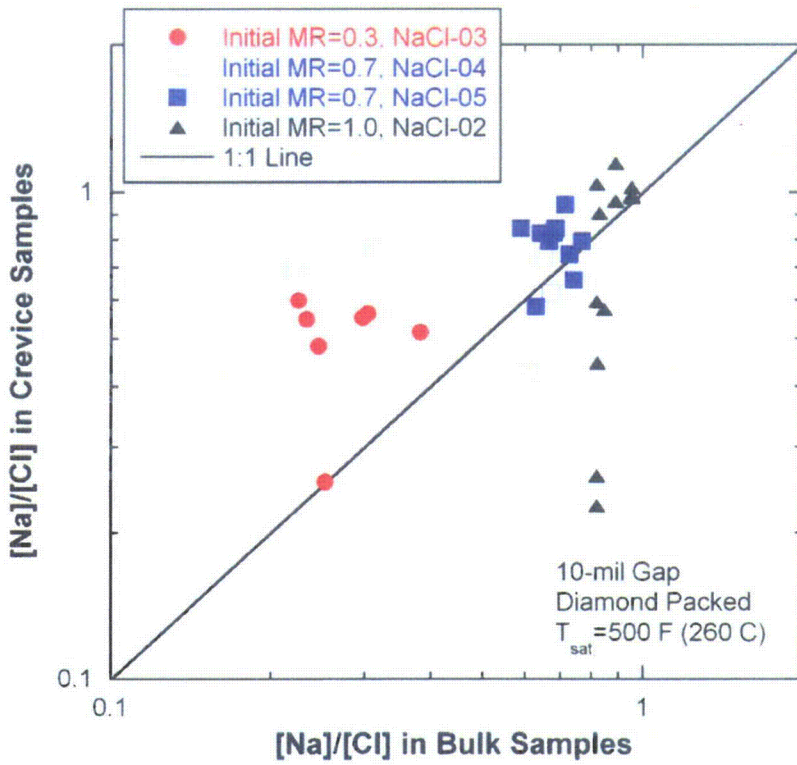


Figure 182.
Molar ratio in crevice sample as a function of the molar ratio in the bulk sample for a diamond-packed crevice.

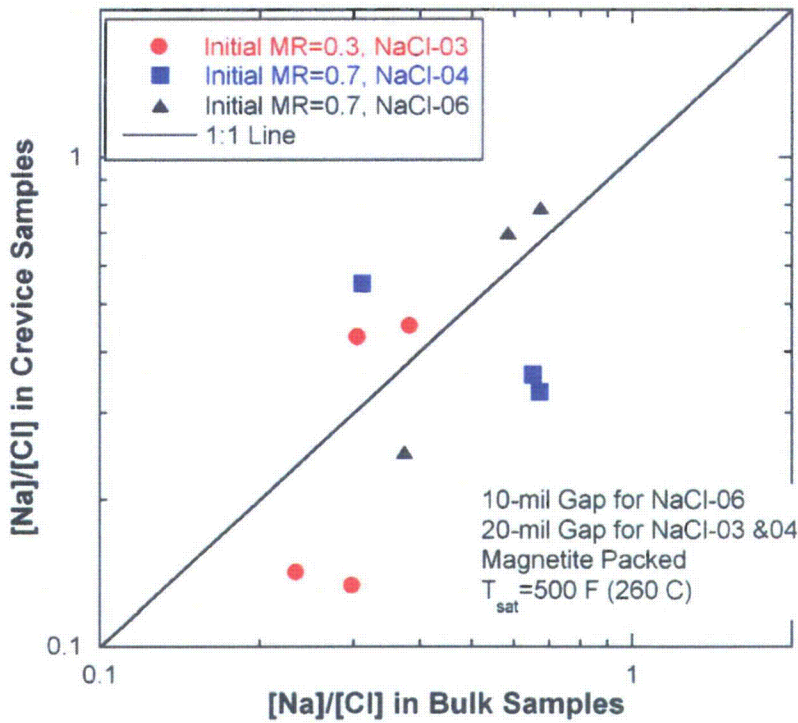


Figure 183.
Molar ratio in crevice sample as a function of the molar ratio in the bulk sample for a magnetite-packed crevice.

6.3.5 Cl Adsorption to Magnetite

The Cl adsorption to magnetite was not likely to be verified experimentally through the MB crevice tests. However, the initial bulk conductivity reduction in the magnetite-packed crevice tests indicates the possibility of Cl adsorption to magnetite. Figure 184 shows the normalized bulk conductivity variation with time from the beginning of each test for $\Delta T=40^\circ\text{F}$. All test results for a magnetite-packed crevice showed rapid reductions of bulk conductivity for 1-2 hours from the beginning of the test. Then, the rate of reduction in bulk conductivity became smaller until they were nearly constant. The bulk conductivity data for the diamond-packed crevice tests did not exhibit this behavior. The hideout rate mainly depends on the heat flux and the total area where nucleate boiling can occur. At the given crevice physical and thermal conditions, the hideout rate will not change until it becomes close to the saturation limit. Therefore, the initial rapid reduction in bulk conductivity suggests a different hideout mechanism for the magnetite-packed crevices. The Cl adsorption to magnetite can be considered as a driving force for impurity hideout at the beginning of a test. This factor becomes less significant with time because the available adsorption sites are limited under a given magnetite-packing condition.

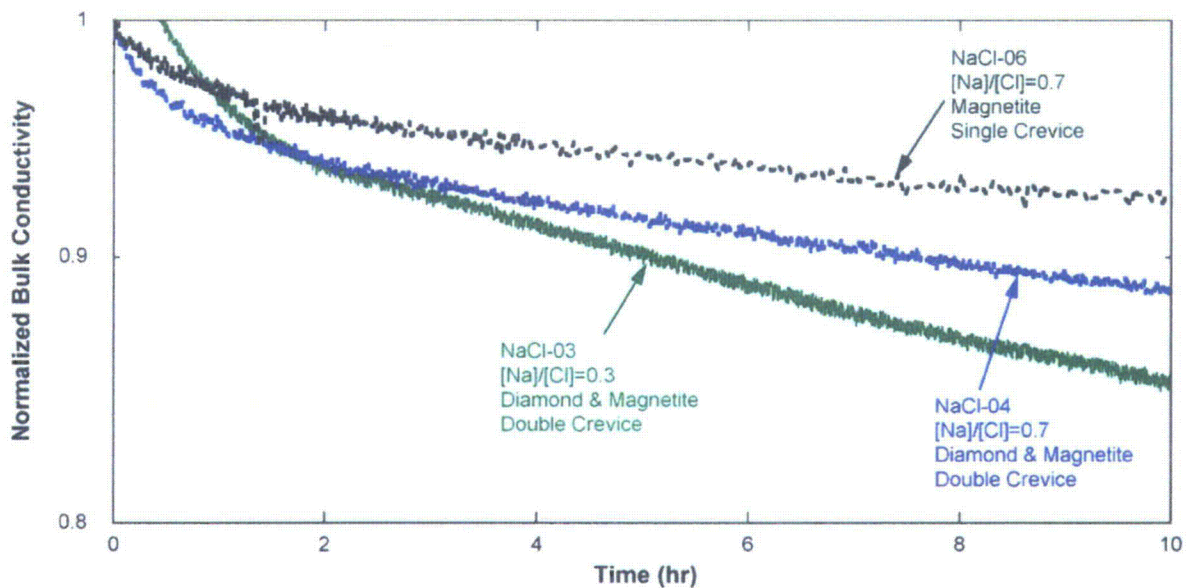


Figure 184. Normalized bulk conductivity variations with time from the beginning of each test at $\Delta T=40^\circ\text{F}$.

6.3.6 Electromigration Effect in the Crevice

Electromigration refers to ion movement due to a difference in electrical potential. The mass transport in solution usually depends on convection and diffusion. If the solution has a charge, electromigration is possible. In a heated crevice where boiling occurs, there are liquid and steam phases. The dissolved oxygen level is very low. Therefore, electromigration is not likely to be a dominant factor for impurity transport. However, electromigration was experimentally observed for some crevice tests. Electromigration requires an electric potential gradient between the crevice and bulk solution. Under a deaerated condition, if metal cations are dissolved in the crevice as a result of tube corrosion or magnetite dissolution, the electric potential in the crevice becomes higher than that in the bulk solution, and this condition drives Cl ions into and Na ions out of the crevice. In the NaCl-03 test, at $\Delta T=60^\circ\text{F}$ the bulk

conductivity increased slightly when the bulk Na concentration increased and Cl concentration remained almost constant, as shown in Figure 53. In the NaCl-05 test at the same ΔT , the bulk conductivity did not vary significantly but the Na concentration increased and the Cl concentration decreased in the bulk solution, as shown in Figure 117. The post-test examinations for the two tests indicated heavy gouging of the tubing. The two test results appear to prove that electromigration occurred in the diamond-packed crevice. Whether electromigration occurred in the magnetite-packed crevice is not clear from our test results. The tube surfaces after NaCl-06 did not show any gouging, and it is uncertain whether metal cations might have come from the dissolution of the magnetite packing materials. Electromigration in a magnetite-packed crevice, if it will happen, appears to take a long time because the impurity hideout rate is very low. Furthermore, it takes time to reach an impurity level that can generate tube corrosion. In an actual SG crevice packed with deposits, as discussed in Section 6.3.3, the crevice pH would be alkaline or neutral during a typical fuel cycle. In an actual SG crevice, one fuel cycle is not long enough for tube corrosion and electromigration to occur. Also, the high packing density of the actual crevice will hinder the movement of ions. However, if some of impurities remain in the crevice after each fuel cycle, tube corrosion and electromigration may occur after several fuel cycles.

6.3.7 Hard Scales Formed on the Tube Surfaces

Black and hard magnetite deposits were observed on the tube surfaces in the crevice region during several crevice tests: NaOH-03 and NaCl-05 packed with diamond and NaCl-06 packed with magnetite. In the NaOH-03 test, black deposits were found mainly near the crevice mouth region, as shown in Figure 102. Similar black deposits were also found in the NaCl-05 test at similar locations, as shown in Figure 123. At the crevice mouth region, mixing between the crevice and bulk solution is active so that concentration of the impurities will be relatively low, and the resultant chemical condition such as pH will not be severe, near to a neutral condition. Therefore, magnetite solubility is expected to be low, and this low solubility makes it easy for magnetite deposits to be formed in that area. Deeper into the crevice, the impurities are further concentrated, and the resultant crevice pH becomes corrosive. Consequently, tube corrosion occurs so that the black deposits are not likely to be formed.

In the NaCl-06 test, black deposits were also formed in the crevice mouth area, as shown in Figure 152. Since the magnetite particles filled the crevice, the hard magnetite deposits appear to form and consolidate easier than for the two tests packed with diamond powders. In an actual SG, the bulk Fe concentration is roughly estimated as 1 ppb, and the total operation time for one cycle is roughly 10^4 hours. Therefore, the total Fe exposure is 10 ppm-hr. The bulk Fe concentration in the NaCl-06 test was within the range of 0.5-1.0 ppm, and the total test time was 700 hours. The total test times of NaOH-03 and NaCl-05 tests were 400 and 700 hours, respectively. If the bulk Fe concentration of the three tests were within the same range, the estimated total Fe exposure of our tests would be 200-700 ppm-hr, which is equivalent to at least 20 fuel cycles for an actual SG. Since we do not know when the deposits actually started to form during the MB tests, the deposits in actual SGs are expected to form earlier than 20 cycles.

7. Summary

7.1 Conclusions

At Argonne National Laboratory, a MB system that can simulate prototypical thermal hydraulic and chemistry conditions of the secondary side of SGs in PWRs was developed. The facility has prototypic crevice heat fluxes and temperatures thus permitting the development of more prototypic crevice chemistry conditions. A crevice simulator equipped with various instrumentations, including thermocouples, ECP electrodes, pH electrodes, conductivity probes, and solution sampling lines, was developed and successfully operated. To measure the pH in the bulk solution and crevice, we used a tungsten/tungsten oxide (W/WO_x) electrode. The W/WO_x electrode served as a pH electrode in the pH range of 4-8 under NaCl or NaOH water chemistry. The potential slope with respect to pH variation was -103 mV/pH, which is close to the Nernstian slope of -106 mV/pH at 260°C (500°F). The behavior of the W/WO_x electrode was consistent with that reported in earlier work²⁹.

We reached the following conclusions from the MB test results:

- ◆ Diamond powder has a very high thermal conductivity as compared with magnetite powder, which can enhance the boiling rate and lead to higher impurity hideout rates. High permeability of diamond packing allows active mixing inside the crevice and the liquid and steam phases can transport easily in and out of the crevice. In some tests, the diamond-packed crevice concentration did not reach the thermodynamic limit, while in the magnetite-packed crevice the concentration was thermodynamically limited under the same thermal conditions. To simulate actual SG crevices, a magnetite-packed crevice having a lower permeability is more appropriate than a diamond-packed crevice, since a diamond-packed crevice can lead to an overestimate of the crevice hideout rate.
- ◆ In a magnetite-packed crevice test (NaCl-06), bulk sample analyses indicated that Na was preferentially concentrated until it reached the thermodynamic limit at a given ΔT , followed by delayed Cl preferential concentration. The W/WO_x electrode installed near the tube wall supported the observations of these Na and Cl concentrations and also the W/WO_x electrodes indicated the radial chemistry gradients in the magnetite-packed crevice, which is consistent with literature information³.
- ◆ Based on the hideout rates for Na and Cl in the magnetite-packed crevice (NaCl-06), the chemistry variation in the deposits in an actual SG crevice near the tube wall was estimated. During a typical fuel cycle, the crevice chemistry was in a transient rather than a steady-state condition, mainly because of the low impurity concentration in the bulk solution. The estimated average crevice pH was always alkaline because of the initial preferential Na concentration unless some impurities remain and accumulate in the crevice after each fuel cycle. The kinetic data for the crevice hideout with low bulk impurity concentration are helpful for estimating the actual variations in SG crevice chemistry.
- ◆ Based on the analyses of the crevice and bulk solution samples at a saturated state, the volatility effect of Cl for the diamond-packed crevices becomes significant as the MR decreases. For the magnetite-packed crevice, available data are limited, but it is likely that the volatility effect of Cl at a saturated state is not as significant as it is for the diamond-packed crevice and it is not dependent on the bulk MR variation.
- ◆ The Cl adsorption onto magnetite was not verified through our current series of tests. However, the reduction in bulk conductivity from the initial value in the magnetite-packed crevice tests indicates possible Cl adsorption to magnetite.
- ◆ Electromigration in the crevice was observed especially when the tube corrosion was severe

under strongly acidic crevice chemistry. But in an actual SG crevice, electromigration in the packed crevice is not likely because bulk impurity concentration is very low and one fuel cycle (about 10^4 hr) is not long enough for tubes to corrode to the point that it results in electromigration unless some impurities remain in the crevice after each fuel cycle and accumulate over several fuel cycles.

- ◆ The crevice pH predicted by the MULTEQ[®] code was compared with the measured crevice pH as a function of boiling point elevation. The test results in diamond-packed crevices followed the “steam retained” option. In a magnetite-packed crevice, the measured pH at steady state was lower than that in the diamond-packed crevice and deviated from the “steam retained” option. In a less permeable crevice, the volatility of Cl becomes less significant because Cl does not easily escape. This condition led to a lowering of the crevice pH near the tube wall. However, since the transient behavior is more important in actual SG crevice deposits, the calculations with a thermodynamic equilibrium code have limited applicability.
- ◆ The MB tests showed some initial evidence that once a crack is formed, the crack itself can act as a crevice. In the NaOH bulk chemistry, this crack can grow even if the sludge or debris is cleaned out of the SG. It would be valuable to confirm whether the crack itself can act as a crevice in other bulk water chemistry regimes such as a NaCl chemistry regime.

7.2 Future Work

From the current test results and analyses, the following additional investigations may provide a better understanding of SG heated crevices:

- ◆ Conduct MB experiments to determine whether a 50 % through-wall crack would grow in the absence of any crevice or packing under NaOH or NaCl bulk water chemistry.
- ◆ Further evaluate the permeability effect on the crevice hideout kinetics in magnetite-packed crevice tests with a lower packing porosity. Considering the porosity of actual SG crevice deposits, a porosity of less than 50 % is required.
- ◆ Conduct MB hideout tests with magnetite-packed crevice and MR=0.3 and 1.0 for comparison with the MR=0.7 test results. From these tests, the molar ratio effect on the crevice hideout behavior in the magnetite-packed crevice can be further explored.
- ◆ Perform MB tests with low impurity concentration in the bulk solution. The impurity level in the secondary water of an actual SG is in the ppb range. Since the total impurity exposures of Na and Cl during one fuel cycle are around 100 ppm-hr, tests having 1-ppm bulk impurity may be appropriate. However, the volatility effect of Cl tends to become significant as the Cl concentration becomes low. Therefore, theoretical modeling should be considered for extrapolating the MB test results to actual SG crevices.
- ◆ Explore the complex solution chemistry involved with sodium, chloride, and sulfate. Sulfate is another major impurity in the secondary water of SGs. Since the concentration of sulfate is likely to be affected by adsorption onto magnetite powder, the magnetite-packed crevice tests with sulfate water chemistry should be considered.

8 References

1. D. R. Diercks, W. J. Shack, and J. Muscara, "Overview of Steam Generator Tube Degradation and Integrity Issues," *Nucl. Eng. Design*, 194: 19-30, 1999. Copyright permission is granted by EPRI.
2. G. M. W. Mann and R. Castle, "Hideout and Return of Chloride Salts in Heated Crevices Prototypic of Support Plates in Steam Generators," EPRI NP-5015, Electric Power Research Institute, January 1987. Copyright permission is granted by EPRI.
3. Allen Baum, "Experimental Evaluation of Tube Support Plate Crevice Chemistry," *Proc. 10th Int. Conf. Environmental Degradation of Materials in Nuclear Power Systems-Water Reactors*, National Association of Corrosion Engineers, 2002.
4. L. Albertin et al., "Characterization of Deposits in Dampierre-1 Steam Generator Support Plate Crevices," *Proc. 7th Int. Symp. Environmental Degradation of Materials in Nuclear Power Systems-Water Reactors*, Breckenridge, Colorado, National Association of Corrosion Engineers, pp. 399-409, 1995.
5. A. Baum and K. Evans, "Modeling Concentrated Solution Transport and Accumulation in Steam Generator Tube Support Plate Crevices," *12th Int. Conf. Environmental Degradation of Materials in Nuclear Power System-Water Reactors*, Minerals, Metals & Materials Society, 2005. Copyright permission is granted by TMS.
6. A. J. Baum, "Restricted Geometries and Deposits," in *The ASME Handbook on Water Technology for Thermal Power Systems*, ed., P. Cohen, American Society of Mechanical Engineers, Chapter 6-3, 1989.
7. R. W. Staehle and J. A. Gorman, "Progress in Understanding and Mitigating Corrosion on the Secondary Side in PWR Steam Generators," Special Bonus Paper, *Proc. 10th Int. Conf. Environmental Degradation of Materials in Nuclear Power Systems-Water Reactors*, Lake Tahoe, Nevada, National Association of Corrosion Engineers, Aug. 5-9, 2001.
8. "Heated Crevice Seminar," NUREG/CP-0189, U.S. Nuclear Regulatory Commission, Washington D.C., February 2005.
9. R. E. Hermer, R. J. Jacko, A. Kishida, and H. Takamatsu, "The Measurement of Simulated Steam Generator Crevices," *Proc. 3rd Int. Symp. Environmental Degradation of Materials in Nuclear Power Systems-Water Reactors*, Traverse City, Michigan, Metallurgical Society, pp. 199-207, 1987.
10. Damien Feron, "Electrochemical Measurements in PWR Steam Generators to Follow Crevice Chemistry," Paper No. A-44, *Proc. JAIF Int. Conf. Water Chemistry in Nuclear Power Plants*, Fukui City, Japan, 1991.
11. A. M. Brennenstuhl, A. McBride, and D. Graham, "An Assessment of High Temperature Electrochemical Noise to Monitor the Effects of Chemical Excursions on the Corrosion Response of UNS N08800 Nuclear Steam Generator Tubes," *Proc. 8th Int. Symp. Environmental Degradation of Materials in Nuclear Power Systems-Water Reactors*, Amelia Island, FL, American Nuclear Society, pp. 3-10, 1997.

12. J. B. Lumsden, G. A. Pollock, P. J. Stocker, P. J. Millett, and C. Fauchon, "Hideout in Prototypic Tube/Tube Support Plate Heated Crevices," Proc. 8th Int. Symp. Environmental Degradation of Materials in Nuclear Power Systems-Water Reactors, Amelia Island, FL, American Nuclear Society, pp. 108-112, 1997.
13. J. B. Lumsden, G. A. Pollock, P. J. Millett, N. Torigoe, and H. Takamatsu, "Effects of the Feedwater Sodium/Chloride Ratio and Hydrazine on Crevice Chemistry," Proc. 9th Int. Symp. Environmental Degradation of Materials in Nuclear Power Systems-Water Reactors, Newport Beach, CA, Minerals, Metals, and Materials Society, August 1-5, 545-554, pp. 1999.
14. H. Kawamura and H. Hirano, "Estimation of Impurity Concentration Factor on Boiling Heat Transfer Surface within Tube-Tube Support Plate Crevice using Corrosion Potential Measurement Technique," Proc. Int. Conf. Water Chemistry in Nuclear Power Plants: Water Chemistry '98, JAIF, Kashiwazaki, Japan, pp. 546-553, October 1998.
15. H. Kawamura and H. Hirano, "Estimating the Impurity Concentration Factor on the Boiling Heat Transfer Surface of a Simulated Steam Generator Tube-Support-Plate Crevice Using an In Situ High-Temperature Conductivity Measurement Technique," Nucl. Tech. 129: 398-406, 2000.
16. A. Baum, "Relationships between Boiling Regimes and Chemical Concentration Processes in Tube Support Plate Crevices," Int. Conf. Water Chemistry in Nuclear Power Systems, SFEN, Avignon, France, April 2002.
17. P. V. Balakrishnan and G. L. Strati, "Laboratory Experiments on Steam Generator Crevice Chemistry," Heated Crevice Seminar, NUREG/CP-0189, U.S. Nuclear Regulatory Commission, Washington D.C., p. 319, February 2005.
18. C. B. Bahn, S. H. Oh, B. G. Park, I. S. Hwang, I. H. Rhee, U. C. Kim, and J. W. Na, "Impurity Concentration Behaviors in a Boiling Tubesheet Crevice: Part II. Packed Crevice," Nucl. Eng. Design, 225: 145-157, 2003.
19. P. J. Millett, "Theoretical and Experimental Investigation of Local Concentration Processes in PWR Steam Generators," Ph.D. Thesis, University of Connecticut, 1991.
20. P. J. Millett and J. M. Fenton, "A Modeling Study of Parameters Controlling Local Concentration Processes in Pressurized Water Reactor Steam Generators," Nucl. Tech. 108: 256-265, 1994.
21. G. R. Engelhardt and D. D. Macdonald, "Transport Processes in Steam Generator Crevices. I. General Corrosion Model," Corr. Sci. 41: 2165-2190, 1999.
22. G. R. Engelhardt, D. D. Macdonald, and P. J. Millett, "Transport Processes in Steam Generator Crevices. II. A Simplified Method for Estimating Impurity Accumulation Rates," Corr. Sci. 41: 2191-2211, 1999.
23. Céline L. Fauchon, "Development and Testing of an Electrochemical Model for PWR Steam Generators Crevice Environment," Master Thesis, Massachusetts Institute of Technology, February 2000.

24. "MULTEQ: Equilibrium of an Electrolytic Solution With Vapor-Liquid Partitioning," Volume 3, *Theory Manual*, EPRI NP-5561-CCML, Electric Power Research Institute, Palo Alto, CA, August 1992.
25. K. E. Kasza, J. J. Oras, B. L. Fisher, J. Y. Park, J. E. Franklin, and W. J. Shack, "Argonne Model Boiler Facility: Topical Report," NUREG/CR-6880, U.S. Nuclear Regulatory Commission, Washington D.C., 2005.
26. Gilbert W. Castellan, *Physical Chemistry*, 3rd Ed., Addison Wesley Publishing Company, Reading, MA, p. 378, 1983.
27. S. E. S. El Wakkad, H. A. Rizk, and I. G. Ebaid, "The Electrochemical behavior of the Tungsten Electrode and the Nature of the Different Oxides of the Metal," *J. Phys. Chem.* 59: 1004-1008, 1955.
28. L-A. Yao, F-X. Gan, Y-X. Zhao, C-L. Yao, and J. L. Bear, "Microelectrode Monitoring the Crevice Corrosion of Titanium," *Corrosion* 47(6): 420-423, 1991.
29. L. B. Kriksunov, D. D. Macdonald, and P. J. Millett, "Tungsten/Tungsten Oxide pH Sensing Electrode for High Temperature Aqueous Environments," *J. Electrochem. Soc.* 141(11): 3002-3005, 1994.
30. D. D. Macdonald, A. C. Scott, and P. Wentzcek, "External Reference Electrodes for Use in High Temperature Aqueous Systems," *J. Electrochem. Soc.* 126(6): 908-911, 1979.
31. M. J. Danielson, "A Long-Lived External Ag/AgCl Reference Electrode for Use in High Temperature/Pressure Environments," *Corrosion* 39(5): 202-203, 1983.
32. Gilbert W. Castellan, *Physical Chemistry*, 3rd Ed., Addison Wesley Publishing Company, Reading, MA, pp. 770-773, 1983.
33. S. Bakhtiari, K. E. Kasza, D. S. Kupperman, S. Majumdar, J. Y. Park, W. J. Shack, and D. R. Diercks, "Second U.S. Nuclear Regulatory Commission International Steam Generator Tube Integrity Research Program Final Project Summary Report," NUREG/CR-6804, U.S. Nuclear Regulatory Commission, Washington, D.C., 2003.
34. *CRC Handbook of Chemistry and Physics*, ed., David R. Lide, 83rd Ed., CRC Press, Boca Raton, LA, 2002.
35. J. Molgaard and W. W. Smeltzer, "Thermal Conductivity of Magnetite and Hematite," *J. Appl. Phys.* 42(9): 3644-3647, 1971.
36. James F. Shackelford, *Introduction to Materials Science for Engineering*, 5th Ed., Prentice Hall, New Jersey, p.65, 2000.
37. "PWR Secondary Water Chemistry Guidelines," Revision 5, TR-102134-R5, Electric Power Research Institute, Palo Alto, CA, p. 2-21, May 2000.
38. A. S. Quist and W. L. Marshall, "Assignment of Limiting Equivalent Conductances for Single Ions to 400°C," *J. Phys. Chem.* 69(9): 2984-2987, 1965.

39. A. Baum, "Limits to Crevice Concentration Processes," Heated Crevice Seminar, NUREG/CP-0189, U.S. Nuclear Regulatory Commission, Washington D.C., pp. 203-240, February 2005.
40. M. N. Panda and L. W. Lake, "Estimation of Single-Phase Permeability from the Parameters of a Particle-Size Distribution," AAPG Bulletin 78(7): 1028-1039, 1994.
41. J. Lumsden, "Heated Crevice-Design, Experimental Methods, and Data Interpretation," in Heated Crevice Seminar, NUREG/CP-0189, U.S. Nuclear Regulatory Commission, Washington D.C., pp. 98-136, February 2005.

Appendix A: Preliminary Crevice Test with NaOH Bulk Chemistries

A.1 Packed Crevice Test: NaOH-01

Packed crevice tests were conducted for two crevice simulators with radial gap sizes of 10 and 20 mils, respectively. Each crevice was filled with synthetic diamond powders. The secondary bulk solution contained 11.5-ppm Na as NaOH, as was the case for the unpacked crevice test. The test solution was poured into the secondary chamber before heat-up. A high-pressure injection pump was not available at that time. More information for the crevice simulator and crevice/bulk instrumentations is given in Sections 2.2 and 2.3.

A.1.1 Test Results

Four initial series of tests were conducted. The primary/secondary temperature was maintained at 600/500 °F. The first test involved about 2 days of testing, after which the model boiler (MB) was shut down and allowed to cool over a weekend. The second test involved about 4.5 days of testing and was performed as a check on the reproducibility of the first test and the possibility of achieving increased concentration of the impurity with longer time. The third test extended for 14 days to explore the ultimate crevice concentration achievable and the influence of the micro-bore tube sampling procedures on the impurity concentration data. Also evaluated was the influence of upsetting a crevice by extracting large volumes of crevice contents and determining the time constant associated with re-establishment of crevice hideout. The fourth test involved, without interrupting the third test, raising the primary temperature from 316°C to 329°C (600°F to 625°F), as was done for the unpacked crevices, to determine if crevice hideout changes.

Test Series 1

Figure A1 shows the temperature variations with time in the 10-mil radial gap crevice as well as the primary water temperature (T_p). Thermocouple (TC) T3 shows more gradual temperature elevation than the others. The temperature elevations are dependent on the location of the thermocouples. Figure A2 shows the temperature variations in the 20-mil gap crevice. All thermocouples are close to the secondary saturation temperature of 500°F, except the TC labeled T6. Based on the post-test examination, the diamond packing in the 20-mil gap crevice had blown out during the test, which might explain the lower temperature in this crevice. For test series 1, a maximum Na concentration of 5930 ppm, corresponding to a hideout factor of 560, was observed in the 10-mil gap crevice. For the 20-mil gap crevice, the maximum Na concentration was 54 ppm, corresponding to a hideout factor of 5. The MB was shut down and cooled during the weekend. This 2-day test appeared to be too short to evaluate the steady-state concentration in the crevice. Without opening the MB, test series 2 was conducted under the same test conditions.

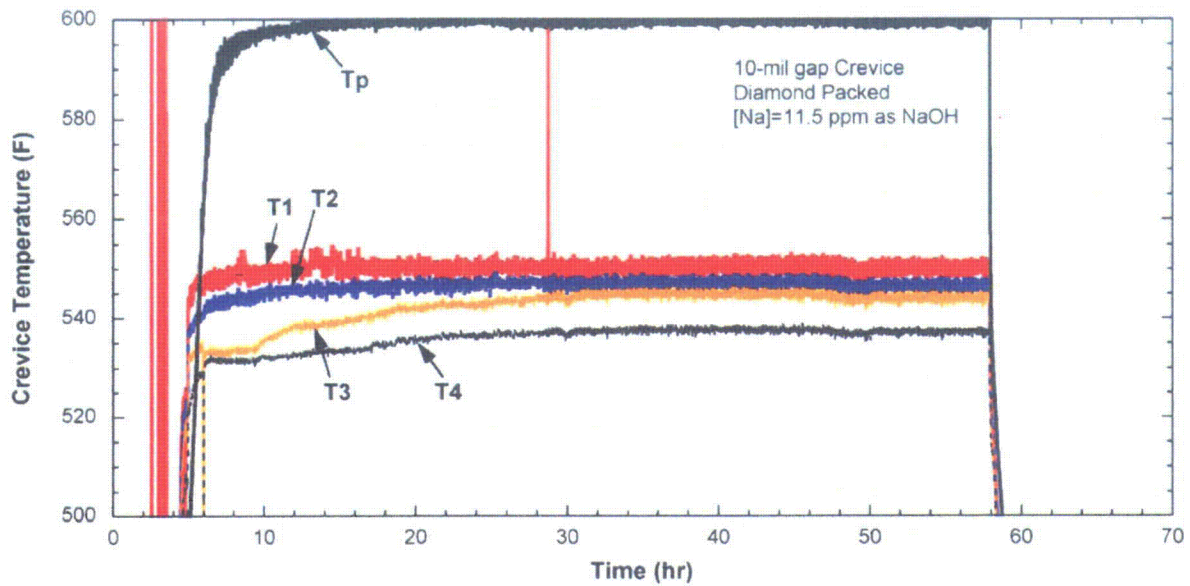


Figure A1. Primary water ($T_p=600^\circ\text{F}$) and crevice temperature variations with time in 10-mil gap crevice packed with diamond powder during series 1 of NaOH-01 test.

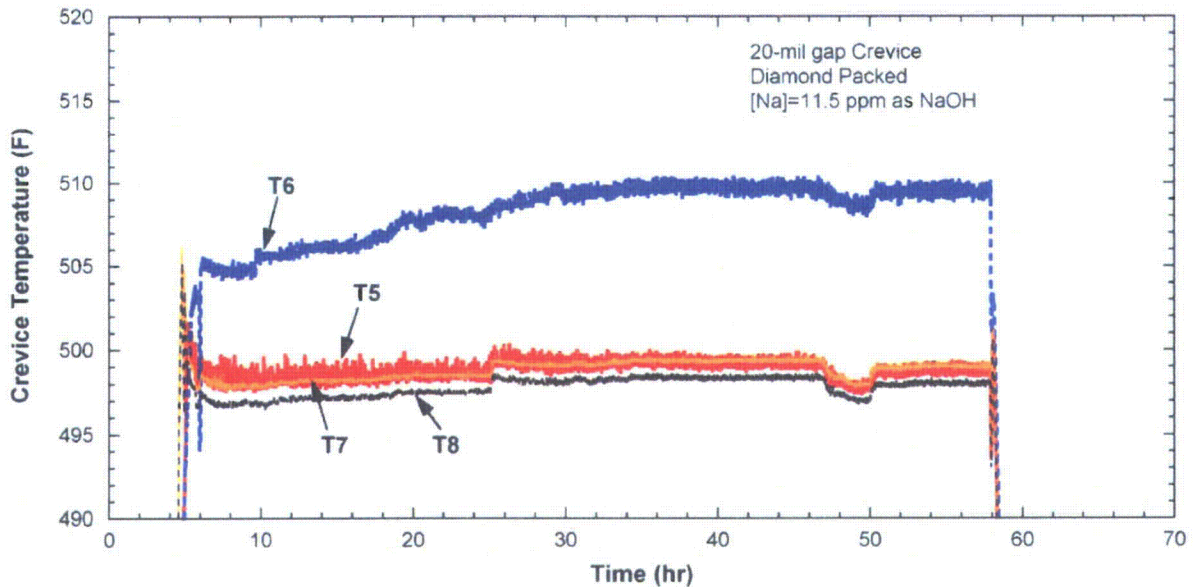


Figure A2. Crevice temperature variations with time in 20-mil gap crevice packed with diamond powder during series 1 of NaOH-01 test.

Test Series 2

Figure A3 shows the crevice temperature variation with time in the 10-mil radial gap crevice. Substantial crevice superheating was observed, in marked contrast to the unpacked crevice of the same gap. As compared with the series 1 results shown in Figure A1, the temperatures did not undergo gradual elevation after the stabilization of the primary water temperature, which might be an effect of the series 1

test. The maximum stabilized temperatures varied from 279°C to 287°C (534°F to 549°F), depending on the TC location. These temperatures are 19°C to 27°C (34°F to 49°F) higher than the secondary bulk temperature of 260°C (500°F). Figure A4 shows the temperature variations with time in the 20-mil gap crevice. As observed in the series 1 test shown in Figure A2, temperatures did not undergo significant elevation.

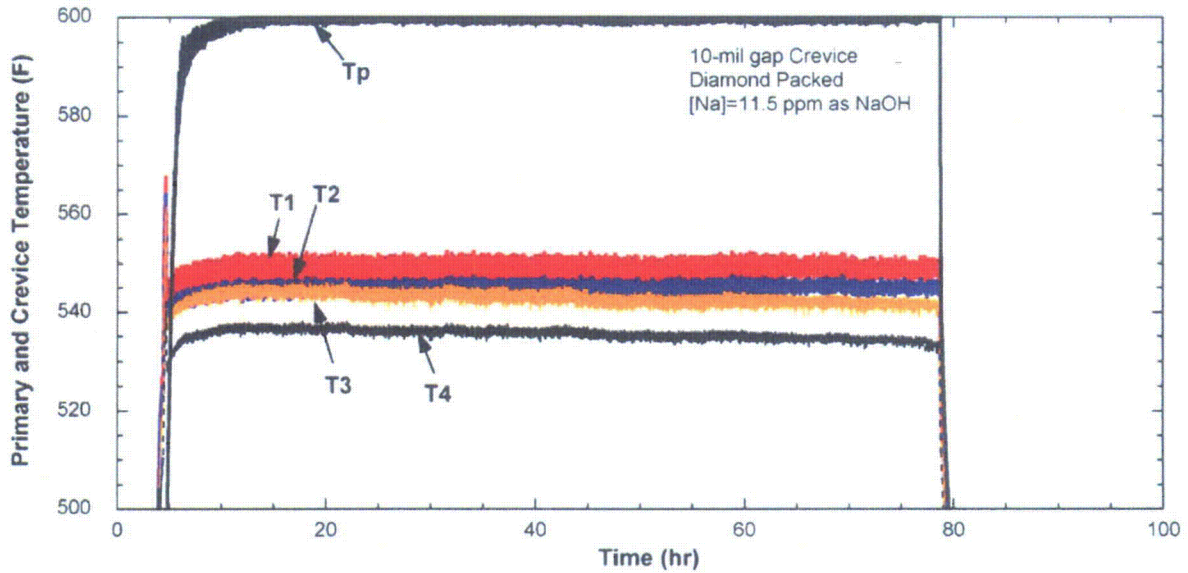


Figure A3. Primary water and crevice temperature variations with time in the 10-mil gap crevice packed with diamond powder during series 2 of NaOH-01 test.

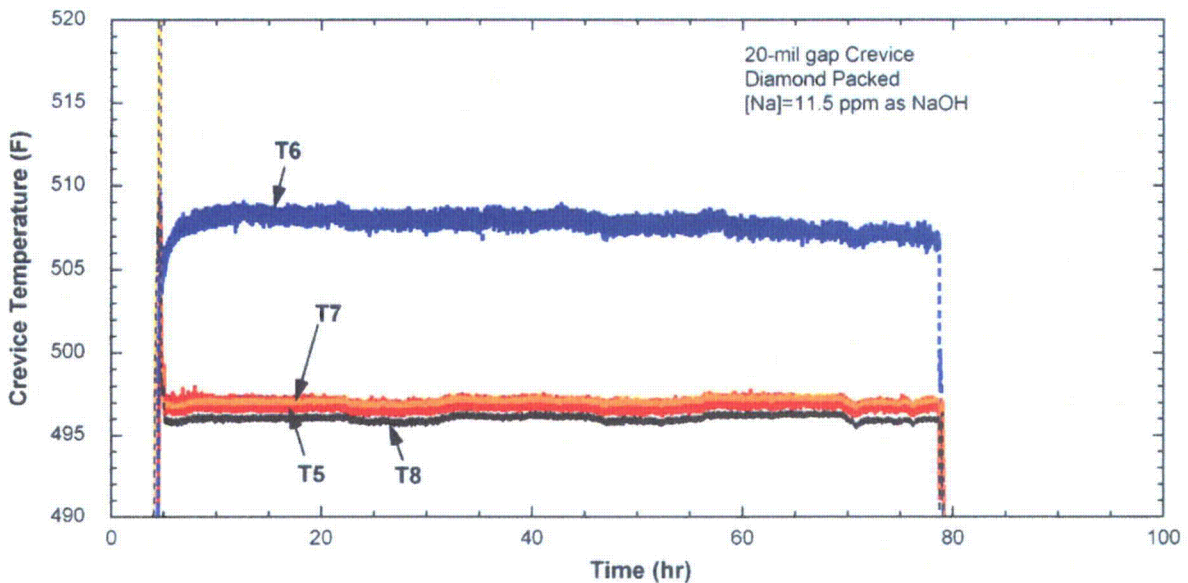


Figure A4. Crevice temperature variations with time in the 20-mil gap crevice packed with diamond powder during series 2 of NaOH-01 test.

For this longer duration test under the same conditions as test series 1, the maximum Na concentrations were 67,700 ppm (concentration factor of 8,600) and 31 ppm (concentration factor of 4) in

the crevices in the 10-mil and 20-mil radial gap, respectively. The increased concentration for the test series 2 appears to be due to the micro-bore extraction tube/valve volumes resulting in a time-delay effect. The calculated internal volume of the micro-bore extraction tubing is about 70 μL . The dead volume of the valve could not be evaluated but should be less than that of the extraction tubing. Assuming that the sampling volume is roughly 50 μL , at least three samples are needed to obtain the actual crevice solution. Since only three samples were taken in the test series 1, the third sample could represent only the beginning stage of the crevice concentration, which led to such a lower Na concentration. With the longer running time and the more frequent sampling of test series 2, we achieved truer indications of maximum hideout. By taking into account the extraction line volume, we are able to better understand the time delay observed in the sampling results compared with the temperature data. As described in the next section, the post-test examination revealed that the diamond powder in the 20-mil gap crevice had been blown out during the test. This result explains the low Na concentration observed in this crevice.

The crevice hideout estimated by the MULTEQ code predicts a maximum Na concentration factor of 45,000 and pH of 11.07, with a neutral pH of 4.88 at the maximum available superheat of 100°F. The estimated concentration factor at the observed maximum superheat of 49°F is 43,000. The maximum concentration factor of 8,600 is less than the MULTEQ predicted value by a factor of five. This discrepancy might be due to significant dilution during the sampling by mixing with secondary water. The samples for the 10-mil crevice were tinted brown. This tinting may indicate dissolved metallic ions, e.g., ferric or ferrous ions or some other species. The ICP/OES analysis confirmed 15-40 ppm Fe in the samples.

Test Series 3 and 4

Figure A5 shows the temperature variations with time in the 10-mil gap crevice. The two thermocouples (T1 and T2) did not work properly presumably because of the thermocouple tip's corrosion in NaOH solution. The crevice temperatures (T3 and T4) did not vary significantly with time except for the period of 20-60 hours. During this period, crevice upset testing caused the temperature fluctuation. Micro-bore tubing crevice extraction was performed to intentionally upset the hideout of the 10-mil gap crevice. An extraction rate of one drop every three seconds had less significant influence on crevice superheat, but a rate of one drop per second caused a significant fluctuation of the crevice temperature at the thermocouple nearest the micro-bore tube (thermocouple T4). With the cessation of crevice extraction, the superheat returned to the initial undisturbed value. Figure A6 shows the temperature variations in the 20-mil gap crevice. The temperature behaviors are almost the same as in the series 2 test shown in Figure A4.

Series 4 involved raising the primary temperature from 315°C to 329°C (600°F to 625°F), as was done for the unpacked crevices, without interrupting the long-term test of series 3. The increased temperature difference between the primary and secondary chambers caused the superheat in the 10-mil gap crevice to increase up to 7-10 °F, as shown in Figure A5. The temperature changes in the 20-mil gap crevice were minor, as shown in Figure A6.

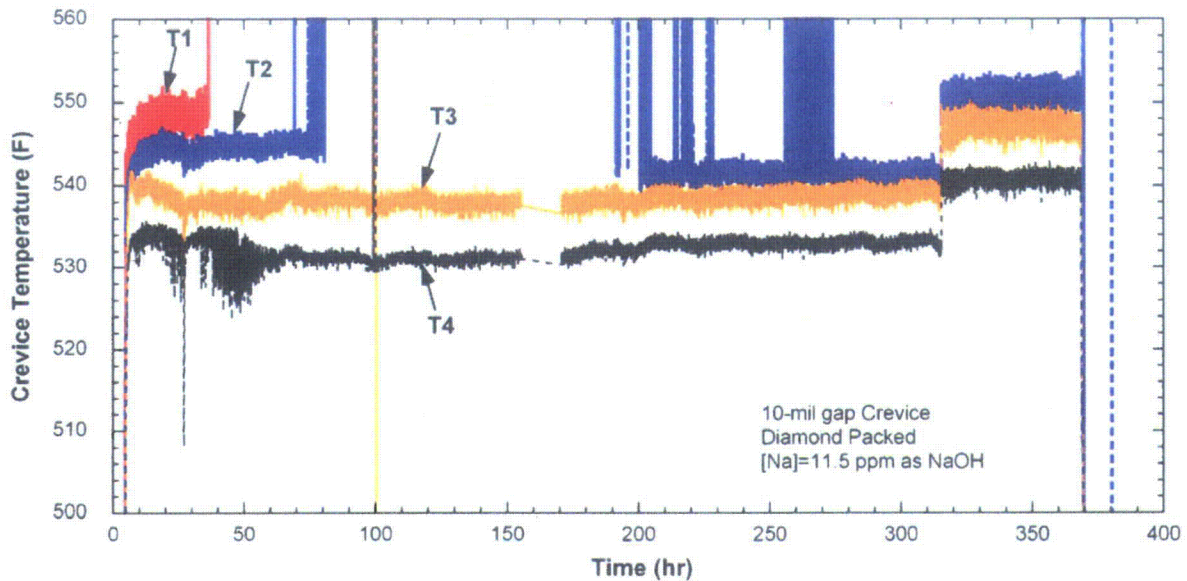


Figure A5. Crevice temperature variation with time in the 10-mil gap crevice packed with diamond powder during series 3 and 4 of NaOH-01 test.

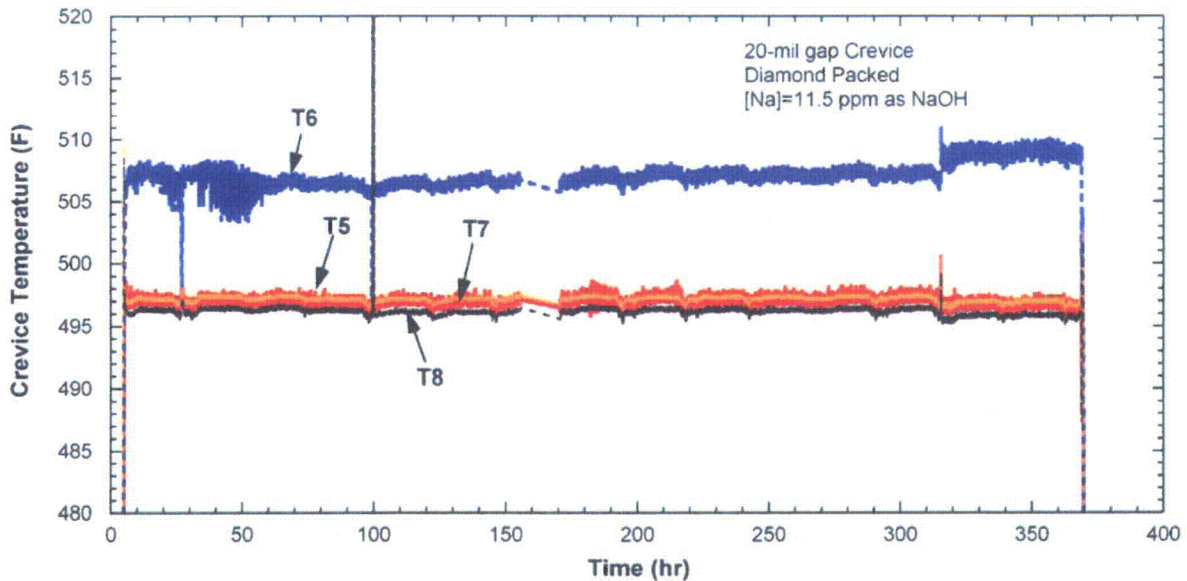


Figure A6. Crevice temperature variation with time in the 20-mil gap crevice packed with diamond powder during series 3 and 4 of NaOH-01 test.

A.1.2 Post-Test Examination

Post-test examination revealed that most of the diamond packing in the 20-mil radial gap crevice had been blown out because of a tear in the nickel foam placed over the crevice entrance. Figures A7 and A8 show the torn nickel foam membrane on the 20-mil gap crevice and the absence of diamond packing

in the crevice, respectively. As evident in Figures A9 and A10 for the 10-mil gap crevice, the nickel foam membrane is intact, and the crevice retains its packing. This finding explains why substantial crevice superheating, approaching 27°C (49°F), was observed in the 10-mil crevice, while only minor superheat occurred in the 20-mil crevice, similar to our previous result for an unpacked crevice of the same radial gap size.

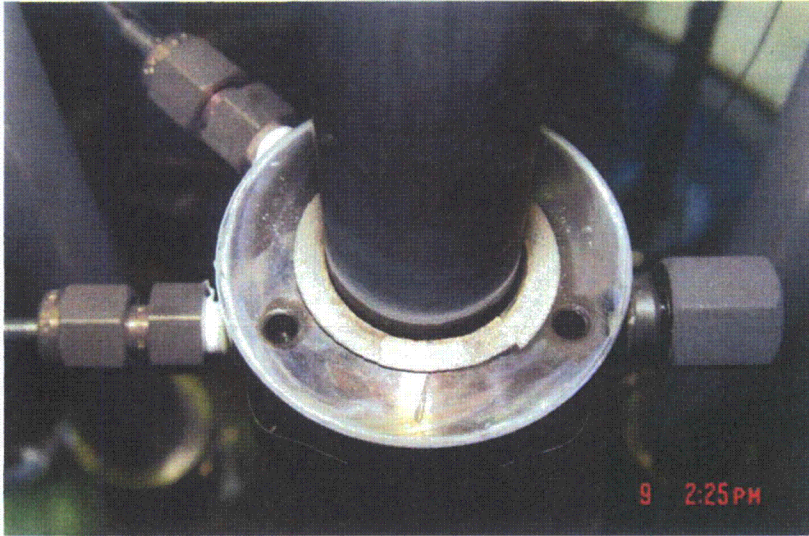


Figure A7.
Photograph of torn nickel membrane on the 20-mil gap crevice and the absence of diamond packing in the crevice.



Figure A8.
Photograph of 20-mil gap crevice and the absence of diamond packing in the crevice.



Figure A9.
Photograph of 10-mil gap
crevice with intact nickel
membrane.



Figure A10.
Photograph of 10-mil gap
crevice with diamond packing.

The inspection of the two steam generator (SG) tubes showed that the outer tube wall in the vicinity of the 10-mil gap crevice had undergone considerable gouging at the end of the NaOH-01 test, as shown in Figure A11. This crevice exhibited a NaOH hideout factor approaching 8,600, and the total time under these conditions was 490 hours. Considering the intergranular attack (IGA) growth rate of alloy 600 MA at a crevice pH of 11 and temperature of 315°C (599°F),¹ the estimated IGA attack depth during the 490-hour exposure is around 25 μm (1 mil), which is comparable to the observation results in Figure A11. No gouging/pitting occurred on the larger 20-mil gap crevice, where the hideout factor was only 5. These same SG tubes and crevices were used in the NaOH-02 test.

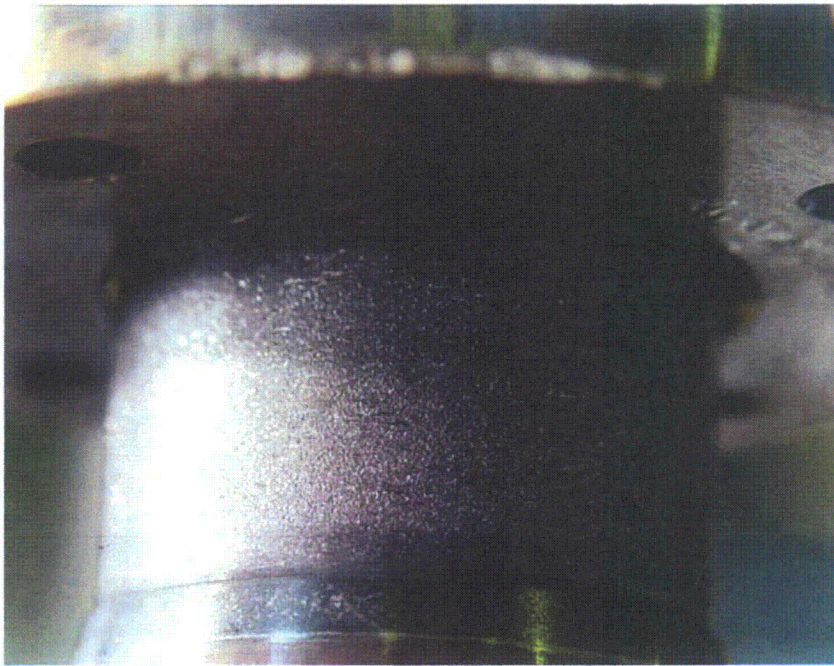


Figure A11.
Photograph of gouging in
tube wall in the vicinity of the
10-mil gap crevice.

A.1.3 Summary

In summary, the first packed crevice test, NaOH-01, involved four phases. For the 10-mil radial gap crevice, the nickel membrane was intact and the crevice retained its packing. This crevice exhibited a NaOH hideout factor approaching 8,600. Inspection of the crevices revealed that most of the diamond packing in the 20-mil gap crevice was blown out because of a tear in the nickel foam membrane placed over the crevice exit. This occurrence explains why crevice superheating approaching 27°C (49°F) was observed in the 10-mil crevice, while only minor superheat occurred in the 20-mil gap crevice, similar to our previous result for an unpacked crevice of the same radial gap size. The inspection also showed that the outer tube wall in the 10-mil gap crevice region at the end of NaOH-01 had undergone considerable gouging. No gouging/pitting occurred on the 20-mil gap crevice, where the hideout factor was only 5, mainly because the packed diamond powder had been blown out of the crevice.

A.2 Packed Crevice Test: NaOH-02

A.2.1 Experimental Setup

With completion of the NaOH-01 test, the MB secondary chamber was opened, and the crevices were inspected and cleaned. The 10- and 20-mil gap crevices were repacked, and new nickel-foam grit retention membranes were installed. The 10-mil gap crevice was packed with 50:50 mixture of two mesh sizes of diamond grit (127-165 μm and 75-97 μm), the latter being smaller than that used in the NaOH-01 test in an attempt to achieve a higher packing fraction and further restrict the flow into and out of the crevice. The 20-mil gap crevice was packed with the same grit size (127-165 μm) as used in the NaOH-01 test to obtain data for this grit and crevice size that were not obtained previously because grit was blown out of the crevice through a faulty retention membrane. The estimated crevice porosity is 40 % and 29 %

for the 10- and 20-mil gap crevices, respectively. The larger gap crevice has the same porosity as the NaOH-01 test, but the porosity of the smaller gap crevice was larger even though mixed diamond powders were used.

A.2.2 Test Results

The NaOH-02 test was conducted under the same primary and secondary bulk temperatures and bulk chemistry as the NaOH-01 test. After two days of testing, with the MB achieving a stable thermal-hydraulic state and the two crevices both showing superheat above the bulk saturation temperature of 260°C (500°F), a test was conducted involving 30 min of steam purging from the secondary chamber. The purpose of the steam purging was to remove the possible buildup of hydrogen gas in the secondary chamber, which might have originated from the corrosion of internal metal surfaces, including the secondary chamber and alloy 600 tubing, and to eliminate its influence on the electrochemical potential (ECP) instrumentation. The steam was purged at a rate that ensured maximum nucleate-boiling heat transfer of the SG tube and steam condensation in the vertical finned heat rejection pipe. This purging had no measurable influence on the ECP instrumentation. Hence, the build-up of hydrogen gas in the secondary chamber and its effect appear to be negligible.

Figure A12 shows the temperature versus time in the 10-mil gap crevice. The temperature varied depending on the circumferential location. The temperature variations might have occurred because the thermocouples were located at different locations from the tube surface. Closer locations to the tube surface will show higher temperature. The smaller gap crevice showed nominally the same crevice superheat as the NaOH-01 test packed with the diamond powder of only one grit size (127-165 μm). Figure A13 shows the temperature variations in the 20-mil gap crevice. In the NaOH-01 test, recall that the diamond grit was blown from the 20-mil crevice through a torn nickel membrane and the crevice behaved like an unpacked crevice. In contrast, the 20-mil gap crevice in the NaOH-02 test retained the diamond packing and achieved superheats in the range of 0-20°F, depending on crevice location. The temperature oscillations shown in Figure A13 appear to indicate the active mixing of liquid and steam phases. As described in the next section, axial through-wall cracks were detected in the 10-mil gap crevice region. The temperature oscillations shown in Figure A12 are attributed to a primary-to-secondary leak through the cracks.

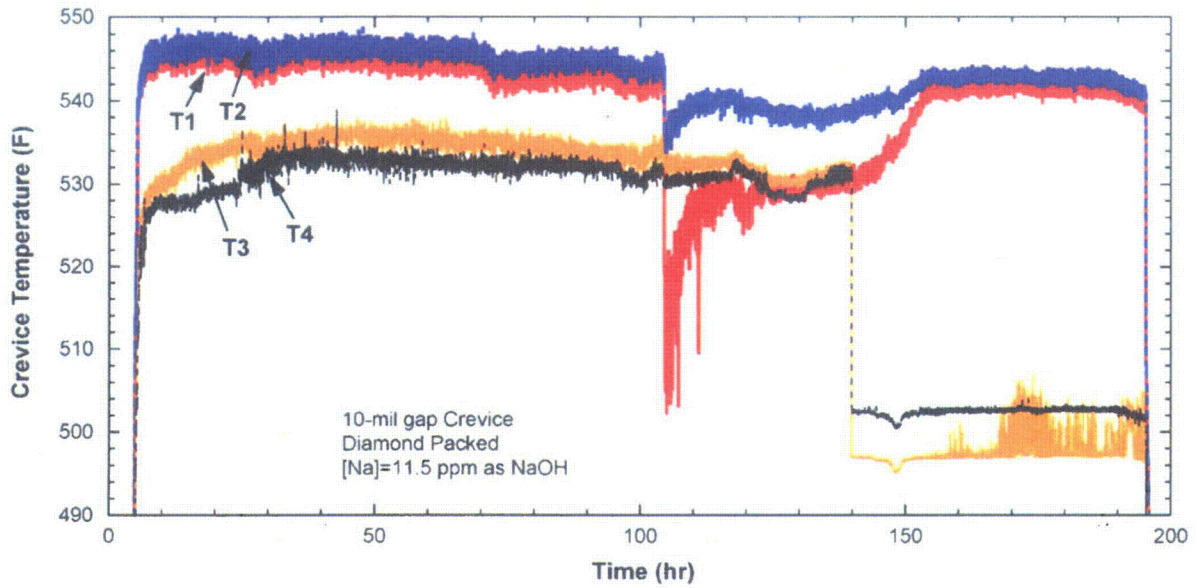


Figure A12. Crevice temperature variation with time in the 10-mil gap crevice packed with diamond powder for NaOH-02 test.

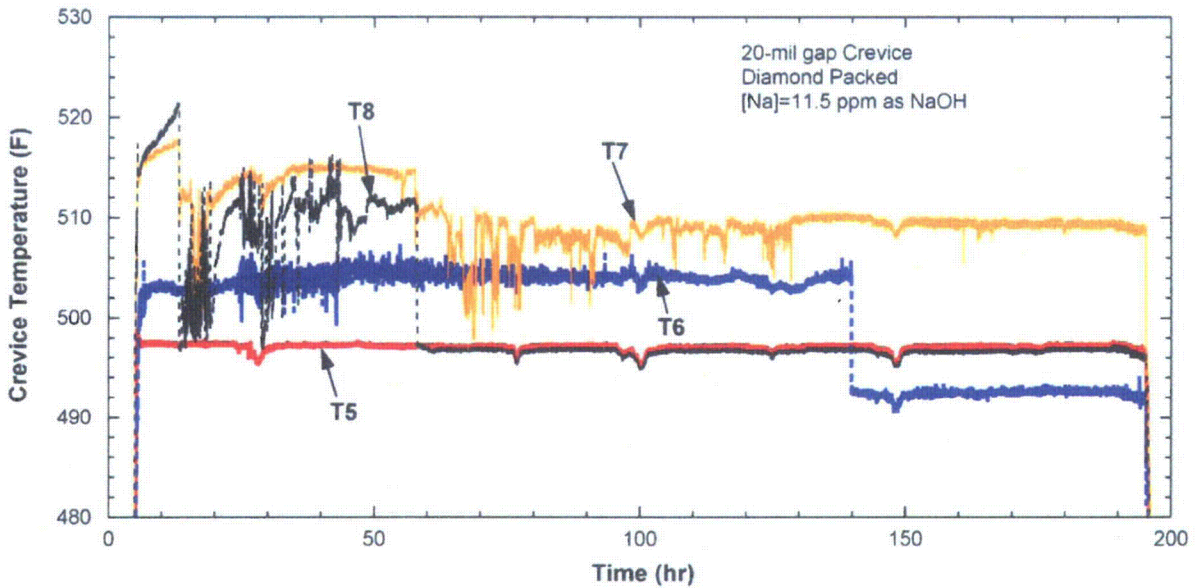


Figure A13. Crevice temperature variation with time in the 20-mil gap crevice packed with diamond powder for NaOH-02 test.

A large temperature drop occurred in the 10-mil gap crevice at about 100 hours, as shown in Figure A12. Another temperature drop occurred at 140 hours. The drastic temperature drops are attributed to the beginning of a leak from the through-wall cracks. Post-test examinations, as discussed in the next section, verified through-wall cracks in the crevice region. To accurately determine the time when the leakage started, the cooling fan speed and the resistances of the level sensors in the bulk water are plotted as a

function of time in Figure A14. The first small change of cooling fan speed was caused by the secondary-chamber purging test. The second change of fan speed occurred at the same time as the drastic temperature drop, at about 100 hours. Also, the resistance of the lower level sensor started to decrease at the same time. This decrease suggests the increase of bulk Na concentration caused by the leakage. The change in the upper level sensor readings indicated a leak from the primary side to the secondary chamber. The time of this event coincided with the time at which two of the 10-mil gap crevice thermocouples indicated the loss of superheat. After running the NaOH-02 test for 190 hours at 316°C (600°F) primary- and 260°C (500°F) secondary-side temperatures, the MB was shut down. After cooling, the secondary chamber was opened to find the source of the primary-to-secondary leak. The total accumulated exposure time of the cracked tubing over the two consecutive series of diamond-packed crevice testing, during which the crevice hideout factor reached 8,600, is 590 hours. The bulk secondary water for all these hours initially consisted of 11.5 ppm Na (20 ppm as NaOH) in deionized water, which decreased to 4.2 ppm due to the Na hideout in the crevices. Considering the stress corrosion crack (SCC) growth rate of alloy 600 MA under a crevice pH of 11 and temperature of 315°C (599°F),¹ we estimated the crack length during the 590-hour exposure to be about 67 mil, which is comparable to the tube wall thickness of 50 mil.

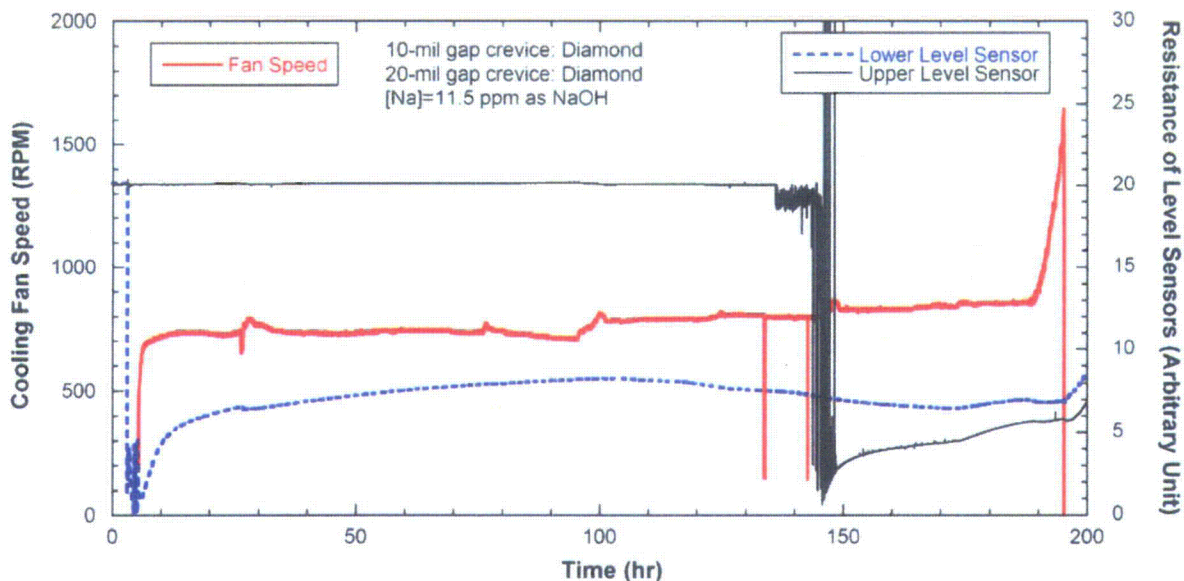


Figure A14. Cooling fan speed and resistance of lower and upper level sensors with time for NaOH-02 test.

A.2.3 Post-Test Examination

After opening the secondary chamber, we examined the two packed crevices prior to disassembly by filling the crevices with water and pressurizing the primary chamber to 4.8 MPa (700 psi) with nitrogen. The outlet of the 10-mil gap crevice exhibited repeated bubble release, as shown in Figure A15, indicating through-wall penetration. Under our primary and secondary chamber test temperatures of 316°C and 260°C (600°F and 500°F), respectively, the pressure differential across the tube was 5.7 MPa (827 psi).

The leaking tube was then removed from the MB, and a low-pressure nitrogen-gas bubble test was performed in a water bath. At 0.34 MPa (50 psi), bubbles were generated at several sites along a ≈ 10 -mm (0.4-in.) long axial SCC located in the bottom half of the crevice, as shown in Figure A16. No other leakage was seen. Because the flaw was very tight, we applied dye penetrant to allow it to be studied and photographed. As shown in Figure A17, the axial SCC flaw on the outside diameter (OD) is longer than 18 mm (0.71 in.).

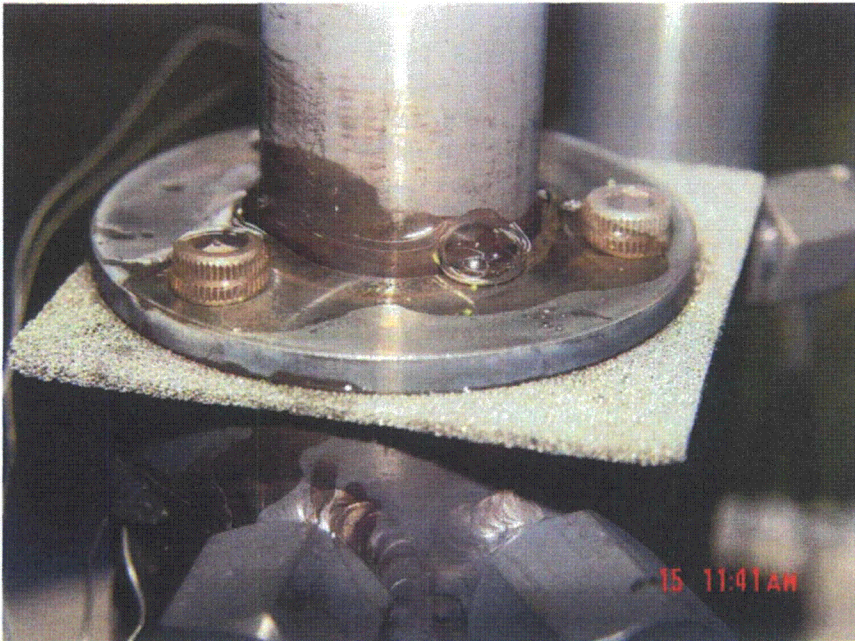


Figure A15.
Photo indicating repeated bubble generation and release at the crevice exit due to an SG SCC flaw in the packed-crevice region for 10-mil gap.

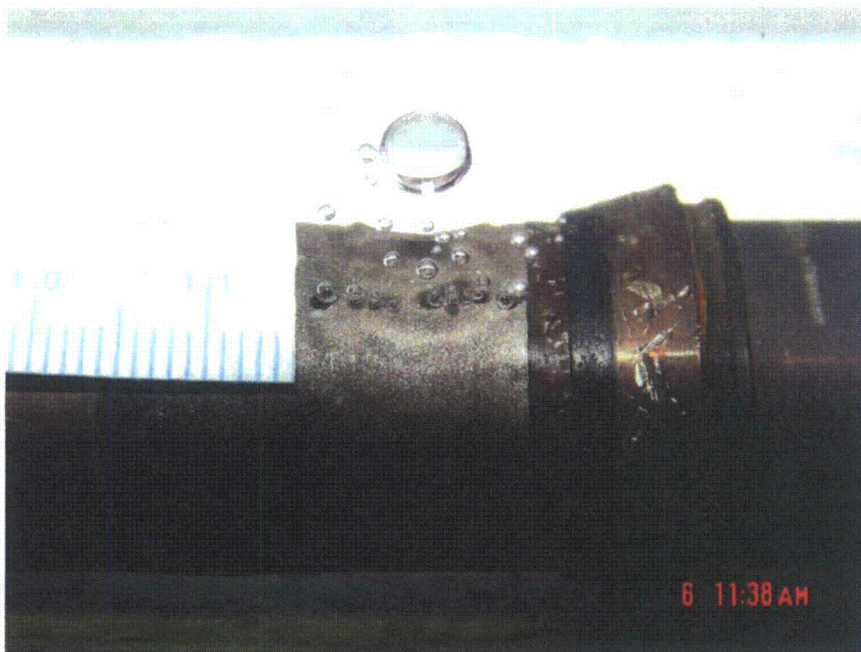


Figure A16.
Low-pressure bubble test of MB crevice flaw at 0.34 MPa (50 psi) showing bubbles at several sites along an ≈ 10 -mm (0.4-in.)-long axial SCC located in the bottom half of the crevice.

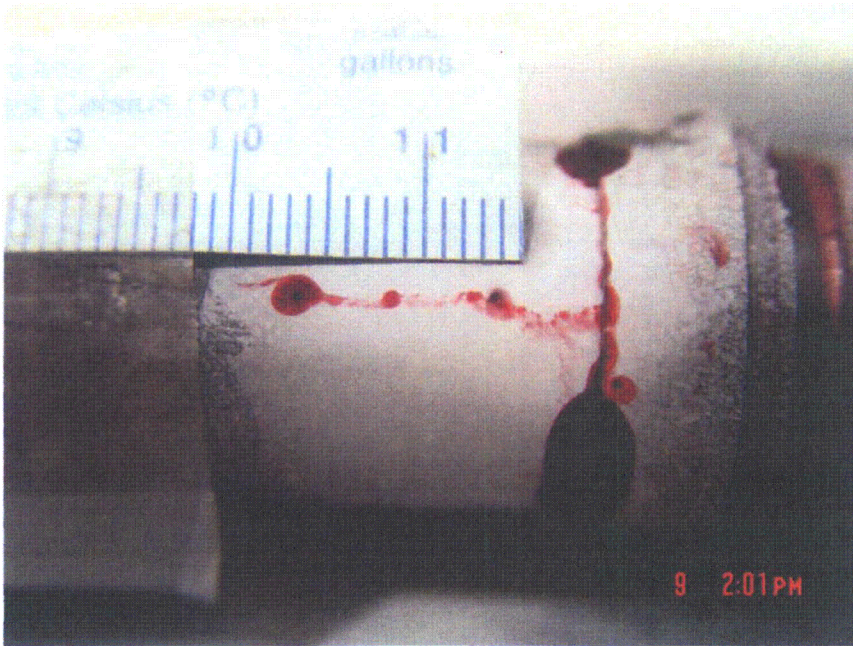


Figure A17. Crevice SCC flaw photographed using dye penetrant to enhance visualization. The flaw is longer than 18 mm (0.71 in.).

A.2.4 Eddy-Current Examination of Cracked Tube

After photographing the flaw, we initiated eddy-current non-destructive examinations to permit further characterization of the tube crevice region. A +Point coil operating at 300 kHz was used to profile the cracks. Standard industry practice was used for all depth measurements. An electro-discharged machine notched reference tube (18 notches) was used for calibration. Figure A18 shows the +Point c-scan for the tube. Four prominent cracks (numbered 1-4) are visible, all axial ODSCC. The maximum +Point voltage for these four cracks was about 6 V.

The profile for each crack was established by determining the eddy current depth at intervals along the crack. The depth profiles for the four SCC flaws are shown in Figure A19 through A22. Flaws MB1-1 and MB1-3 are located in the crevice ring-simulator region, and flaws MB1-2 and MB1-4 are located immediately below this region under the Swagelok cone and ring fittings used to seal the bottom of the crevice, as shown in Figure A16. The crevice hideout region produced by the Swagelok fittings is formed by the line contact associated with the fittings and the tube, resulting in a reduced flow region that hinders nucleate-boiling heat transfer. This hideout region has a different flow communication path with the bulk secondary path than the crevice formed by the crevice simulator ring. For MB1-2 and MB1-3, we could not clearly locate one end of the crack from the eddy-current signal. Any signal indicating an EC depth of 90% through-wall or greater is presumed to be a through-wall flaw location. The only crack that leaked during the low-pressure bubble tests and the only one that clearly showed at the tube OD under the initial dye penetrant exam is MB1-1, as shown in Figures A16 and A17. Table A1 shows the crack identifier, maximum +Point voltage, total length, and length where the crack is estimated to be through-wall for all four flaws. As will be discussed shortly, after pressurizing the tube to 8.3 MPa (1200 psi) for the purpose of leak testing, we could see all four cracks, but only MB1-1 exhibited an active leak.

Table A1. Maximum +Point voltage, length, and estimated through-wall length for the four prominent axial ODSCC flaws in tube MB1.

SCC Identifier	Maximum Point, Volts	Eddy-Current Length, mm (± 1 mm)	Estimated Through-wall Length, mm
MB1-1	5.6	28	15
MB1-2	6.2	≈ 20	6
MB1-3	6.6	≈ 20	8
MB1-4	5.6	30	4

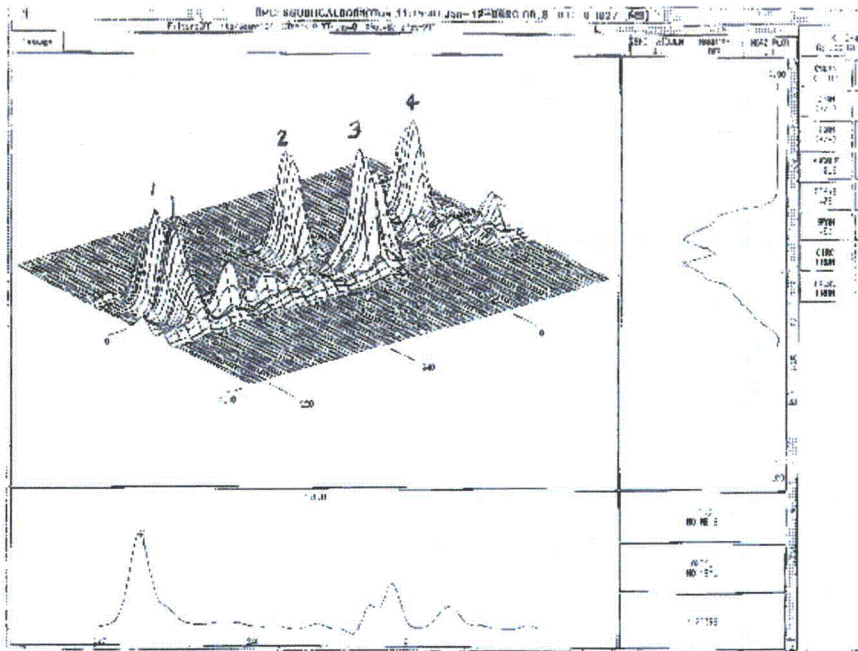


Figure A18.
C-scan of MB tube MB1
using +Point probe at
300 kHz. Four axial
ODSCCs are evident.

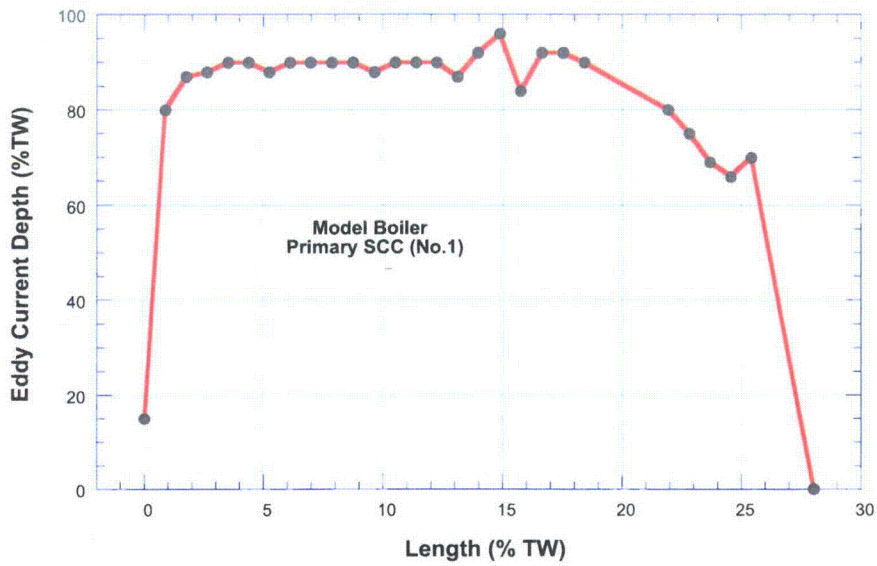


Figure A19.
Eddy current profile for
the primary axial
ODSCC MB1-1.

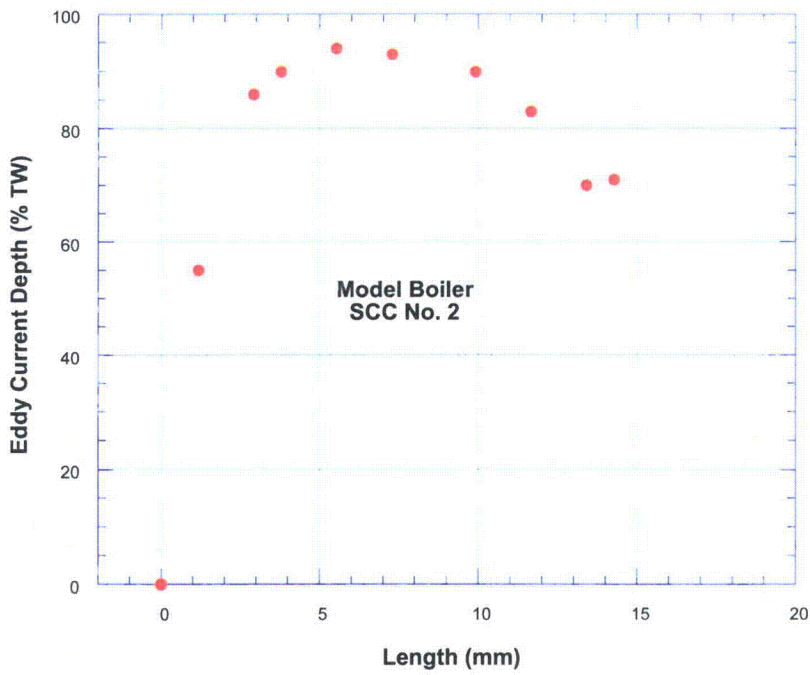


Figure A20.
Eddy current profile for the
axial ODSCC MB1-2.

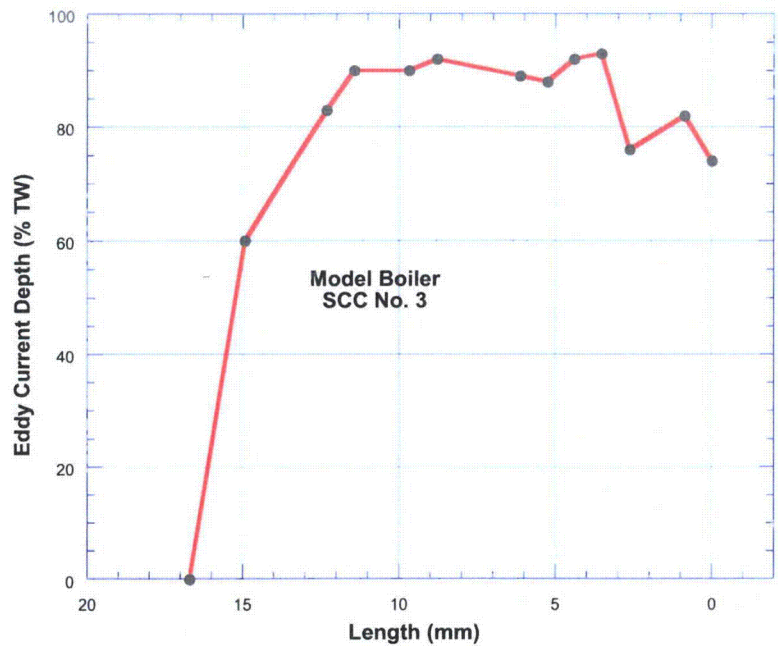


Figure A21.
Eddy current profile for the axial ODSCC MB1-3.

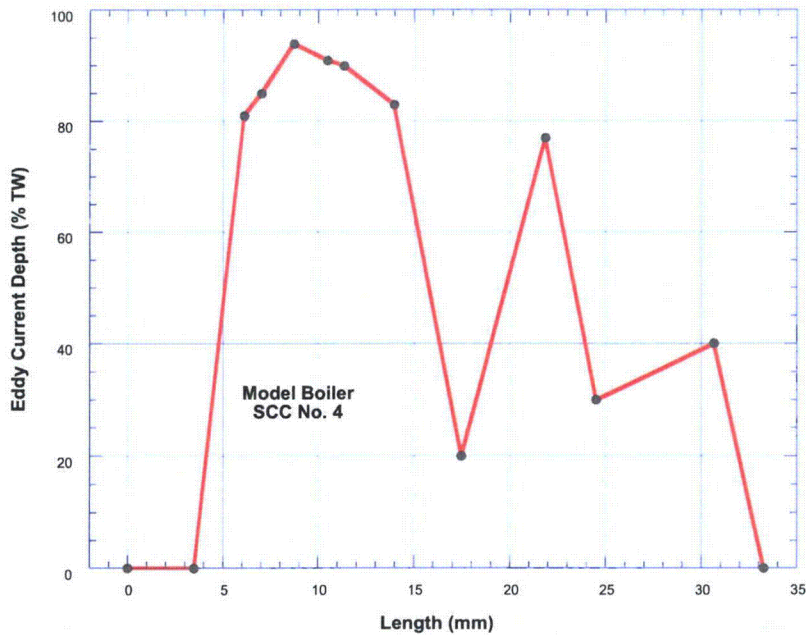


Figure A22.
Eddy current profile for the axial ODSCC MB1-4.

A.2.5 High-Pressure Leak Test for Cracked Tube

After the eddy-current examination, the flaws were heat tinted and subjected to a constant-pressure leak test at 8.3 MPa (1200 psi) in our Room-Temperature High-Pressure Leak Testing Facility.² The objective was to study the leak characteristics and determine if the flaw would exhibit time-dependent constant-pressure tearing. The leak testing was performed by increasing the flow in 1.0 MPa (150 psi)

increments from 0 to 8.3 MPa (0 to 1200 psi) with 2-3 minutes of hold at each intermediate plateau. At each plateau, we monitored the leak. The flaw zone MB1-1 showed no signs of leakage until a pressure of 3.1 MPa (450 psi). The leak was in the form of a single drop with no cyclic behavior. As stated above, our bubble immersion test with nitrogen gas at 0.34 MPa (50 psi) showed active bubble generations at several locations over about 10 mm (0.4 in.) of the OD crack length. At 5.2 MPa (750 psi), we saw drop formation from two distinct locations, one being MB1-1 and the other outside of the crack region highlighted by the bubble test. At 6.2 MPa (900 psi), active multiple jets were issuing from the 10-mm (0.4-in.) axial zone of flaw MB1-1. At 7.2 MPa (1050 psi), the jets became very strong. No other locations showed active jetting. An additional point of water droplet formation may have occurred in another region, but firm confirmation was not possible due to water spray inside the jet confinement tank.

The test pressure was then raised to 8.3 MPa (1200 psi), and the flow rate was measured as a function of time. After 15 min at this pressure, the leak rate was 1.69 kg/min (3.72 lb/min), and 10 min later the leak rate had increased to 2.08 kg/min (4.60 lb/min), which is quite a rapid increase. We stopped the leak test and photographed the leaking flow as well as other regions of cracking suggested by the pretest eddy-current nondestructive evaluation. As shown in Figure A23, the main axial flaw labeled MB1-1 had widened and grown significantly compared with its pretest length shown in Figures A16 and A17. Figure A24 to Figure A26 show the three additional ODSCC flaw areas on the tube, namely, MB1-2, MB1-3, and MB1-4. The photographic images of the flaws at the OD after leak testing agree well with the flaw locations determined by eddy current techniques, though these flaws did not produce active jets. Flaws 1 and 3 were in the crevice simulator ring region, and flaws 2 and 4 were in the zone of the Swagelok fittings that seal the crevice at the bottom of the crevice simulator ring.

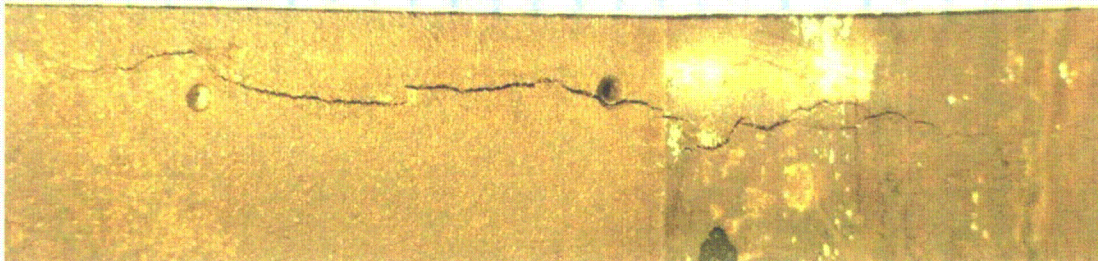


Figure A23. Photograph of crevice SCC OD flaw MB1-1 after leak testing at 8.3 MPa (1200 psi).

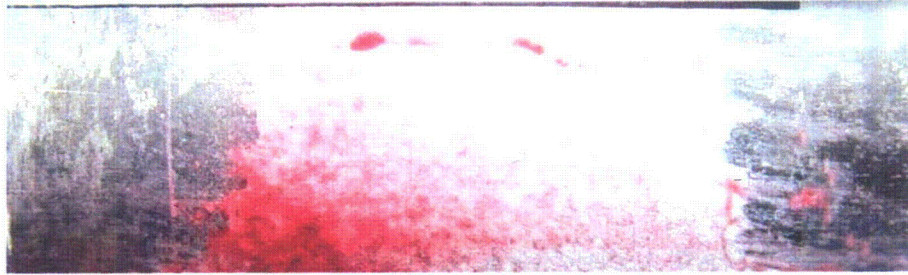


Figure A24. Photograph of crevice SCC OD flaw MB1-2 after leak testing at 8.3 MPa (1200 psi).



Figure A25. Photograph of crevice SCC OD flaw MB1-3 after leak testing at 8.3 MPa (1200 psi).

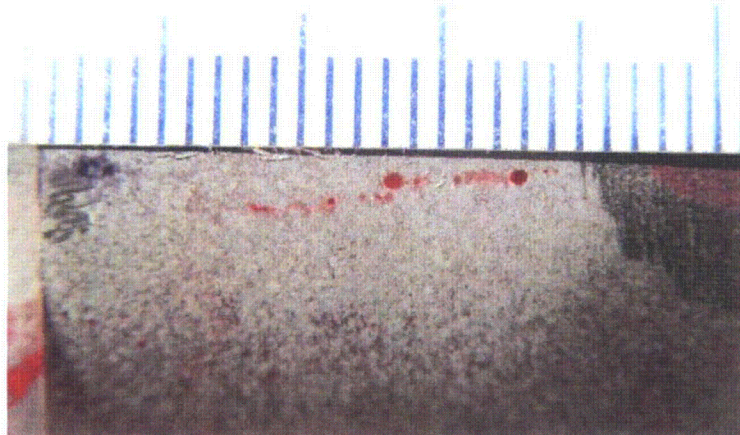


Figure A26. Photograph of MB crevice SCC OD flaw MB1-4 after leak testing at 8.3 MPa (1200 psi).

The MB appears to be a good facility for studying not only chemical hideout induced by prototypic SG-tube crevice heat transfer, but also, in a reasonable length of time, can be used to study the potential for cracking of tubes exposed to various chemicals under a variety of crevice geometry, thermal hydraulic, and tube material conditions. There is the possibility that, in the presence of corrosive chemicals concentrated by crevice hideout, the vigorous nucleate boiling at an SG tube outer surface accelerates the growth of SCC above that which takes place in the absence of heat transfer and nucleate boiling. The MB also allows us to grow SCC flaws in a prototypic heat transfer environment and further evaluate the potential for using eddy-current non-destructive examination to characterize the SCC.

References

1. "PWR Secondary Water Chemistry Guidelines-Revision 5," TR-102134-R5, Electric Power Research Institute, Palo Alto, CA, May 2000, p. 2-21.
2. K. Kasza, S. Majumdar, J. Park, and J. Franklin, "Results for Pressure and Leak-Rate Testing of Laboratory-Degraded Steam Generator Tubing," NUREG/CR-6789, U.S. Nuclear Regulatory Commission, Washington, D.C., 2002.

Appendix B: Mass Balance Analysis with Simple Analytical Model

A simple analytical model for crevice concentration was adopted from earlier work by Cleary and Lindsay.¹ The crevice hideout rate can be established by using a mass balance equation like Eq. (B1).

$$\rho_f \varepsilon V \frac{dc}{dt} = \dot{m}_i c_o - \dot{m}_o c - (\dot{m}_i - \dot{m}_o) \gamma c - \Gamma (c - c_o) \quad (B1)$$

where ρ_f : liquid density in crevice

ε : porosity in crevice

V : total volume in crevice

\dot{m}_i : mass flow rate of liquid into the crevice

\dot{m}_o : mass flow rate of liquid out of the crevice

c : crevice concentration

c_o : bulk concentration

γ : liquid - vapor distribution coefficient

Γ : mass transfer coefficient for diffusion

On the right-hand side of Eq. (B1), the first term reflects the incoming rate of impurity from bulk water and the second term, the mechanical carry-over by the outgoing liquid flow.

For algebraic simplicity, the parameter K_f is defined as follows:

$$K_f = \dot{m}_i / \dot{m}_o \quad (B2)$$

In most cases K_f is much larger than 1. The difference between the incoming and outgoing mass flow rates is equal to the evaporation rate inside the crevice, which can be formulated as follows:

$$\dot{m}_i - \dot{m}_o = \alpha \pi D L q'' / h_{fg}$$

where α : the fraction of wetted length in the crevice

D : steam generator tube diameter

L : crevice depth

q'' : heat flux in the crevice

h_{fg} : heat of vaporization

(B3)

$$\dot{m}_i - \dot{m}_o = \dot{m}_i \left(1 - \frac{1}{K_f} \right) \approx \dot{m}_i = \alpha \beta' q''$$

where $\beta' = \pi D L / h_{fg}$

(B4)

Equation (B1) can be reformulated by using Eq. (B2)-(B4) and assuming $K_f \gg 1$:

$$\begin{aligned}
\rho_f \varepsilon V \frac{dc}{dt} &= \dot{m}_i \left[c_o - \left(\frac{1}{K_f} + \left(1 - \frac{1}{K_f} \right) \gamma \right) c \right] - \Gamma (c - c_o) \\
&= \alpha \beta' q'' \left[c_o - \left(\frac{1}{K_f} + \gamma \right) c \right] - \Gamma (c - c_o) \\
&= (\alpha \beta' q'' + \Gamma) c_o - \left[\alpha \beta' q'' \left(\frac{1}{K_f} + \gamma \right) + \Gamma \right] c
\end{aligned} \tag{B5}$$

Since the MB system is closed, the accumulation rate in the crevice should be balanced by the reduction rate in bulk water, as follows:

$$\begin{aligned}
\rho_o V_o \frac{dc_o}{dt} &= -\rho_f \varepsilon V \frac{dc}{dt} \\
\text{where } \rho_o &: \text{density of bulk water} \\
V_o &: \text{volume of bulk water}
\end{aligned} \tag{B6}$$

The reduction rate of the impurity concentration in the bulk water can be determined by using

$$\begin{aligned}
\rho_o V_o \frac{dc_o}{dt} &= -(\alpha \beta' q'' + \Gamma) c_o + \left[\alpha \beta' q'' \left(\frac{1}{K_f} + \gamma \right) + \Gamma \right] c \\
\frac{dc_o}{dt} &= -\frac{\alpha \beta' q'' + \Gamma}{\rho_o V_o} c_o + \frac{\alpha \beta' q'' \left(\frac{1}{K_f} + \gamma \right) + \Gamma}{\rho_o V_o} c
\end{aligned} \tag{B7}$$

If the second term on the right-hand side does not vary much with time, Eq. (B7) can be integrated and formulated as follows:

$$\begin{aligned}
\ln \frac{c_o - A_i}{c_o^o - A_i} &= -G_i t \\
\text{where } c_o^o &: \text{initial bulk concentration} \\
A_i &= \frac{\left[\alpha \beta' q'' \left(\frac{1}{K_f} + \gamma \right) + \Gamma \right] c}{\alpha \beta' q'' + \Gamma} \text{ and } G_i = \frac{\alpha \beta' q'' + \Gamma}{\rho_o V_o}
\end{aligned} \tag{B8}$$

To estimate A_i and G_i in Eq. (B8), impurity concentration behavior data are needed for the bulk water. Figure B1 shows the theoretically estimated conductivity as a function of Na concentration for the Na-to-Cl molar ratio of 0.7. Since the theoretical calculation assumes an infinitely dilute condition, this calculation method is not applicable to the higher impurity concentration observed inside the crevice. Figure B2 shows the calculated Na and Cl concentrations from the bulk conductivity data. The calculated concentrations are in good agreement with the chemical analysis.

The parameter A_i can be determined by a graphical method as shown in Figure B3 through B5. The A_i value is changed by trial and error until the best-fit linear regression is achieved. The bulk concentration variation data shown in Figure B2 were used to determine A_i and G_i values as a function of ΔT . Only bulk conductivity data logged before reaching the steady-state conditions at each ΔT were used for this analysis. As shown in Figure B3 through B5, the best value of A_i is zero. In the case of $\Delta T=40^\circ\text{F}$ it was difficult to find a best value of A_i . To determine a general trend, the best value of A_i at $\Delta T=40^\circ\text{F}$ was assumed to be zero as used in other cases. If we assume the mass transfer coefficient is small enough to neglect, A_i is dependent on K_f , the liquid-vapor distribution coefficient, and the crevice concentration. Since $1/K_f$ is usually much less than one and the liquid-vapor distribution coefficient for NaCl or NaOH is negligible, A_i is dependent on the crevice concentration, c . The estimated crevice concentration in this series of tests is around 10^5 ppm range. If $1/K_f$ is in the same range as the crevice concentration, A_i will be close to zero.

The obtained G_i values are plotted as a function of ΔT in Figure B6. The plot for G_i is linear with respect to ΔT . In Eq. (B8), if the mass transfer by diffusion is negligible, G_i is proportional to the fraction of wetted length α and heat flux q'' . If the wetted length is constant and equivalent to the actual depth of the crevice, the heat flux will be proportional to ΔT . Therefore, G_i is proportional to ΔT , as shown in Figure B6. Based on the results in Figure B6, the impurity hideout rate is proportional to ΔT . Strictly speaking, the impurity hideout rate depends on the heat flux and the total tube surface area where nucleate boiling occurs in the crevice, excluding steam-dominant areas.

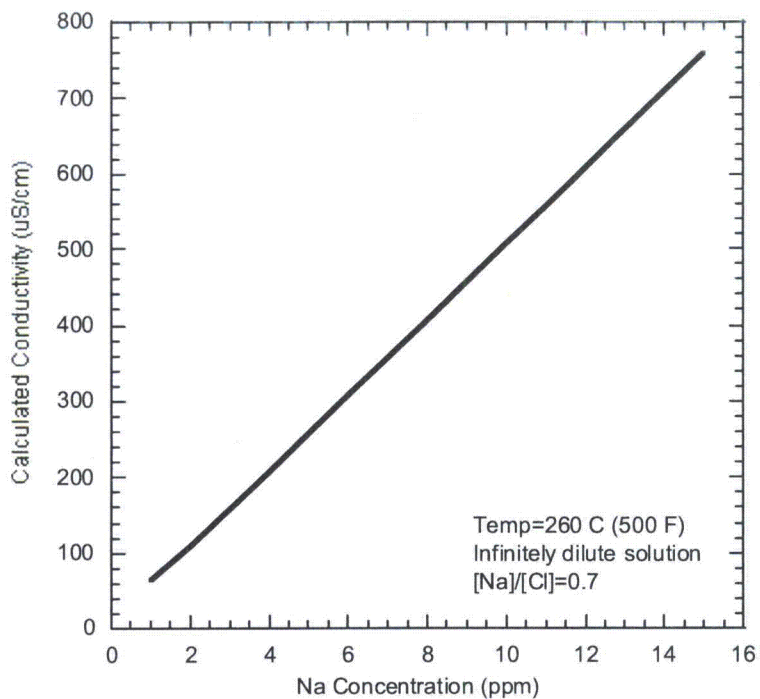


Figure B1.
Theoretically predicted conductivity as a function of Na concentration assuming that Na-to-Cl molar ratio is 0.7.

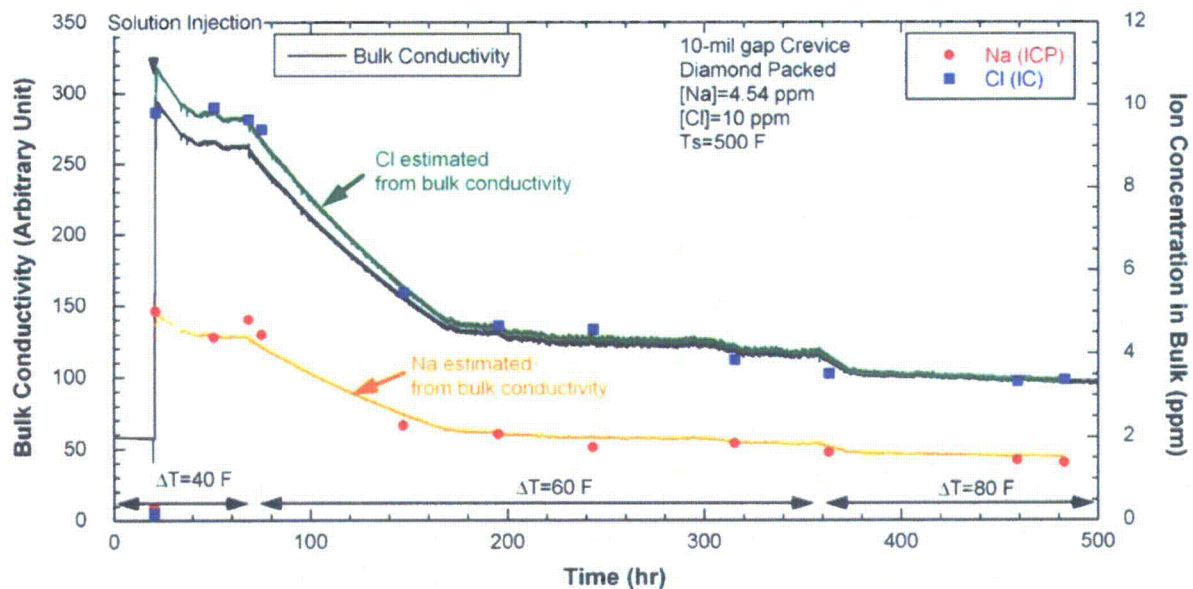


Figure B2. Na and Cl concentration variation estimated from bulk conductivity.

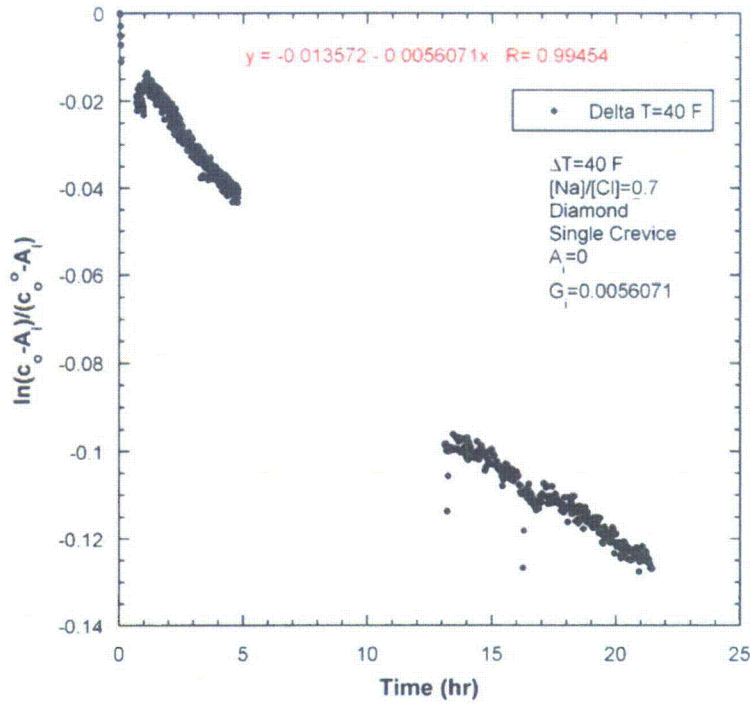


Figure B3.
Normalized bulk concentration variation as a function of time at $\Delta T = 40^\circ\text{F}$.

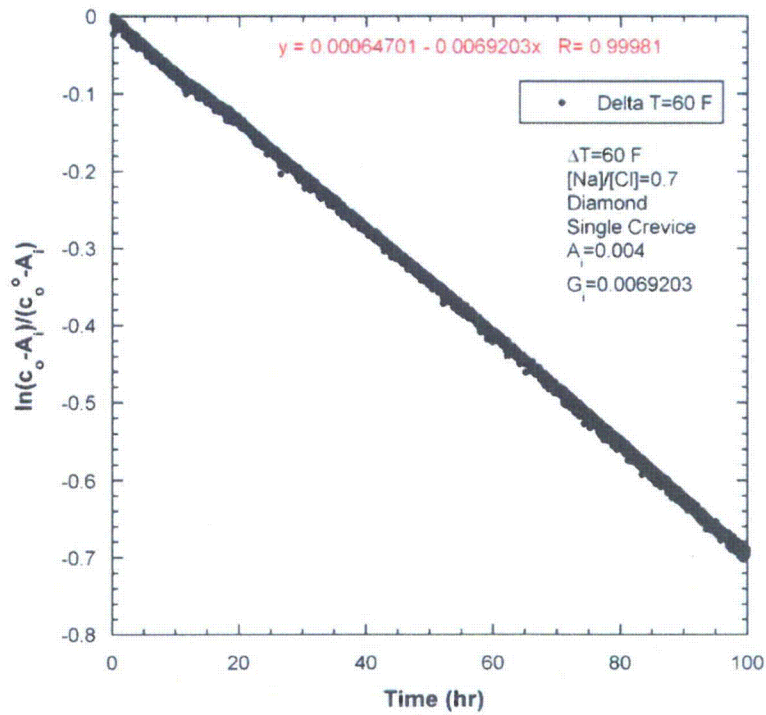


Figure B4.
Normalized bulk concentration variation as a function of time at $\Delta T = 60^\circ\text{F}$.

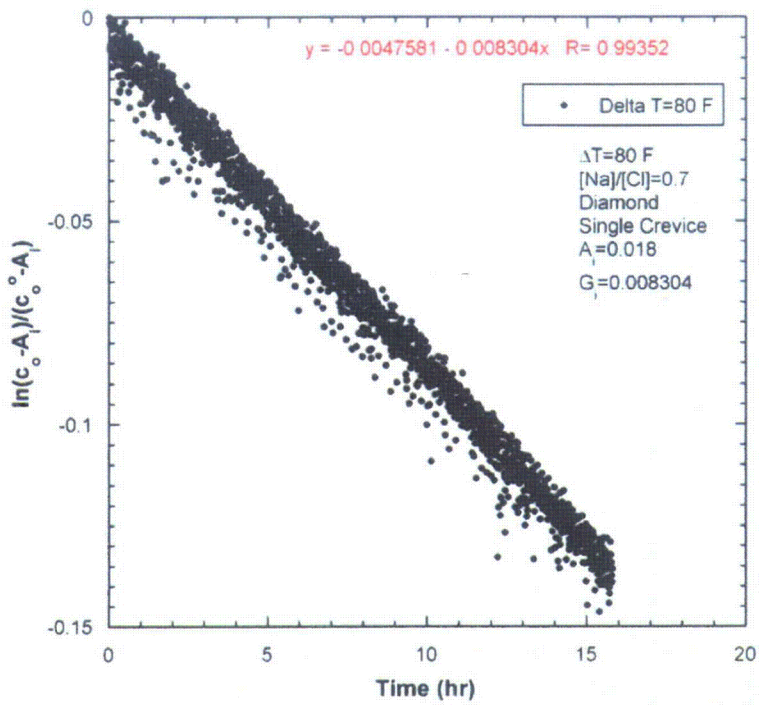


Figure B5.
Normalized bulk concentration variation as a function of time at $\Delta T = 80^\circ\text{F}$.

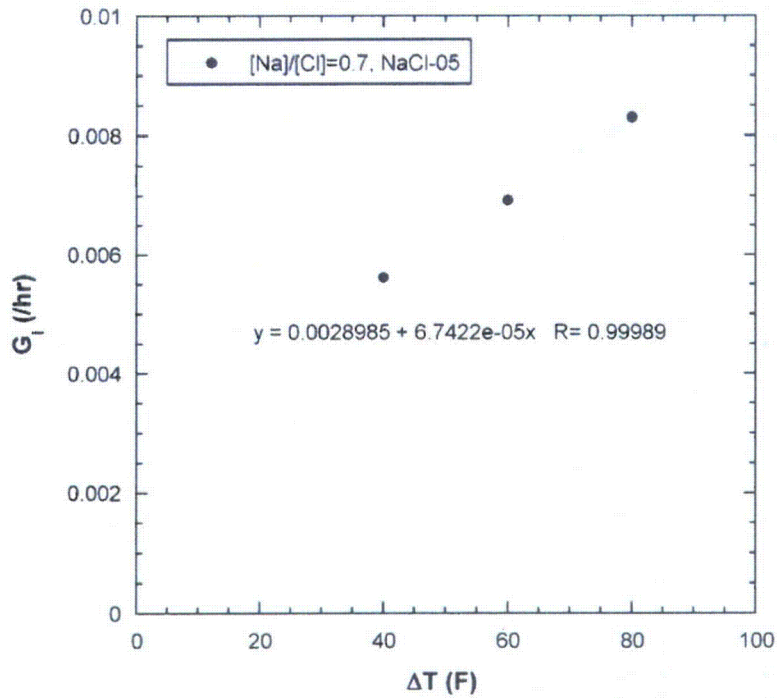


Figure B6.
Time constant G_1 variation as a function of ΔT .

Reference

1. J. G. Cleary and W. T. Lindsay Jr., "Diffusion and Hideout in Crevices, Final Report," EPRI-NP-2979, Electric Power Research Institute, Palo Alto, March 1983.

BIBLIOGRAPHIC DATA SHEET

(See instructions on the reverse)

NUREG/CR-6994

2. TITLE AND SUBTITLE

Argonne Model Boiler Test Results

3. DATE REPORT PUBLISHED

MONTH

YEAR

December

2009

4. FIN OR GRANT NUMBER

N6582

5. AUTHOR(S)

C.B. Bahn, K.E. Kasza, J. Park, C. Vulyak, and W.J. Shack

6. TYPE OF REPORT

Technical

7. PERIOD COVERED (Inclusive Dates)

8. PERFORMING ORGANIZATION - NAME AND ADDRESS (If NRC, provide Division, Office or Region, U.S. Nuclear Regulatory Commission, and mailing address; if contractor, provide name and mailing address.)

Argonne National Laboratory
9700 South Cass Avenue
Argonne, IL 60439

9. SPONSORING ORGANIZATION - NAME AND ADDRESS (If NRC, type "Same as above"; if contractor, provide NRC Division, Office or Region, U.S. Nuclear Regulatory Commission, and mailing address.)

Division of Engineering
Office of Nuclear Regulatory Research
U.S. Nuclear Regulatory Commission
Washington, DC 20555-0001

10. SUPPLEMENTARY NOTES

C. Harris NRC Project Manager

11. ABSTRACT (200 words or less)

Various corrosion phenomena have been observed in the steam generator (SG) tubes of pressurized water reactors. One such type of corrosion involves impurity concentration in the narrow gap between SG tubes and supporting structures or sludge piles ("crevices"). The purpose of this study is to characterize accumulation of impurities in the crevices for varying Na-to-Cl molar ratios in water, temperature, and packing type (diamond or magnetite). This characterization is based on tests carried out at Argonne National Laboratory in a model boiler system which can simulate prototypic SG conditions. Diamond powder, which has a higher thermal conductivity than magnetite powder, can enhance the boiling rate and lead to a rapid rate of impurity accumulation. Magnetite-packed crevices, which have lower permeability, are more appropriate for the simulation of actual SG crevices than a diamond-packed crevice. A radial chemistry gradient was observed in a crevice packed tightly with magnetite powder, a finding supported by earlier experimental work. Near the tube wall, the crevice chemistry tends to vary actively because of the increased volatility effect of Cl at the heated tube wall where boiling occurs. Initially, the crevice pH near the tube wall appears to be alkaline. As the concentration progresses, however, the crevice pH becomes neutralized and even acidic because of preferential Cl concentration, enabled by a reduced boiling rate near the tube wall due to the presence of a Na-rich liquid film. Based on the test results, the chemistry variation in actual SG crevice deposits near the tube wall was estimated. Unless some impurities remain and accumulate in the crevice after each fuel cycle, during most of a typical fuel cycle, the crevice chemistry would be in a transient rather than a steady-state condition because of low impurity concentrations in the secondary system. The kinetic data obtained for the crevice chemistry evolution with low bulk impurity concentration is valuable for the estimation of actual SG crevice chemistries. Based on the crevice and bulk solution sample analyses, the volatility effect of Cl in the diamond-packed crevices becomes significant as the molar ratio decreases.

12. KEY WORDS/DESCRIPTORS (List words or phrases that will assist researchers in locating the report.)

Steam Generator, tube leaks, chemistry, chlorine, Cl, thermal conductivity

13. AVAILABILITY STATEMENT

unlimited

14. SECURITY CLASSIFICATION

(This Page)

unclassified

(This Report)

unclassified

15. NUMBER OF PAGES

16. PRICE